New Approaches to Study Learning-Related Changes in Neuronal Activity Patterns in the Mouse Auditory Cortex

---

Dissertation zur Erlangung

der naturwissenschaftlichen Doktorwürde (Dr. sc. nat.)

vorgelegt der

Mathematisch-naturwissenschaftlichen Fakultät

der Universität Zürich

von

Balazs Laurenczy

von

Chavannes-près-Renens, VD

Promotionskomitee

Prof. Dr. Fritjof Helmchen (Vorsitz)

Prof. Dr. Richard Hahnloser

Prof. Dr. Klaas Enno Stephan

Zürich, 2016

Au fur te seront les lettres données sans que la suite ne saches et devras les inscrire à la trace. Libre sera toujours de l'inscription la surface quoique du quintil le dernier mot ne pourra se graver mais seulement à l'encre humaine s'écrire en coulée une silencieusement finale. Après sûrement mourras mais en sachant ce qu'aucun n'a su puisque tel le livre que lu il efface en blancheur la page et le lecteur.

— Alain Damasio, *El Levir et le Livre*

Abstract

Animals can learn to perceive and discriminate sounds to associate them with a meaningful outcome. Using simple discrimination learning, it was shown that the topographic map of the auditory cortex in mice can undergo extensive and specific changes upon learning. However the associated changes on the neuronal level have not been studied so far. Recent advances in genetically encoded calcium indicators and in two-photon calcium imaging in mouse neocortex allow to chronically record the neuronal activity of the cortex in specific cell types and cortical layers over time periods spanning from days to months.

In this thesis, an auditory discrimination learning paradigm combined with two-photon calcium imaging was established. This combined learning task and imaging technique was used to investigate the learning-related changes in the frequency tuning properties and activation patterns of layer 2/3 neurons of the auditory cortex during a goal-directed auditory discrimination task. Preliminary findings suggest that neuronal populations of expert animals have lower responsiveness to auditory stimulation compared to naive animals, while keeping high information content. However these findings were not fully conclusive due to several technical limitations (movement artefacts, viral toxicity).

Furthermore, learning-related changes in neuronal population activity patterns were also studied across multiple cortical regions. A delayed auditory discrimination task combined with wide-field calcium imaging was established. Training of the animal in the delayed auditory discrimination was pursued until reaching a very high performance level. An analysis workflow was developed to select learning trials where body movement was minimized, in order to avoid movement-related contamination in the calcium imaging signal. Preliminary findings suggest that activity in auditory cortex is suppressed for the target but not for the distractor sound. Furthermore, cortical regions potentially retaining behavior-related information during the delay period were identified. However, as more animal numbers are still currently analysed, these findings remain preliminary and will need to be confirmed.

Finally, interactive visualization and automated analysis tools were developed to meet the challenges of the large and complex data sets produced by combined behavior and calcium imaging experiments. These tools were integrated in a framework composed of several independent modules that performed various tasks, like data management, semi-automated image segmentation, calcium imaging data analysis, custom plotting and analysis, joint tracking, single trial visualization and analysis, and finally behavior experiment control.

Zusammenfassung

Geräusche können von Tieren wahrgenommen und unterschieden werden um diese als überlebenswichtige Information zu verarbeiten. Experimente, welche einfache Lernparadigmen zum Unterscheiden von Geräuschen benutzten, konnten zeigen, dass die topographische Repräsentation dieser Geräusche im auditorsichen Cortex erhebliche und spezifische Änderungen unterlaufen. Die Änderungen im Gehirn, die durch das Unterscheiden von Geräuschen oder Tönen hervorgerufen werden, wurden nicht erforscht. Die kürzlich erzielten Fortschritte in der Erzeugung von genetisch modifizierten Mauslinien, sowie die Weiterentwicklung von Zweiphotonen Mikroskopie im Maus Neocortex erlauben es neuronale Aktivität im Cortex in einer schicht-spezifischen Art über längere Zeit zu verfolgen und zu messen.

In dieser Doktorarbeit wird aufgezeigt, wie ein neuartiges auditorisches Lernparadigma mit Zweiphotonenmikroskopie etabliert wurde. Das neuartige Lernparadigma - in Kombination mit neuen bildgebenden Verfahren - wurde benutzt, um die lernspezifischen Änderungen im Gehirn bezüglich der Unterscheidung verschiedener Tonfrequenzen zu studieren. Dieses Paradigma wurde mit genetischen Werkzeugen auf Schicht 2/3 des auditorsichen Cortex beschränkt und bezog sich auf ein zielgerichtetes Diskriminierungsverfahren von Tonfrequenzen. Voruntersuchungen deuten darauf hin, dass neuronale Populationen von Tieren auf Expertenniveau ein niedriges neuronales Antwortniveau, jedoch hohen Informationsgehalt, verglichen mit naiven Mäusen, aufweisen. Jedoch konnten diese neuen Erkenntnisse aufgrund vielfältiger Limitationen (Bewegungsartefakte, virale Toxizität) nicht vollständig validiert werden.

Des Weiteren wurden die lernspezifischen Änderungen neuronaler Ensembleaktivität auf kortikalem Niveau studiert. Dazu wurde ein zeitverzögerter Test zur Unterscheidung von Tonfrequenzen mit „wide-field“ Aufnahmeverfahren kombiniert. Das Training von Tieren mit dieser Zeitverzögerung wurde durchgeführt, bis die Tiere eine sehr hohe Trefferquote erzielten. Ein neuartiges Analyseverfahren wurde entwickelt um Experimente, welche Artefakte hervorgerufen durch Bewegungen des Tiers aufwiesen, vom Endresultat zu entfernen. Vorläufige Resultate dieser Analysen deuten darauf hin, dass die Aktivität im auditorischen Cortex für das Zielgeräusch im Gegensatz zum Ablenkungsgeräusch unterdrückt wird. Basierend auf diesen Versuchen konnten kortikale Areale identifiziert werden, welche verhaltensrelevante Informationen während der Verzögerungsperiode verarbeiten. Jedoch müssen noch mehr Tiere diesem Testverfahren unterzogen werden, um diese Befunde zu untermauern.

Um die hier präsentierten neuen Paradigmen und Daten zu verarbeiten, wurden automatisierte Analyse- und Visualisierungsroutinen entwickelt, da die hier präsentierten Daten von hoch komplexer Natur sind. Diese neuen Analyseverfahren wurden in einem Analysepaket zusammengeführt, welches aus mehreren unabhängigen Modulen aufgebaut ist. Diese Module beinhalten die Kontrolle und Ausübung mehrerer komplexer Aufgaben. Diese beinhalten die Datenverwaltung von Experimenten, benutzerdefinierte Visualisierung der Daten, die Analyse von Tierbewegungen und die Kontrolle über Verhaltensexperimente.

Table of Contents

1 Introduction

1.1 The auditory system of rodents

Hearing is a key sensory system in many species throughout the animal kingdom and a very useful complementary sense in many other. Hearing provides critical information about the environment in a fast and very sensitive manner, which helps animals survive better and react faster, both as preys or as hunters. The information provided by the auditory system is not only detection of changes in the environment, but also the location, distance, direction and most crucially the nature of the sound source, as the sound can be recognized by comparing it to the previously heard sounds. This comparison relies very much on another key ability in the animal kingdom, which is the ability of animals to learn and adapt their behavior. Learning a new behavior, or in other words learning new associations of external stimuli and appropriate responses to them, is a key feature of the nervous system, presumably the most complex one.

During my PhD, I was interested in how animals can learn and what happens in their brain during the learning process. More specifically, I worked on understanding how they solve a learning task and what changes are associated to this learning in the brain. To do this, I focused on the auditory system by using auditory discrimination tasks in the mouse, which is a very useful model species because of the genetic tools available for it. To investigate the changes happening in the brain during this learning task, I mainly used calcium imaging of cortical neurons, either using two-photon microscopy or wide-field imaging.

1.1.1 Hearing and the auditory research community

The auditory system is one of the five sensory modalities in mammals, together with the visual, somatosensory, olfactory and gustatory modalities. As such, auditory information is one of the five type of inputs to the central nervous system, which are incoming channels that link the brain to the external world. Investigating this input channel is one of the ways to try to understand the brain and more precisely, how it processes external information.

In today's neuroscience research, the auditory community is still smaller compared to the visual and somatosensory research communities. But the auditory community is growing quickly, as the auditory modality enables arguably easier and better controlled stimuli presentation, while still being a strongly relevant modality for animal behavior.

The auditory system was studied in many different species, including rodents (Harris et al., 2011), cat (Winer and Lee, 2007), bats (Kössl et al., 2015), owls (Pena and DeBello, 2010), ferrets (King et al., 2007) and humans (Hackett, 2015). In human research, a great amount of literature is devoted to study tinnitus (for a review see Eggermont (2015)). Tinnitus is the hearing of a sound without external sound being present, and it is the symptom of various hearing-related illnesses. The following introduction will focus on the rodent auditory system, as all experiments of this thesis were carried out in mice.

The following subsections give an overview of the anatomy of the ascending mouse auditory pathways from the hearing organ, the ear, to the highest step of processing, the auditory cortex. A number of feedback descending pathways also exist but will only be mentioned sparsely for simplicity. This chapter is mostly based on the auditory system chapter by Malmierca and Ryugo (2012) from the book *The Mouse Nervous System* by Watson et al. (2012).

1.1.2 The path to the auditory cortex

The auditory system is processing sounds that are perceived through the ears. Sounds are air pressure waves of different frequencies, and different species have different frequency ranges of hearing: 2 to 100 kHz for mouse (Koay et al., 2002), 1 to 80 kHz in rat (Malmierca and Ryugo, 2012) and 0.5 to 85 kHz in cat (Heffner and Heffner, 1985). For comparison, the hearing range of humans is between 0.02 and 20 kHz.

As said, sounds are a *physical phenomenon* processed by the auditory system and as such, they can be described with various parameters. The main properties describing sounds are the frequency and intensity, measured in hertz (Hz) and decibels (dB) respectively. Intensity of sounds is also often measured using the sound pressure level (SPL), which is a measure of the pressure of a sound at a specific distance and relative to a *reference value*. SPL is defined by the following equation:

$$\mathrm{SPL} = 20 \log_{10}\left(\frac{p}{p_{ref}}\right) \mathrm{dB}$$

where p is the root mean square sound pressure and p_{ref} is the reference sound pressure, commonly set to 20 $\mu\mathrm{Pa}$ (threshold of human hearing). In natural conditions, sounds are usually not present as pure tones with a single frequency but rather as a combination of many different pure frequencies, creating an *assemblage* that our ears perceive and can usually easily identify. Other

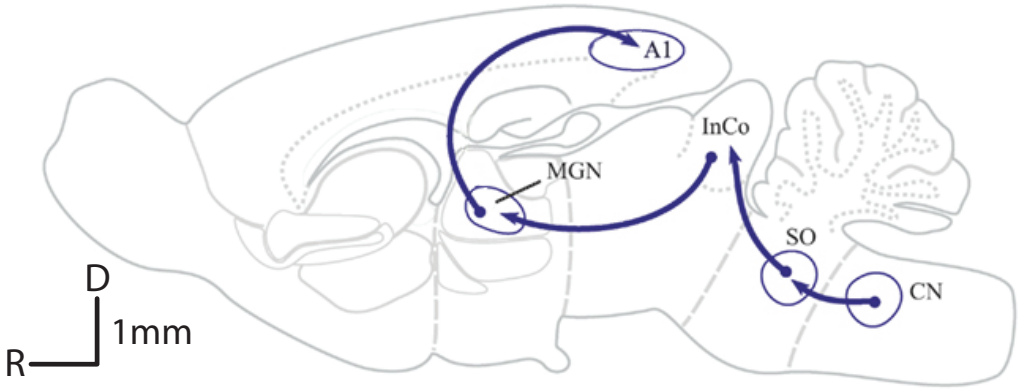

Figure 1.1: The ascending rodent auditory pathway: *The major relays of the ascending rodent auditory pathway. Scale bar: 1 mm. Abbreviations:* R *rostral;* D *dorsal;* CN *Cochlear Nuclear;* SO*, Superior Olive;* InCo *Inferior Colliuculs;* MGN*, Medial Geniculate Nucleus;* A1*, Primary Auditory Cortex.* Modified from Mueller (2012).

features linked to the perception of sounds are also commonly associated to the sounds. In organisms with two ears placed on each side of the head, inter-ear intensity and inter-ear time difference can be measured. These can help distinguish the distance or the physical location of the sound's source relative to the ear perceiving it.

Sound waves enter the ear and are propagated to the inner ear, where the transduction into action potential happens (Figure 1.2). The organ of Corti is sensing the mechanical vibrations produced by the sound, using the sensory hair cells. These cells use the deflections of their stereocilia to transform the mechanical vibrations into action potentials. Moreover, the organ of Corti is shaped as a spiral and along its length, several properties of the basilar membrane (progressive increase of the stiffness, decreasing width and increased thickness from apex to base) give rise to a mapping of the different frequencies of the sound along the length of the organ of Corti. This mapping is called the *cochleotopy*, or cochlear frequency map. It is the first appearance of a frequency-dependent topographic organization in the auditory system.

1.1.3 Sub-thalamic and thalamic auditory system

The auditory nerves conduct the produced action potentials to the cochlear nucleus complex (*CNC*) in the brainstem, where the physical properties of the sound are already analysed (Figure 1.2). From there, the dorsal, intermediate and ventral acoustic striae conduct the auditory information to the superior olive complex (*SOC*) and then to the inferior colliculus (*IC*). The medial nucleus of the trapezoid body (*MTz*) is located at the most medial part of the SOC. It receives projections from the contralateral ventral cochlear nucleus and has extensive projections to the ipsilateral SOC. The IC is itself composed of several nuclei, the central nucleus (*CIC*), the dorsal cortex (*DCIC*), the lateral cortex (*LCIC*) and the rostral cortex (*RCIC*). These nuclei are mostly

defined by cytoarchitectural properties rather than by the physiological responses of the neurons they contain. The neurons of the inferior colliculus show a large variety of response properties to the sound stimuli.

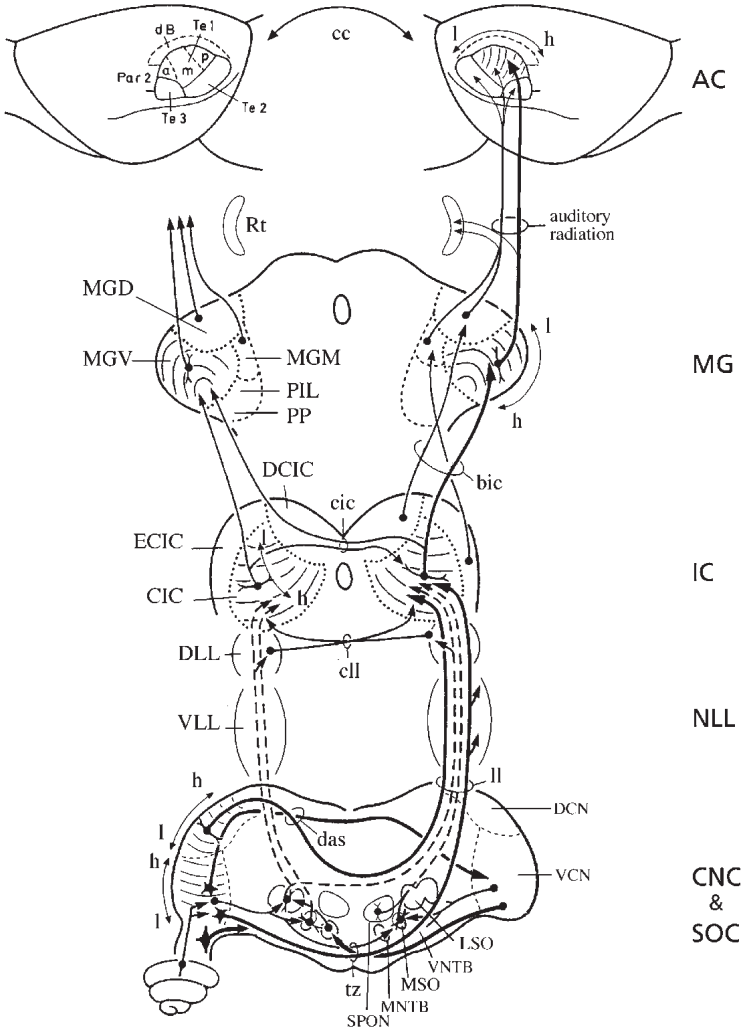

Figure 1.2: Detailed schematic of the mouse auditory pathway: *The ascending mouse auditory pathway from the cochlea (bottom) to the auditory cortex (top). Abbreviations:* CNC *Cochlear Nuclear Complex;* SOC*, Superior Olivary Complex;* DCN *dorsal cochlear nucleus,* VCN *ventral cochlear nucleus,* tz *trapezoid body,* SPON *superior paraolivary nucleus,* MTz *medial nucleus of trapezoid body,* MSO *medial superior olive,* VTz *ventral nucleus of trapezoid body,* LSO *lateral superior olive,* ll *lateral lemniscus,* DLL *dorsal nucleus of lateral lemniscus,* VLL *ventral nucleus of lateral lemniscus,* cll *commissure of lateral lemniscus,* LCIC *lateral cortex of inferior colliculus,* DCIC *dorsal cortex of inferior colliculus,* cic *commissure of inferior colliculus,* bic *brachium of inferior colliculus,* PP *peripeduncular nucleus,* PIL *posterior intralaminar nucleus,* Rt *auditory sector of reticular thalamic nucleus,* cc *corpus callosum,* Te *temporal areas (1,2,3).* Modified from Malmierca and Ryugo (2012).

The inferior colliculus sends its output to the auditory thalamic nucleus, the medial geniculate nucleus (*MG*), which is again subdivided into a dorsal (*MGD*), ventral (*MGV*), and medial part (*MGM*). The thalamus was often reported as being solely a relay structure or a gateway of the sensory information to the cortex. During the last years, it has been shown that the auditory thalamic nuclei can alter the nature of the auditory information in a dynamic way, as it receives not only auditory information but also somatosensory, vestibular, visual and nociceptive inputs. Finally, the targets of the auditory thalamus projections include of course the primary auditory cortex, but also the striatum and the amygdala. Amygdala and the auditory pathway have been shown to be connected via circuits involved in fear conditioning (Herry and Johansen, 2014).

To summarize, the path from the ascending auditory information has several major relay points,

described above, with mainly four synaptic relays until it reaches the auditory cortex. These relay points all convey the tonotopic organization described at the cochlear level, although with different degrees of fidelity. On top of this, there are multiple convergences and cross-connections, notably from pathways other than the auditory path, and this organization is made even more complex by the seven commissures of the central auditory system.

1.1.4 The auditory cortex

The auditory cortex is one of the sensory cortices of the brain, focused on processing auditory information. In mice, the auditory cortex is thought to be divided in 4 or 5 functionally distinct subregions: the primary auditory cortex (AI), the secondary auditory cortex (AII), the anterior auditory field (AAF), the ultrasonic field (UF) and sometimes the dorsal posterior cortex (DP) (Figure 1.3 top left, Stiebler et al. (1997)). Surrounding the core auditory region, *belt* auditory cortices have been reported to also process and receive auditory-related information. There is however no specific labelling at this time to reveal them unambiguously (Malmierca and Ryugo, 2012).

The auditory cortex, like the other cortices, contains different types of neurons. Based on the action they have on their target, two main categories of neurons can be defined: the excitatory (glutamatergic) and the inhibitory (GABAergic) neurons. The glutamatergic neurons are *activating* their targets, making them more likely to fire an action potential, whereas the GABAergic neurons are *deactivating* their targets, making them less likely to fire an action potential. Neurons can also be categorized according to their morphology. In the cortex, mostly long-range projecting pyramidal neurons and locally connected interneurons are present. All these different categories of neuron are distributed in the six layers of the cortex. Pyramidal cells are the majority of the neurons in the cortex as they represent about 75% of all neurons. There are a number of subtypes of pyramidal neurons, but they mostly lack clear genetic markers to be unambiguously identified.

Interneurons subtypes are usually better defined using a wide range of genetic markers, combined with specific morphologies, connectivity and intrinsic action potential firing properties (Kepecs and Fishell, 2014). These different subtypes have various roles within the cortical circuitry. For example, the targets of vasointestinal peptide-containing (VIP) interneurons are mostly somatostatin- (SST) and parvalbumin-containing (PV) interneurons. This interneuron to interneuron circuitry leads to the disinhibition of the pyramidal neurons targeted by the SST and PV interneurons (Wolff et al., 2014; Pi et al., 2013).

The main inputs incoming to the primary auditory cortex are from the ventral part of the auditory thalamic nucleus, called the medial geniculate nucleus MGV. The anterior auditory field also receives input from the thalamus from the dorsal part of the same nucleus (MGD, Llano and Sherman (2008)). The different layers of a sensory cortex are thought to be wired together and with the

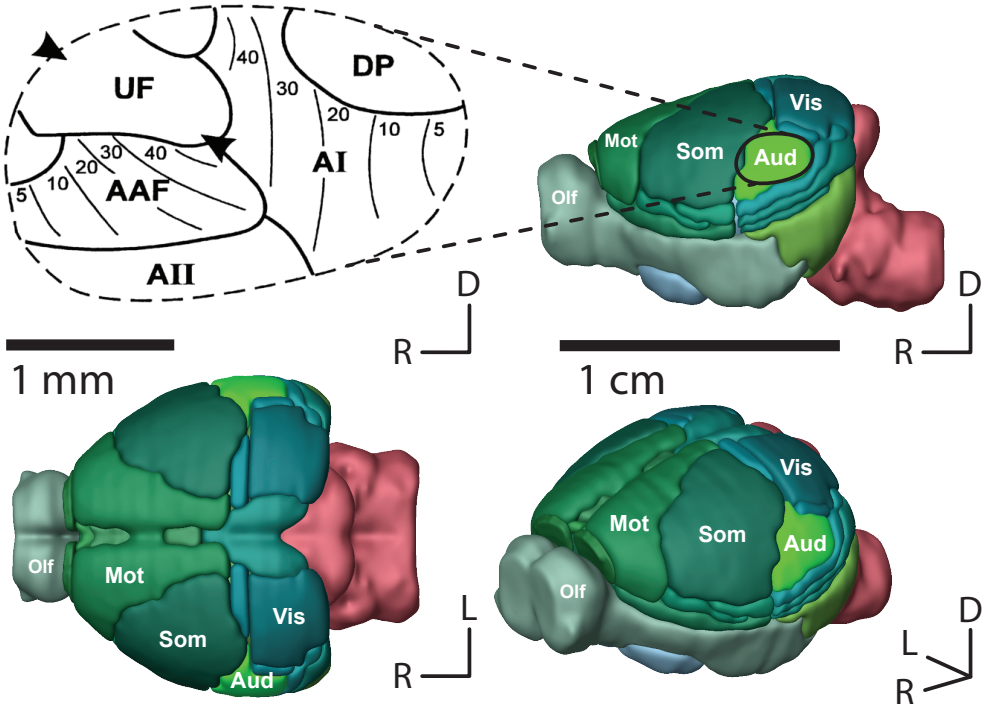

Figure 1.3: The location and division of the auditory cortex: Top left*: The divisions of the auditory cortex in mice. Abbreviations:* R *rostral;* D *dorsal;* L *lateral;* AI *primary auditory field;* AII *secondary auditory field;* AAF *anterior auditory field;* UF *ultrasonic field;* DP *dorsal posterior cortex. Modified from* Stiebler et al. (1997). ***Top right****: Sagital view of a mouse brain with the main sensory areas labelled. Abbreviations:* Olf *olfactory bulb;* Mot *Somatomotor;* Som *somatosensory;* Aud *auditory;* Vis *visual. Images from the* Allen Brain Explorer *(Lau et al., 2008).* ***Bottom left and right****: Same as top right, but with horizontal and tilted views, respectively.*

other cortices and brain regions according to a canonical microcircuit (Douglas and Martin, 2004). The projections from the thalamus mostly arrive in layer 4 of the cortex. Layer 2/3 received the input from layer 4, and are forming networks within their sensory cortex as well as with the other cortices. Layer 5 and 6 are the main source of outgoing connections from the auditory cortex, targeting either the thalamus, the striatum, the amygdala or the other hemisphere via the callosal projections.

1.2 Measuring neuronal activity in the auditory cortex

There are many different methods to measure the activity of the neurons in the auditory cortex. These methods have different advantages and drawbacks, as well as different temporal and spatial resolutions, as illustrated in Figure 1.4. These techniques have also different degree of impact on the physiology of the cortex during the recording, as they are more or less invasive recording methods. Finally, the ease of access to the auditory cortex, given its lateral position on the head (Figure 1.3), is also a relevant factor when choosing a method to study the auditory cortex. The following section is a condensed description of the main methods used in this thesis to record activity from the auditory cortex of mice.

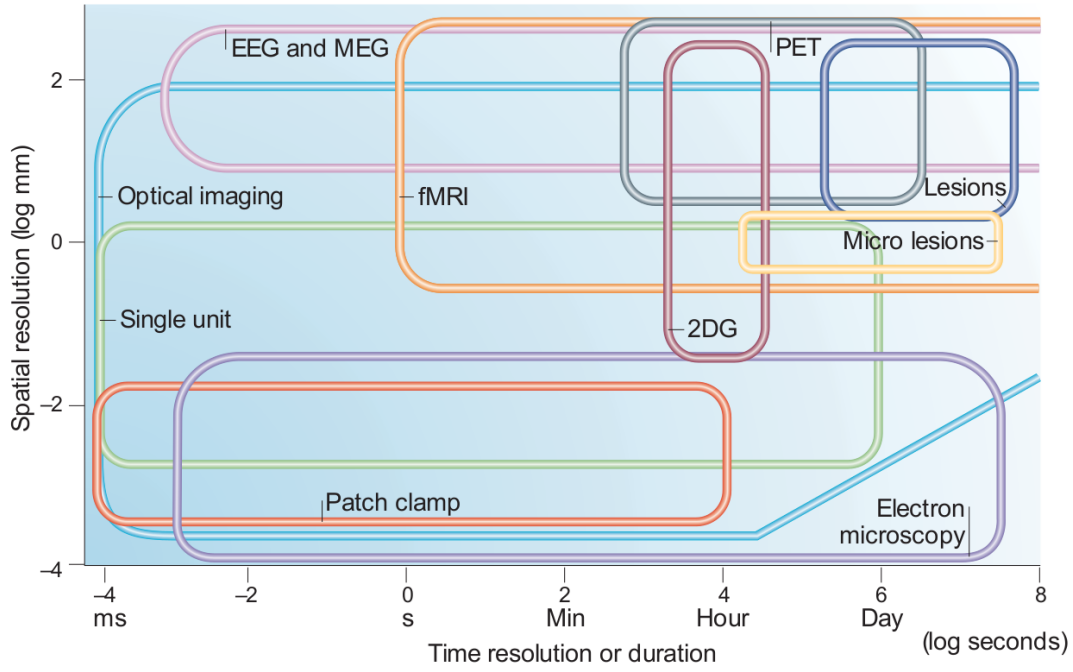

Figure 1.4: Measuring neuronal activity in the auditory cortex: *Different techniques used to measure activity in the cortex. The spatial and temporal resolution of each method is shown with a rectangle. Optical imaging methods have a very wide range of resolution. These include voltage-sensitive dye imaging (VSDI), intrinsic signal optical imaging (ISOI), calcium imaging, confocal imaging, multiphoton imaging. Abbreviations: EEG, electroencephalography; fMRI, functional magnetic resonance imaging; MEG, magnetoencephalography; PET, positron emission tomography; 2DG, 2-deoxyglucose post-mortem histology. From* Grinvald and Hildesheim (2004).

1.2.1 Electrophysiological recordings

Electrophysiolgy is one of the oldest and most *traditional* recording method available in neuroscience. Already in 1952, Hodgkin and Huxley performed electrophysiology experiments by recording intracellularly from the giant squid axon (Hodgkin and Huxley, 1952), for which they re-

ceived a Nobel prize in 1963. Electrophysiolgy techniques consist in recording the changes in electrical potential of cells or groups of cells. It is arguably the method that is "*closest*" to record the physiology of neurons, as the changes in the electric potential is what defines best the *activity* of neurons. Two main categories of electrophysiolgical recordings exist: intracellular and extracellular.

Intracellular recordings measure the voltage or the current across the membrane of a neuron, therefore allowing the measurement of the sub-threshold activity of neurons (changes bellow the action potential threshold). Usually, the tip of a metal microelectrode or a glass micropipette is inserted inside the cell, so that the membrane potential can be measured compared to a reference electrode located outside of the cell. Several different *modes* of intracellular recordings exist. Voltage and current clamp modes are settings were either the voltage or the current are set to a given value (*clamping*), respectively. The instruments then record the amount of current or voltage that is required to maintain the clamped voltage or current, respectively.

Another intracellular recording mode, developed by Neher and Sakmann and named *patch clamping*, allows the recording of very small voltage or current changes by inserting a micropipette that fuses with the membrane, creating a seal with a very high resistance. If the seal is then opened up, a full access to the inner membrane potential of the neuron is obtained, with a very low access resistance (Neher and Sakmann, 1992). This whole-cell mode is widely used in neuroscience and in the auditory research for the completeness of the information it provides about the measured neuron. It should be noted that this whole-cell configuration is a difficult procedure *in vivo*, having an acceptable success rate only in the hand of experienced electrophysiologists. This mode has nevertheless be used in the auditory cortex of living animals (Chen et al., 2015).

Extracellular electrophysiology can record the potential changes of either a single neuron or of a group of neurons. Typically, only the supra-threshold activity can be recorded, which means that membrane potential changes that do not lead to an action potential cannot be seen. When recording from a single neuron, the potential change of a specific neuron can be recorded by placing a metal microelectrode or a glass pipette in its close proximity. When using a glass pipet, this approach is often referred to as the cell-attached or juxta-cellular mode. In this configuration, the patch pipette is pushed against the targeted neuron, a tight seal is formed, but the seal is not opened up as in the whole-cell mode described above. Therefore only the spiking activity (the firing of action potentials) of the neuron is recorded. This cell-attached mode was the method used in some of the experiments in this thesis. It was combined with two-photon guiding, which will be described in a later section.

When using metal electrodes, different filtering can be applied to the recordings to extract different biological signals. In these extracellular recordings, a metal electrode is placed in the

vicinity of neurons and the combined membrane potential change of several neurons is recorded as a group. Depending on the frequency band that is then filtered, either slower variations, called local field potential (LFP) can be extracted, or the spiking activity of the neurons can be recorded. For LFPs, the signal is low-pass filtered with a cut off at ~300 Hz. By using a low impedance electrode and positioning it in an appropriate manner, the activity of a large number of neurons can be recorded. The low-pass filter removes the spiking contribution from the signal. The remaining LFP signal is thought to reflect the synchronized synaptic inputs to the measured region.

When filtering out the signal with a high-pass filter with a cut off above ~1 kHz, only the spiking component remains. In these so-called multi-unit recordings, the action potentials of many neurons can contribute to the observed signal. It is then often necessary to perform a spike sorting step, to tease out which and how many neurons contributed to the recorded signal. The aim and result of the spike sorting is to attribute the recorded spikes to the neurons they were recorded from. Some electrophysiology techniques use recording *probes* with several electrodes at the same time, with a regular spacing of typically ~50 µm between the electrodes. Using the signal recorded in several channels can help differentiating the contribution of the neurons during the spike sorting step. The spiking activity of each neuron can then be identified and used for further analysis, either individually (single unit activity) or as a group (multi-unit activity, see Figure 1.6 and Figure 1.7, Guo et al. (2012); Polley (2006); Hackett et al. (2011); Stiebler et al. (1997)).

1.2.2 Intrinsic signal optical imaging

Intrinsic signal optical imaging (ISOI) is a functional imaging technique used to record activation regions in the cortex. The experimental setup required by ISOI is very simple but with low spatial and temporal resolution. This method is based on changes in blood oxygenation caused by physiological activity of the neural tissue measured (for a review, see Zepeda et al. (2004)). Indeed, the activation (firing) of neurons in a specific location of the cortex requires energy and therefore oxygen. As the oxygen is brought to a specific region, an increased blood flow and blood oxygenation can be observed. This is usually done by shining red light on the surface of the brain and recording the reflected light. As more oxygenated blood is present in a region, the lower the reflectance will be. Therefore, the changes measured by ISOI are *decreases* of reflectance.

Usually, ISOI is used to visualize the approximate location of a specific sensory cortex, or a specific region within a sensory cortex. For example, the cortical region associated with individual whiskers, called *barrels*, can be visualized by stimulating the whisker and recording the activity in the cortex with ISOI (Aronoff and Petersen, 2007; Polley et al., 2004). A similar approach can be used in the olfactory bulb to identify regions within the olfactory bulb that are associated with different odors (Bozza and Mombaerts, 2001). In this thesis, the very same was done to obtain an

approximate location of the auditory cortex.

ISOI was also used a lot in the visual cortex to map ocular dominance (Cang et al., 2005) or retinotopy (Lantz, 2014). The typical experimental paradigm for ISOI is based on repetitions and averaging. Usually, the reflectance before and after a stimulus is compared using a standard normalization formula:

$$\Delta R/R = \frac{R_{stim} - R_{base}}{R_{base}}$$

where R_{base} is the reflectance measured during the baseline period (before the stimulus) and R_{stim} is the reflectance measured after the stimulus. As the measured signal is directly linked to the blood flow, a lot of factors can add noise and artefacts to the measured signal. Therefore, a high number of stimulus presentation are necessary to average out the noise and artefacts. In addition, the hemodynamic signal recorded with ISOI is relatively slow (several seconds), with the consequence that a relatively long inter-repetition time must be waited after each stimulus in order to return to the baseline condition (typically 15-30 seconds).

Another experimental paradigm that circumvents these disadvantages was developed by Kalatsky and Stryker. *Fourier optical imaging* is a technique to acquire and analyse intrinsic signal optical images of the brain's activity, using continuous stimulus presentation and continuous data acquisition (Kalatsky and Stryker, 2003). This method is very useful to obtain the topographic map of a specific sensory stimulus feature, like visual retinotopic maps, visual orientation maps and auditory tonotopic maps. A temporally periodic stimulus is presented and the component of the recorded response at the frequency of stimulation is extracted and analysed using a Fourier analysis. By extracting the phase of the response at the stimulation frequency, the preference for the stimulus feature can be obtained. Indeed, since the stimulus space was presented sequentially, each phase of the response corresponds to a specific stimulus within the presented stimulus sequence.

To obtain *absolute* tonotopic maps, the hemodynamic response delay Φ_d must be corrected for. This can be done by presenting the stimulus sequence in a reversed order. By then subtracting the two responses from the forward stimulus presentation Φ^+ and the reverse stimulus presentation Φ^- , the *absolute* tonotopic map can be obtained. This process is described by the following equations:

$$\Phi^+ = {\Phi_s}^+ + \Phi_d \tag{1.1}$$

$$\Phi^- = {\Phi_s}^- + \Phi_d \tag{1.2}$$

where Φ^+ is the measured phase for the *forward* presentation (including the delay), Φ^- is the measured phase for the *reverse* presentation (including the delay), ${\Phi_s}^+$ is the absolute phase for the *forward* presentation (without the delay), ${\Phi_s}^-$ is the absolute phase for the *reverse* presentation (without the delay) and Φ_d is the hemodynamic response delay. Since the stimulus sequence is

cyclic:

$$\Phi_s{}^- = -\Phi_s{}^+ \tag{1.3}$$

Therefore, one can obtain the *absolute* phase by subtracting the two measured phases via the following equation:

$$\Phi^+ - \Phi^- = \Phi_s{}^+ + \Phi_d - (\Phi_s{}^- + \Phi_d) \tag{1.4}$$

By replacing $\Phi_s{}^-$ using 1.3:

$$\Phi^+ - \Phi^- = \Phi_s{}^+ + \Phi_d - (-\Phi_s{}^+ + \Phi_d) \tag{1.5}$$

$$\Phi^+ - \Phi^- = \Phi_s{}^+ + \Phi_d + \Phi_s{}^+ - \Phi_d \tag{1.6}$$

$$\Phi^+ - \Phi^- = 2\Phi_s{}^+ \tag{1.7}$$

Finally:

$$\Phi_s{}^+ = \frac{\Phi^+ - \Phi^-}{2} \tag{1.8}$$

This *Fourier* paradigm is faster to acquire and more robust to all the artefacts that can be present in the intrinsic optical signal recordings from awake animals (ventilation, vasomotor signals, heart beat, etc.). This method can also be use to obtain topographic maps in a more precise and faster was, compared to the traditional manner if averaging the responses to episodic, randomly interleaved stimulus presentations (*standard* paradigm). In this thesis, both the *standard* and the *Fourier* paradigms were used to obtain tonotopic maps of the auditory cortex, similarly to what has been done before in the auditory cortex (see Figure 1.6, Kalatsky et al. (2005); Nelken (2004)).

1.2.3 Calcium imaging and calcium indicators

Calcium imaging is an optical method to record the activity of neurons via the measurement of the intracellular calcium concentration (for reviews, see Helmchen and Waters (2002); Grewe and Helmchen (2009); Grienberger and Konnerth (2012); Peron et al. (2015)). Indeed, in many neuron types, the firing of action potentials is closely associated with large and rapid increases of the intracellular calcium concentration (Kerr et al., 2005, 2007). This increase of calcium concentration can be used to read out the activity of neurons using calcium indicators. Calcium indicators are synthetic molecules or proteins that can bind free calcium ions and therefore react to the presence and concentration of calcium by changing their three-dimensional conformation. In addition, these indicators are usually associated with a fluorescent domain, designed in a way that the change in conformation due to the presence of calcium alters their fluorescence emission properties. This change in emitted light is what is finally measured in the calcium imaging experiments.

The changes in emitted fluorescence is therefore a *proxy* for the change in calcium concentration, which is itself a *proxy* for the spiking activity of the neurons (action potentials).

Many different calcium indicators are available nowadays. These indicators can be categorized according to many criterion: synthetic versus genetically encoded, emission and absorption wavelengths, temporal resolution, fluorescence emission amplitude for a given calcium concentration, fluorescence half-time (extinction), ratiometric indicators versus single-fluorophore, etc. These properties will be briefly described hereafter and a few common calcium indicators will be described.

A broad class of calcium indicators are the synthetic calcium indicator molecules. The oldest indicators are synthetic molecules that needed to be injected in the brain tissue or directly into the neurons. These were the *quin*, *fura*, and *fluo* indicator families (Tsien, 1989). Later, the *Oregon Green BAPTA-1* synthetic indicator (OGB-1) was a major synthetic calcium indicator used to measure the activity of cortical networks in a number of studies (Stosiek et al., 2003; Kerr et al., 2005, 2007; Hofer et al., 2011). OGB-1 was often used in combination with *Sulforhodamine 101*, which is a specific marker of astroglia in the neocortex (Nimmerjahn et al., 2004; Nimmerjahn and Helmchen, 2012). This allowed distinguishing between neurons and glial cells within the pool of neurons labelled with OGB-1.

Genetically encoded calcium indicators (GECIs) are another more recent class of calcium indicators. GECIs are proteins that can act as calcium indicators due to the different protein domains they contain. Typically, a calcium binding domain (e.g. calmodulin) and a fluorescent protein (e.g. GFP or any color variant of it) are encoded in a DNA sequence. This sequence can either be integrated to cells via a virus vector or more recently via the creation of transgenic animals that can express these proteins without external intervention. These mouse lines can be combined to obtain inducible, temporally and spatially specific expression of a calcium indicator, for example in a specific cell type or a particular cortical layer (Madisen et al., 2015). The most commonly used indicators are the *GCaMP* family (Chen et al., 2013b), the red variant *RCaMP* family (Ohkura et al., 2012) and the Yellow-Cameleon ratiometric indicator family (Horikawa et al., 2010).

GCaMP6 is the latest version of the GCaMP indicator family (Chen et al., 2013b). These indicators are based on the GFP fluorescent protein and can typically excited with a ~470 nm blue light (940 nm in two-photon mode) and they emit in the ~520 nm regime. The latest version GCaMP6 is thought to provide great sensitivity, large calcium transient amplitudes, fast rise and decay times. For a single action potential using the fast variant GCaMP6f (Chen et al., 2013b), the detection efficiency is 84%, the amplitude is ~20% $\Delta F/F$, and the time constants are τ_{onset} = 45 ms, τ_{decay} = 142 ms (Chen et al., 2013b). This fast variant (GCaMP6f) was used through the use of a transgenic animal in this thesis (see Methods) and the medium variant (GCaMP6m) was used

via viral vector (see Methods).

The RCaMP1.07 indicator is a red shifted variant calcium indicator using the red fluorescent protein mApple (Ohkura et al., 2012). This indicator is a derivative of the R-GECO red shifter indicators (Zhao et al., 2011). Red indicators were shown to be very useful to image in deeper tissues (Pilz et al., 2016), especially when combined with non-linear microscopy techniques like two-photon microscopy (Helmchen and Denk, 2005).

Finally, the third variant of GECIs are the ratiometric indicators, which include the *Yellow-Cameleon* (YC) family (Nagai et al., 2004). These indicators are different from the previously described GCaMP and RCaMP families as they contain two fluorescent domains (CFP and YFP in the YC family) and can therefore use the principles of *fluorescence resonance energy transfer* (FRET). FRET is an energy transfer phenomenon observed between two light-sensitive molecules or domains when they are close to each other. When the concentration of free calcium in the cell is low, these two fluorescent domains are separated by a distance that is too big to allow FRET. In presence of calcium, the molecule changes its three-dimensional conformation and brings the two fluorescent domain close to each other, therefore allowing the FRET process to take place. The consequences of this is that without calcium binding, when one of the fluorophore is excited with its specific wavelength, mostly that fluorophore will emit light, since the other fluorophore is too far away to benefit from the FRET. However, in presence of calcium, the second fluorophore will also emit more light due to the energy transferred by the closely located first fluorophore. It is possible to record the fluorescence emitted by both fluorophores in separate channels, as the fluorophores have different emission spectra.

By calculating a ratio R of the two fluorescence signals, a more robust measure of the fluorescence can be obtained, since this ratio would be insensitive to the perturbation and artefacts present in both signals. Typically, movement artefacts, which often happen when recording from living animals, affect both channels in a similar way and are therefore at least partially corrected for when using ratiometric indicators. These artefacts would however be present in the GCaMP and RCaMP indicators described before. The recorded fluorescence signal from a ratiometric calcium indicator can also be calibrated in order to be able to measure the intracellular free calcium concentration $[Ca^{2+}]_i$ (Helmchen, 2011).

In this thesis, the *Yellow-Cameleon Nano 140* (YC-Nano140) was used (Horikawa et al., 2010). As all the calcium imaging experiments of this thesis were carried out in living and sometimes even behaving animals, the ratiometric property of YC-Nano140 and therefore its robustness to movement artefacts was a clear advantage to use it instead of the other alternatives.

This section described the properties and uses of calcium indicators in the context of calcium imaging. The next sections will address the microscopy tools to actually excite the calcium indica-

tors, as well as the recording techniques to collected the emitted light from the indicators.

1.2.4 *In Vivo* two-photon calcium imaging

The two-photon absorption phenomenon

Calcium imaging is very often performed in combination with *two-photon laser scanning microscopy* (2PLSM), originally developed by Denk and colleagues (Denk et al. (1990); for reviews, see Helmchen and Waters (2002); Helmchen and Denk (2005); Gobel and Helmchen (2007); Grewe and Helmchen (2009); Peron et al. (2015)). 2PLSM is a microscopy technique based on the two-photon absorption phenomenon (reviewed in the context of neuroscience in Svoboda and Yasuda (2006)). Two-photon absorption refers to the nonlinear process where two low-energy photons cooperate to excite a fluorescent molecule to a higher excitation state. In this process, the absorption depends on the square power of the light intensity. This two-photon absorption phenomenon is used in 2PLSM to record activity from the cortex using calcium indicators, as described below.

There are two main advantages of using two-photon excitation over single photon in the context of calcium imaging. First, the wavelength of the two-photon excitation is longer than with single photon excitation, as the combined energy of the two-photon should correspond to the energy of the single photon excitation. As consequence when recording from the brain, the two-photon excitation will scatter less in the tissue, due to the longer wavelength. Second, in order to have a two-photon excitation, the two photons must arrive nearly at the same time and at the same place (same fluorophore molecule) in a very precise way. The second photon must arrive right after the first photon (on the order of 10^{-15} seconds, which is the lifetime of the virtual state created by the absorption of the first photon). Therefore, only the very specific location where the laser beam is focused will have a high enough probability to have a two-photon excitation. In other words, the fluorescent molecules above and below the focus will not be excited, as the *concentration* of photon will not be sufficient. This leads to the *optical sectioning* of the sample, and therefore removes the need of spatial filtering on the detector side, like the pinholes in confocal microscopy, which is a certain advantage over other microscopy techniques. Indeed, in 2PLSM, any photons emitted from a fluorophore and recorded at a given time are known to come from the location excited at that given time. With these conditions and appropriate optics (described below), it is relatively easy to reach the micrometer spatial resolution and therefore image from single neurons.

The two-photon microscope

To produce an image, the properties of two-photon excitation can be used and therefore it is possible to simply scan a laser beam over the sample. Since only the location where the beam is

focused will two-photon excite the molecules, all the emitted light recorded by the detectors can be collected and read out as the light intensity coming from that specific location. This differs from other microscopy techniques, where pinholes or other strategies must be used to know where the recorded light originally came from.

Several challenges have to be met in the design of a two-photon microscope used for 2PLSM (Helmchen, 2009). First, in order to achieve a high enough photon density at the focus, *ultra fast femtosecond pulsed lasers* should be used. These lasers concentrate photons in time to have a higher probability of two-photon absorption at the focus. In order to have a high concentration, the pulses must be extremely short (on the order of ~100 femtoseconds) but still be spatially close to one another (typical repetition rate of such a laser is ~80 MHz, 12.5 ns between pulses). The scanning of the beam is usually done with 2 galvanometric mirrors, one for each scanning axis (X and Y). The speed at which the scanners can scan a frame determines the sampling rate of the microscope (frame rate). Z-axis focusing (up and down) can be achieved with a piezoelectric element moving the objective along the optical axis. More recently, electrical tunable lenses (ETL) were developed, which can be integrated to the optical path (Grewe et al., 2011). These ETLs remove the need of mechanically moving the objective, therefore allowing Z-axis focusing at very high speeds ($100\,\mu m$ focus shift in less than 15 ms). In addition to the previous components, Pockel cells are used to control the laser beam intensity and a telescope system is used to magnify the beam diameter. To direct the beam, a so-called *4f* (4 focal length) system is often used. This system, composed of two large lenses (the tube and the scan lens) creates a *stable* optical plane that fills the back aperture of the objective, in such a way that the filling of the objective is kept constant and stationary independently of the X or Y scanning and independently of the focusing depth (Z axis). As all collected light is part of the meaningful signal, large numerical aperture objectives are usually preferred to collect the emitted light from the excited fluorophore. The emitted light is then typically detected using photo-multiplier tubes, one per color channel if ratiometric indicators are used. All the major components described here assembled together with some additional helping optical or mechanical elements (dichroic mirrors, shutters, motor stages, etc.), form a two-photon microscope.

Two-photon calcium imaging in the auditory cortex

2PLSM with calcium imaging has been performed in many sensory cortices with various experimental conditions, and among these studies, a number of them were done in the auditory cortex. Some of these key calcium imaging studies from the auditory cortex are briefly summarized here.

Rothschild et al. (2010) and Bandyopadhyay et al. (2010) were the first to use two-photon calcium imaging in the primary auditory cortex of mice. They demonstrated that sound evoked

calcium transients could be recorded from single neurons in the primary auditory cortex, which in itself is already an achievement for that time due to the difficulty of establishing stable imaging conditions in the auditory cortex because of its lateral position (Figure 1.3). Furthermore, they both showed that local populations in the primary auditory cortex were heterogeneous regarding the frequency tuning, even though they are embedded in the large-scale tonotopic organization.

Grienberger et al. (2012) recorded population calcium signals in the auditory cortex of mice using an optical fiber. Because they used a fiber, they did not have cellular resolution but rather recorded the combined activity from several neurons. They could however characterize the spontaneous and sound-evoked calcium signals of these populations of neurons.

Chen et al. (2011) used a high-speed two-photon microscopy device to do high-resolution two-photon imaging in single dendritic spines. They recorded calcium signals evoked by sound stimulation in cortical neurons of the auditory cortex and showed the high heterogeneity of NMDA-receptor-dependent single-spine synaptic inputs that arrive to the same dendrite.

Letzkus et al. (2011) used fear conditioning and calcium imaging to test the involvement of disinhibitory circuits in the auditory cortex. They found that disinhibition is driven by foot-shock-mediated cholinergic activation of layer 1 interneurons, which in turn generates inhibition of layer 2/3 parvalbumin-positive interneurons. They demonstrated that stimulus convergence in the auditory cortex is necessary for the associative fear learning of complex sounds, which suggests that layer-1-mediated disinhibition is an important mechanism for learning and information processing in the context of fear learning.

Bathellier et al. (2012) used *in vivo* two-photon calcium imaging in the auditory cortex of mice to study category discrimination. They showed that local network activity evoked by sounds is constrained to few response modes, corresponding to the sound categories the neurons responded to. They tested how transitions between response modes happen by presenting mixed categories of sounds. They saw abrupt changes when the networks switched from on category to the next, suggesting attractor-like discrete dynamics in the context of sound categorization. Overall, they showed that nonlinear dynamics can spontaneously generate sound categories in the auditory cortex.

Winkowski and Kanold (2013) compared the tonotopic homogeneity of two different layers of the auditory cortex. They used in vivo two-photon calcium imaging and showed that the spatial organization of frequency tuning in layer 3b/4 was more homogeneous than in layer 2/3, concluding that a transformation of sensory representations occurs between layers within the auditory cortex.

The study from Graber et al. (2013) is different as it was not done in mice or rodents but rather in the zebra finch. Using two-photon calcium imaging, they characterized the spatio-temporal structure of the spontaneous activity and of auditory evoked responses in the songbird's motor

area HVC. They found strong correlations between the calcium signal fluctuations in nearby cells of a given type.

Issa et al. (2014) did an extensive study of the tonotopic organization of the mouse auditory cortex. They were trying to address the question of the weakly organized tonotopic arrangement at the level of individual neurons, highlighted by Rothschild et al. (2010) and Bandyopadhyay et al. (2010). They made good use of GCaMP3 transgenic animals by using imaging techniques on multiple scales, including wide-field calcium imaging and two-photon single cell calcium imaging.

It is interesting to notice that only few of these studies used transgenic animals that genetically encoded the calcium indicator. The usage of transgenic animals as *vectors* for calcium indicators was only emerging recently. Combining behavior training in these animals and calcium imaging is even more recent and only done by a handful of groups around the world. Another great property of calcium imaging can be added to this kit: the ability to optically identify neuronal types. Indeed, transgenic animals can express fluorescent protein reporters (GFP, RFP, tdTomato, etc.) under the control of specific genetic markers associated with well-defined cell types, as for example the somatostatin, parvalbumin or vasointestinal peptide interneuron types. These fluorescent reporters can also be introduced via viral vectors. In both cases, by using two-photon imaging, it is possible to visually identify the neurons that are labelled by these fluorescent reporters, which therefore provides cell type information.

1.2.5 Wide-field calcium imaging

Wide-field calcium imaging is another technique to record calcium activity from the cortex. Unlike two-photon laser scanning microscopy (2PLSM), wide-field imaging uses single photon excitation and collects the emission light using a high speed camera. All the calcium imaging principles described above are used in the same way, but another major differences compared to 2PLSM is the spatial scale and resolution that can be achieved with wide-field. As mentioned above 2PLSM is working on the neuronal scale and can record from tens, hundreds or maybe even thousands of neurons with single cell resolution. Wide-field imaging is more commonly used to record the activity of cortical regions without single cell resolution (Berger et al., 2007).

Wide-field imaging is particularly well suited to work with transgenic animals expressing a genetically encoded calcium indicator in a layer-specific manner (Madisen et al., 2015). Indeed, wide-field imaging can usually image a large surface of the brain (typically in the order of 3-5 mm) and therefore benefit from the extended, relatively homogeneous labelling provided by the genetic expression of the indicator. Using wide-field imaging, the cortical dynamics and cortical region activity patterns can be recorded, and with a setup and experimental conditions that are arguably easier and more flexible than 2PLSM. Wide-field calcium imaging has been used in the auditory

cortex of mice before (Issa et al., 2014), showing frequency mapping for the entire auditory cortex in a GCaMP3 transgenic animal. They also used the advantage of being able to switch to two-photon microscopy, in order to get a closer look at specific regions identified using the wide-field. This combined two-photon and wide-field calcium imaging is a strong approach to bridge the gap of the different scales with which the brain is studied.

1.2.6 The data analysis challenge

A large part of the work of a scientist, besides observing, measuring and acquiring data, is to extract, analyse, interpret and make sense of the gathered observations. This step of analysis and interpretation is crucial in science, as it gives all the value to otherwise useless and meaningless observations. In today's neuroscience (and in many other fields of science), observations are composed of huge amounts of often very complex data that is produced at high throughput. Thus when studying the brain, the interpretation and analysis of the data is very often the bottleneck, compared to the actual technical challenges of the data collection. The big challenge remains to make sense of all the measurements we have from the brain, because the brain is utmost complex and the interpretations never straightforward.

In the recent years, cluster-based tools have been developed to deal with the increase of data size and complexity (Freeman et al., 2014). The `Thunder` framework was created running on the open-source Apache `Spark` platform for large-scale distributed computing. Together with efficient data storage solutions like the HDF5 file format (The HDF Group, 2016), these advances promises to remove the current data processing and handling bottleneck in neuroscience.

1.3 Physiology of the auditory cortex

1.3.1 The oddball paradigm and stimulus-specific adaptation

The brain is known to be able to detect surprises and mismatches in the environment via the sensory inputs it is provided. Such ability involves a system that can emphasize external stimulus that are different than the ones expected. A very common way to study this surprise or rarity detection property of the brain is by using the *oddball paradigm*. The oddball paradigm is a sensory stimulation paradigm that consists in presenting a sequence of many identical stimuli, called *standards* and then present a new, different stimulus, the *oddball* (also called *deviant*). The response of the standard stimuli and the oddball stimuli are then compared to show a rarity-related change in the response (Squires et al., 1975).

The oddball paradigm has been used in electrophysiological recordings in the human (Näätänen et al., 1978), showing clear differences for a same stimulus depending on the condition it was presented, oddball or standard. This event-related potential recorded with electroencephalograms in humans is referred to as the *mismatch negativity*, due to the negative extra component appearing on the recording for the oddball stimulus.

Recordings from single neurons have also shown similar differences, with the oddball response being larger than the response of the standard stimulus (Ulanovsky et al., 2003). In this single cell context, this phenomenon is referred to as the *stimulus-specific adaptation*, as neurons adapt their response to the standard stimulus and then produce a larger response to the new stimulus. The link between mismatch negativity and stimulus specific adaptation is not fully resolved yet, as the two events have different time windows.

A recent study by Chen et al. (2015) examined the stimulus specific adaptation phenomenon in the auditory cortex of anaesthetized mice, measuring the response of different neuronal types in layer 2/3. They identified two temporally distinct components of the oddball response and examined the NMDA-dependence of the oddball response in 2 interneuron types (somatostatin, parvalbumin) and in the excitatory neurons.

SSA has been mostly studied in the sub-threshold domain, mainly using electrophysiological recordings (Chen et al., 2015; Ulanovsky et al., 2003). As supra-threshold activity involvement in SSA has only been addressed sparsely, exploratory experiments were performed in this thesis using cell-attached electrophysiology and two-photon calcium imaging to address this. It should be however noted that this was not the main topic of this thesis.

1.3.2 Tuning of neurons in the auditory cortex

Neurons in the auditory cortex are activated to represent auditory information. In the case where an external sound stimulus is perceived, neurons in the auditory cortex will show an increased activity, a response to this stimulation. The amplitude of the response of each neuron will depend on many parameters. Many neurons have a preference (or a lack of preference) for certain properties of the perceived sound, depending on their wiring within the network of the auditory cortex. The preference to these properties is referred to as *tuning* (or lack of tuning in the case where no preference is seen). Neurons can be tuned to any physical property of the sound, but tuning is usually the strongest or most well defined for the sound's frequency, and to a lesser extent to its loudness.

Tuning can be measured using the different methods presented before. Tuning of single neurons can be measured individually using electrophysiology (Froemke and Martins, 2011), or for many neurons at the same time using two photon calcium imaging (Winkowski and Kanold, 2013). The combined (averaged) tuning of many neurons in a sub-region of the cortex can be measured with electrophysiology via multi-unit spiking signal Guo et al. (2012), with wide-field calcium imaging (Issa et al., 2014) or with intrinsic signal optical imaging (Kalatsky et al., 2005).

Frequency tuning is usually defined for a single neuron with two metrics:

1. The *characteristic frequency* (CF): the frequency at which the sound intensity threshold for a response is lowest.
2. The *best frequency* (BF): the frequency giving the largest response at a given sound intensity.

These two metrics are often very similar for a neuron (Brown et al., 2004). A typical way of representing the tuning of a neuron is to show a tonal receptive field heat map, which shows the response of a neuron for a combination of different intensities and frequencies (Liang et al., 2014; Guo et al., 2012). The typical pattern obtained from such experiments in pyramidal neurons in layer 2/3 is a V-shaped pattern, where neurons have generally a single characteristic frequency that is activated even at low sound intensity, and then as the sound gets louder, the number of frequencies that evoke a response increases, starting with the frequencies close the characteristic frequency. Such tuning curves can also be obtained from the combined activity of multiple neurons (multi-unit activity, Figure 1.5). A different approach to assess the frequency tuning of neurons is to measure the *spectrotemporal receptive fields* (STRF) of a single neuron, or of a group of neurons. STRFs describe the response of a single or of multiple neurons to different frequencies for a short time window after the sound stimulus.

As said, neurons in the auditory cortex encode auditory information, and this encoding gives

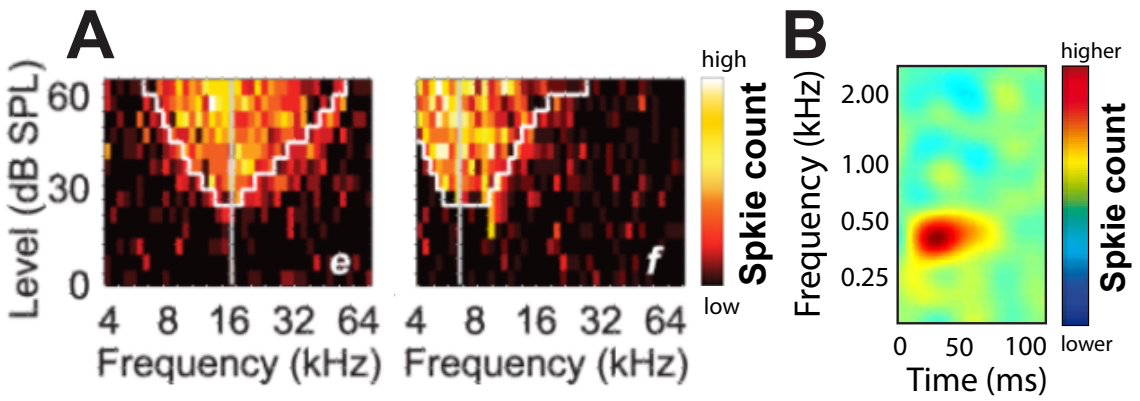

Figure 1.5: Intensity and frequency tuning curve: (A)*: Typical shape of a frequency-intensity tuning curve mapping for 2 example recording sites (multi-unit activity). The colors of the heat map represent spike counts, the lighter the color, the more spikes were recorded. Abbreviations:* SPL *sound pressure level.* Modified from Guo et al. (2012). ***(B)****: example spectrotemporal receptive fields (STRF) recorded from single units in the auditory cortex of ferrets. The X-axis represents time after the stimulus onset. The colors of the heat map represent spike counts relative to baseline.* Modified from Elhilali et al. (2007).

rise to preferences for each neuron in the physical properties of the sound, or to a lack of preference in case of broadly tuned neurons. A relevant question regarding this encoding is how stably the same information is encoded in a neuron. When recording the local field potential in the auditory cortex, which is a bulk signal mixing the responses of a few neurons around the recording electrode, it has been shown that the frequency tuning property of a region in the auditory cortex was shown to be relatively stable across days during several weeks in guinea pigs (Galván et al., 2001), with only small daily changes (~0.2 octaves). Stability of tuning was evaluated in ferrets by measuring STRFs from single unit and multi-unit responses (Elhilali et al., 2007). They found that ~73% of AI neurons exhibited stable receptive fields over periods of 0.5 to 2 hours. Additionally, they showed that the amount of changes during a passive state was much smaller than the changes induced by an auditory task. However, tuning stability was not yet explored on a single neuron level in mice across days.

1.3.3 Topographic maps in the auditory cortex

The previously described tuning properties of neurons have been examined in detail relative to their spatial distribution in the cortex. It has been shown that the tuning of neurons for these properties (frequency, intensity, etc.) is not organized in a random fashion but rather in a topographical manner. The topographic map of the auditory cortex based on the frequency tuning of neurons is the most extensively studied. It is referred to as the *cochleotopic* map or most commonly the *tonotopic* map. This *tonotopic* organization of the neuron arises from the ordered projection received by the auditory cortex from the thalamus, which itself receives it in an ordered manner throughout

all stages of the auditory system back to the cochlea. Tonotopic organisation exists through the entire auditory system, although with different clarity or intensity.

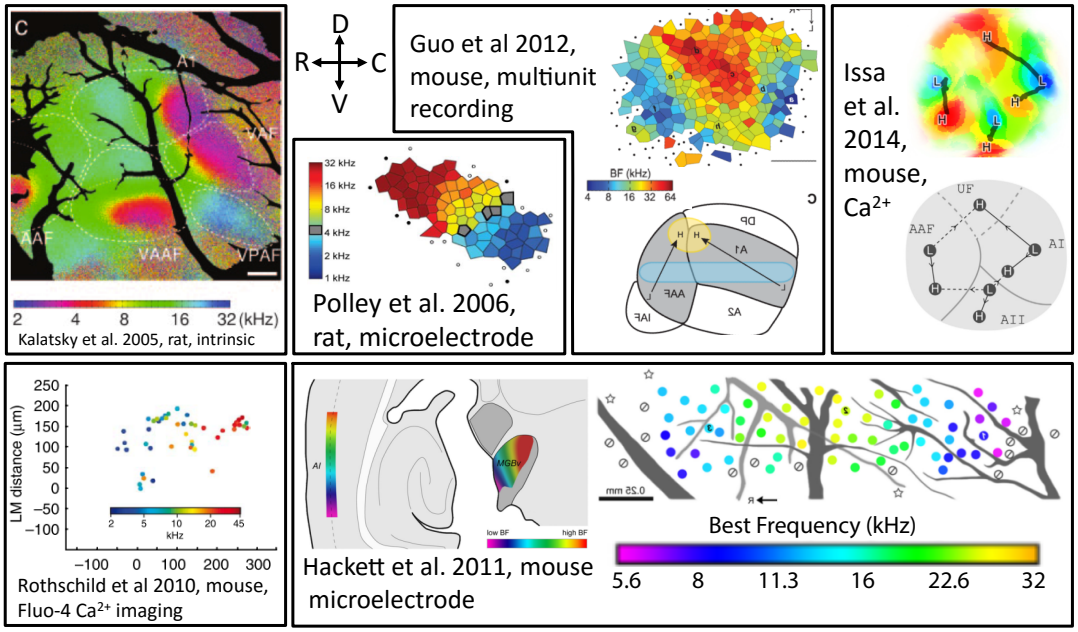

Figure 1.6: Tonotopy in the literature: Tonotopy in the literature (1): *Overview of the tonotopic map representations that can be found in the recent literature. Maps are oriented, flipped or rotated to be in accordance with the orientation shown by the arrows, to ease comparison. The species and the technique of acquisition are annotated. Abbreviations:* R *rostral;* C *caudal;* D *dorsal;* V *ventral.*

Tonotopic maps were described and measured in a quite extensive way in rodents and non-rodents in the cortex, and in the sub-cortical stages of the auditory system (Stiebler et al., 1997; Polley, 2006; Guo et al., 2012). The tonotopic map is usually described as having multiple *tonotopic axes*. Tonotopic axes are the axes going from the low-frequency tuned regions to the high-frequency tuned regions of the tonotopic map. In the auditory cortex of mice, one axis can be defined per division or sub-region for AI, AAF and AII (Stiebler et al., 1997; Guo et al., 2012; Issa et al., 2014). These tonotopic axes are a functional way of delimiting auditory cortical regions. This method can be complemented with tracing experiments from and to the auditory cortex. Projections from the thalamus to the auditory cortex are arriving mainly in the A1 and AAF subregions (Watson et al., 2012), therefore those two sub-regions can usually be well defined using tracing experiments. However, some inconsistencies still exist in the literature regarding the precise outlining from the other auditory cortical regions (Guo et al. (2012); Issa et al. (2014), Figure 1.6, Figure 1.7).

As mentioned, other topographic maps also exist based on other physical properties of the sound, for example sound loudness, or based on features of the processing of the sound, like the response latency maps. All these topographic maps can be seen as overlapping each other,

creating a multidimensional stimulus feature space for each region of the auditory cortex that will define the response of a particular region to a particular stimulus.

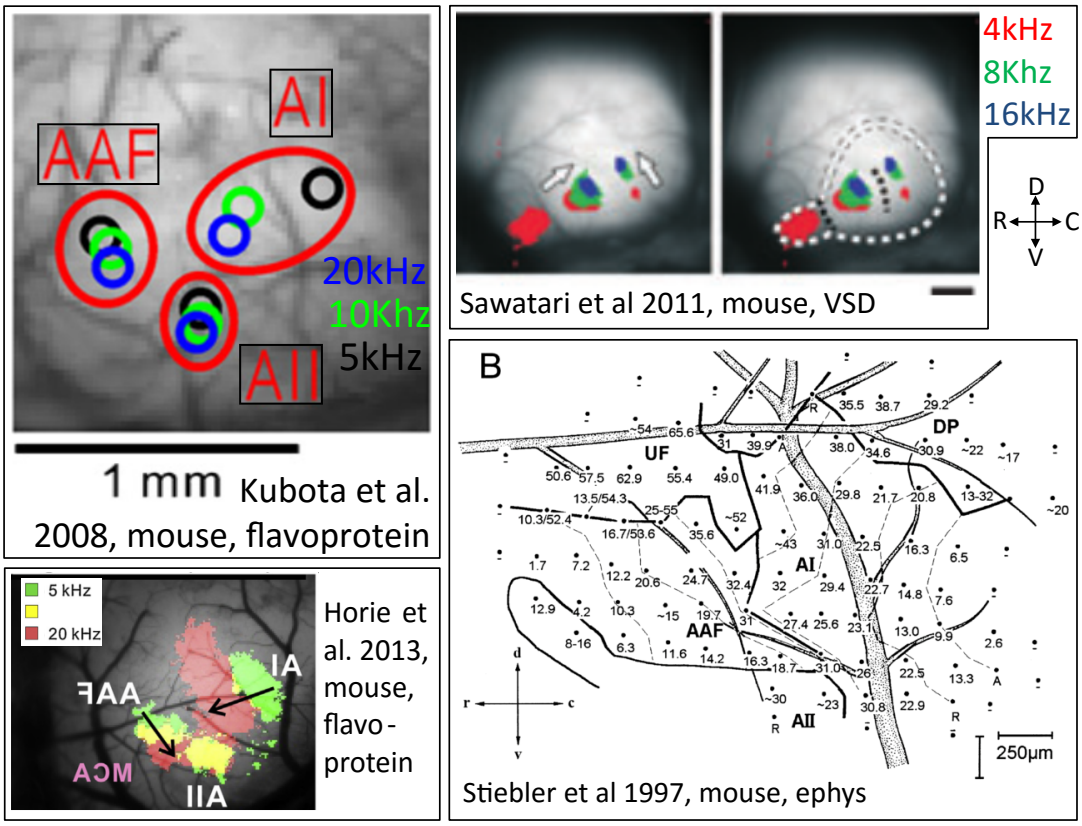

***Figure 1.7: Tonotopy in the literature (2)**: **Tonotopy in the literature (2):** Overview of the tonotopic map representations that can be found in the (less recent) literature. Maps are oriented, flipped or rotated to be in accordance with the orientation shown by the arrows, to ease comparison. The species and the technique of acquisition are annotated. Abbreviations:* R *rostral;* C *caudal;* D *dorsal;* V *ventral;* VSD *voltage sensitive dye.*

1.4 Plasticity of the auditory cortex

One of the most exceptional property of the brain is its capacity to change and adapt itself. The ability to change its output and shape its responses to different stimuli is extremely important, as a hard-wired system would only be able to process a limited, pre-defined number of stimuli. Being able to change allows the brain for an infinite number of responses, as they can always adapt to new conditions. This ability of the brain and its neuronal circuits to change and alter themselves is referred to as *plasticity*. Any learning process involves some form of plasticity in the brain. This section will address the matter of plasticity at the neuronal and synaptic level, and then describe examples of plasticity manipulations in the auditory cortex.

1.4.1 Different types of plasticity

Categories of plasticity can be defined using several criteria: the time scale at which the plasticity happens (short-term versus long-term plasticity), the developmental time point when plasticity is occurring (during development of an individual versus during adulthood), the scale at which plasticity occurs (from the single synapse, the single neuron plasticity up to the entire cortical remapping) and finally the physiological condition in which plasticity occurs (normal healthy, physiological conditions versus disease-related recovery and repair mechanisms). This thesis mainly focused on the long-term adulthood plasticity in physiological conditions.

Plasticity during development and critical periods

It is important to realize that even though the brain keeps a fantastic capacity to change and adapt itself during the adulthood, the most spectacular changes and evolution of the brain happen during the development of an individual. Indeed, the brain has to go through a number of steps to become the complex, precisely wired system that it needs to be to be functional. Neurons have to be created in the right number at the right time, they need to migrate to appropriate location with very precise timing and finally they need to connect to each other in a very specific fashion, sometimes across distances of several orders of magnitude larger than the size of their own cell body.

Mechanisms exist to keep a great amount of flexibility in the wiring and functions of the brain, until the brain is fully formed. Specific time windows were certain sensory modalities can undergo long lasting changes exist. The time windows are referred to as *critical periods*. The external stimuli perceived during these critical periods typically influence the brain much more than if the very same stimuli would happen either before or after the critical period. Critical periods are often

paired with large changes in the morphology of the animal, often related with the sensory modality (eye opening, growing of the whiskers, etc.). These changes in morphology of the animal are usually also paired with changes in the behavior of the animal.

Such a critical period has also been shown to exist for the auditory system of mice. The time period were external stimulus is of greater influence was shown to start around 12 days after birth and last until around 15 days post-birth (Barkat et al., 2011). During this time, exposure to repetitive stimuli or deprivation of certain sound feature can perturb the auditory system and the auditory cortex in a permanent way that will not recover after the end of the critical period. Moreover, the same type of exposure in the adulthood does not lead to the same extended long-lasting changes that it produces during development.

Synaptic transmission and synaptic plasticity

The second form of major plasticity are the less dramatic changes that happen during the adulthood of an animal. These changes mostly rely on synaptic weight changes of the already existing circuits, called *synaptic plasticity*. Plasticity mechanisms and synaptic plasticity are very intensively researched topics and therefore their literature is quite large. The following paragraphs are a summary of this literature, mostly inspired from the reviews of Friauf et al. (2015); Castillo (2012); Sheng and Kim (2002) and Lynch (2004). Many of the findings described here were extensively studied in brain slice preparations, which is an extremely useful and easy to access neuronal preparation for studying interactions and information exchange between pairs of neurons.

In the communication process between two neurons through synaptic transmission via chemical synapses, there is a high degree of change possible (i.e. plasticity). Therefore, synaptic transmission of information between two neurons can be qualified as very dynamic. Synaptic transmission is usually described by referring to the neuron that *sends* the information as the pre-synaptic neuron, and the neuron that *receives* the information as the post-synaptic neuron. The strength of the post-synaptic response evoked by the activation of the pre-synaptic neuron may change dramatically in response to successively triggered synaptic activations. In other words, depending on the sequence, frequency and context in which the pre-synaptic neurons activates the post-synaptic neuron, the strength of this activation can vary a lot. This strength can be increased, for example in case of facilitation or potentiation, or it can be decreased, in case of depression or attenuation. This modification of the strength of a synapse is mediated by different molecular mechanisms, which importantly act either on shorter (hundreds milliseconds to minutes), or on longer time-scales (minutes to hours or even more).

The short-term changes, or short-term plasticity, is typically a change of the synaptic strength that is quickly reversible and that helps to fine-tune the information transfer at the circuit level.

Short-term plasticity is typically involved in mechanisms of neuronal habituation or sensitization, due to this short-lived and reversible nature. The long-term changes, or long-term plasticity, are much longer-lived, permanent changes in the synaptic transmission that can even last for years. Therefore, the mechanisms involved in the long-term plasticity are typically associated with learning and memory formation processes.

In the modification of a synapse strength, it is mostly the release of the neurotransmitter vesicles that is modified. Neurotransmitters are the signalling molecules that are stored in vesicles of the pre-synaptic neuron and can bind to the receptors located on the post-synaptic neuron to trigger its activation. The neurotransmitters in the vesicles of the pre-synaptic neuron are released due the depolarization of its membrane, opening voltage-gated calcium channels that release calcium ions into the pre-synaptic neuron. This calcium is necessary for the fusion of the vesicles to the outer membrane, which will release the neurotransmitters into the synaptic cleft. The neurotransmitter will then bind to the post-synaptic neuron's receptors, triggering the opening of ion-channels that will change the membrane potential (post-synaptic potentials). Depending on the neurotransmitter and its receptor, the membrane potential will be changed, and the neuron will either be depolarized (for example in case of glutamate release by an excitatory pre-synaptic neuron) or hyperpolarized (for example in case of GABA release by inhibitory pre-synaptic neuron). The binding of the neurotransmitters can also trigger longer lasting changes by the activation of molecular signalling cascades involved in plasticity mechanisms described hereafter.

Short-term plasticity

When a pre-synaptic neuron is presented with repetitive activation in short succession, it can lead to an increase or a decrease in the efficacy of the synaptic transmission for a short period of time (Friauf et al., 2015). The first mechanism of short-term plasticity is the decrease in strength due to an ineffective clearance of the neurotransmitters from the synaptic cleft, which by accumulation prevent the further binding to the post-synaptic receptors, which will then remain bound to neurotransmitters but in a closes, non-depolarizing state.

A similar short-term depression can also occur on the pre-synaptic neuron side, if the pool of neurotransmitter vesicles closer to the membrane and that can quickly be released in the synaptic cleft is depleted faster than it is replenished. Indeed, the number of vesicle available for immediate release in the pre-synaptic neuron, called the readily releasable pool vesicles, is not infinite, and needs to be replenished from the recycling and the reserve pool (for review, see Denker and Rizzoli (2010)). Therefore, if a pre-synaptic neuron is being activated too rapidly, no further neurotransmitters will be released when the readily releasable pool of vesicles is depleted.

Regarding the strengthening of the synaptic transmission in short time scale, a well-studied

mechanism is the paired-pulse facilitation, in which the second pulse of two successive pulses (happening within hundreds of milliseconds) creates a larger evoked post-synaptic potential than the first one. This facilitation is often explained by an accumulation of residual calcium in the pre-synaptic terminal from the first pulse, which facilitates the binding of vesicles in the second pulse. This accumulation has a particularly strong effect given the non-linear relationship between the pre-synaptic intracellular calcium concentration and the neurotransmitter release in the synaptic cleft. Therefore, accumulation of calcium increases the release probability of the neurotransmitters. This facilitation mechanism interacts in neurons with the depression mechanisms described in the previous paragraph, and the recovery time from each of these processes in different neuron types is critical in defining the processing speed of neuronal circuits. The different mechanisms and variables related to the synaptic transmission and synaptic plasticity can be put in relation to define the amplitude of the evoked post-synaptic current A_{PSC} using the following relation:

$$A_{PSC} = n * P_r * q$$

where n is the number of readily releasable vesicles (rapid pool), P_r the release probability, affected notably by the pre-synaptic calcium concentration, and q, the quantal size, which is defined as the amplitude of the post-synaptic response to the fusion of a single synaptic vesicle. Given this definition, the quantal size is therefore dependent on the number of neurotransmitter molecules within a single vesicle, which is also a mechanism through which different levels of post-synaptic activation can be achieved, by either having more or less neurotransmitter molecules within each released vesicle.

Long-term plasticity

The transmission efficacy changes described above are usually described to last for several hundreds of milliseconds or in certain cases up to a few seconds. However, longer lasting changes have also been reported, which involve different interactions between molecules and ions at the synapses (Castillo, 2012; Sheng and Kim, 2002). A major player in long term plasticity mechanisms is the NMDAR (N-methyl-D-aspartate receptor) protein. In the paragraphs hereafter, a distinction will be made between forms of long-terms plasticity that are involving NMDAR (NMDAR-dependent plasticity) and some that do not (NMDAR-independent plasticity). Furthermore, the outcome of the plasticity regarding the synapse strength will also be categorized into either long-term potentiation (LTP), which increases the synapse strength and long-term depression (LTD), which decreases the synapse strength. Finally, plasticity mechanisms are also categorized depending on whether they occur on the pre- or on the post-synaptic neuron's side.

The most classical and well studied form of pre-synaptic LTP is found in the hippocampus at

the so-called mossy fiber synapses between the granule cells of the dentate gyrus and the CA3 pyramidal neurons (Castillo, 2012). When the mossy fibers are activated at high frequency (100 Hz), a long-term increase in the vesicle release probability is happening in the pre-synaptic neuron, leading to a long-lasting increase in the glutamate release, induced by an activity-dependent increase in calcium concentration within the mossy fiber terminals. The mechanisms underlying the pre-synaptic LTP at the mossy fibers have been shown to be dependent on the R-type voltage gated calcium channels (VGCC) located at the pre-synaptic terminal, which trigger the calcium / calmodulin-dependent adenylyl cyclase, which in turn leads to enhanced pre-synaptic cAMP levels and activation of another messenger (PKA) that triggers the change in vesicle release. It is interesting to note here that in the pre-synaptic forms of long term plasticity, a retrograde messenger can also travel back from the post-synaptic neuron to the pre-synaptic neuron, in order to trigger the signalling cascade that leads to the change in vesicle release. The mossy fiber terminals have also been shown to express pre-synaptic LTD, in the form of a NMDAR-independent long-term reduction in glutamate release, as well as other forms of pre-synaptic LTP (for review, see Castillo (2012)).

Another major type of long-term plasticity is the post-synaptic NMDAR-dependent plasticity, which involves two main proteins. The first protein is the NMDAR, a glutamate receptor that is also a calcium-permeable transmembrane ion channel and that opens in response to glutamate binding only when the post-synaptic neuron is depolarized. The second important protein is the AMPAR (α-amino-3-hydroxy-5-methyl-4-isoxazolepropionic acid receptor), which is a cation channel that opens in response to glutamate binding and that is thought to mediate most of the rapid membrane potential change in the post-synaptic neurons. Finally, the neurotransmitter glutamate is also a key molecule, as it is the major excitatory neurotransmitter and also binds to the two previous glutamate receptors. Glutamate is triggering a signal across the post-synaptic membrane via different classes of glutamate receptors, which can themselves trigger electrical and biochemical events in the post-synaptic neuron, potentially leading to long-term plasticity (Sheng and Kim, 2002).

In the most well described situation, long-term plasticity happens as follows. Glutamate, released in the synaptic cleft by the depolarized pre-synaptic neuron, binds to the post-synaptic AMPA receptors. When at least two glutamate molecules are binding to an AMPA receptor, this will open it and sodium ions will flow into the post-synaptic neuron, resulting in a depolarization often referred to as an evoked post-synaptic potential (EPSP). At the same time, the NMDA receptors also bind glutamate but they do not open directly because the pore in their channel is blocked by magnesium ions. But as the AMPA receptors open and introduce sodium into the post-synaptic neuron, the NMDARs can open since a depolarization of the membrane causes the magnesium ion to move out into the extracellular space. NMDA receptors are therefore acting as

coincidence detectors for both an incoming glutamate release and an existing depolarization in the post-synaptic neuron. Since NMDARs are permeable to both sodium and calcium, calcium enters the post-synaptic neuron and triggers a cascade of signalling molecules (involving CaMKII and PKAII) that ultimately leads to the up-regulation of AMPA receptors to the membrane. This increase in glutamate receptor at the post-synaptic neuron creates long-lasting increase in the amplitude of the EPSP, as more depolarizing channels are present at the synaptic cleft. An additional mechanism is strengthening this LTP, as the entry of calcium can trigger kinases that will phosphorilate the post-synaptic receptors (like the AMPA receptors), which improves their conductance for cations, further depolarizing the post-synaptic neuron (larger EPSPs). Inversely, if phosphorylases are activated rather than kinases, a weakening of the EPSP can be seen, which is then leading to LTD, reducing the strength of the synapse.

In addition to the functional changes described above, structural changes can also occur as neurons are able to change the size and shape of their synaptic bouton, by modulating the cytoskeloton of their dendritic and axonal processes. Therefore, the size of a synapse can be increased in order to increase the available surface for neurotransmitter release and capture. An even more dramatic change can occur in the structure as new synapses can be formed or discarded depending on the activity levels occurring in them. These processes are also closely tied to the NMDA receptor dependent plasticity signalling cascades (Sheng and Kim, 2002).

A remarkable finding is that depending on the pattern of activation of the NMDA receptors, the synaptic transmission can be either reinforced or weakened, leading to either LTP or LTD. The easiest explanation for this is that LTP and its kinase mechanisms only occurs in conditions when very high level of calcium can be found in the post-synaptic neuron, whereas if only moderate levels of calcium are present, it is rather the LTD mechanisms that take place. This explanation does however not account for the precise temporal aspect of plasticity, as it has been shown that the timing of pre- and post-synaptic activation is very important, as the change by just tens of milliseconds in the order of activation can reverse the direction of the synaptic strength modification from LTP to LTD. Therefore it is probably the precise spatio-temporal pattern of post-synaptic calcium concentration that determines which signaling pathway is activated and therefore whether LTP or LTD will be occurring in a given synapse.

1.4.2 Direct manipulations of plasticity

Two main approaches can be used to induce plasticity in an adult auditory cortex: directly manipulate the auditory cortex with electrophysiological or optogenetical tools or use a less invasive approach that does not bypass the auditory sensory organs and the auditory system. Many of the findings described below, using both of these approaches, have been summarized in a remarkable

review by Weinberger (2003).

The first approach involves most of the time a rather invasive manipulation of the studied system, by implanting stimulation electrodes in the tested system. But even though plasticity can be triggered through less invasive ways, like the behavior training paradigms describe later, direct stimulation of particular nuclei or lesions of certain specific regions can tell a lot about the involvement of the studied nuclei and regions in the plasticity process and in the mechanism through which the auditory cortex is modified.

Several methods exist to quantify plasticity and most of them are based on the before and after manipulation comparison. Typically, a quantification of certain properties (responsiveness, frequency tuning, onset latency, etc.) of a single neuron, a group of neuron or the entire auditory cortex is measured, and then measured again after manipulation. For example, single neuron frequency tuning curves, local field potential frequency tuning or even entire tonotopic maps can be compared for plasticity-related changes. Most of the studies mentioned below use such approaches.

Direct manipulation relies on the fact that the inputs to the auditory cortex do not only contain focused projecting sources like the thalamus or the callosal projections, but also some more widespread neuromodulatory projections. A major neuromodulator that has been found to be involved in many plasticity mechanisms is the acetylcholine, from the cholinergic projecting neurons. Cholinergic inputs to the auditory cortex arise from the nucleus basalis (NB). Acetylcholine has been shown to be of great influence in the plasticity experiments performed on various levels. It is however not the only neuromodulator that was shown to play a role in plasticity mechanisms. Norepinephrine, dopamine and serotonin have all been shown to be implicated in some aspect of the plasticity of auditory cortex. However the precise role of each of these modulatory input is not yet resolved.

Classical experiments by Weinberger, Kilgard, Merzenich and others over the last two decades highlighted the influence of NB stimulation when paired with a pure tone frequency (Kilgard and Merzenich, 1998; Weinberger, 2003, 2004). Typically, a single pure tone frequency was presented many times in short temporal conjunction with a nucleus basalis stimulation. This lead to the shift in the preferred frequency of neurons towards the frequency paired with the NB stimulation. Furthermore, lesions or pharmacological inhibition of the NB leads to deficit in memory related tasks and decreases learning performances (Conner et al., 2003; Kilgard, 2003; Conner et al., 2005).

1.4.3 Behaviorally triggered plasticity

The second approach regroups all the manipulations of the auditory system without surgical or electrophysiological intervention in the neural network. This involves training paradigms and conditioning experiments that both rely on the "natural" or physiological functioning of the auditory cortex. These two sub-groups of behaviorally triggering plasticity differ mainly in the active involvement requested by the animal. Conditioning experiments often only expose the animal to certain types of sound stimulation without the animal needing to react to it. Training experiments however involve the animal to greater attention levels as it is required to report or respond in some fashion.

Conditioning experiments, as the training experiments, come in two flavors: the positive and negative reinforcement of a certain stimulus. Negative reinforcement include for example fear conditioning experiments where the animals are exposed to an aversive stimulus, like a foot shock, which is paired with a specific stimulus that will be associated with it. Typically, a pure tone of a certain frequency is played and is predictive to the foot shock. Animals passively learn to distinguish this specific frequency from others that are played without relation to the foot shock. Positively reinforcement conditioning paradigms are very similar except that the association is made between a positive event, like a drug or a sugar pellet, and the paired sound.

Fear conditioning experiments show that specifically the frequency paired with the foot shock evokes an increased response in the auditory cortex but not the other frequencies (Weinberger, 1995). Typically, the response for the frequencies surrounding the paired frequency are decreased. In similar experiments, the preferred frequency of neurons tends to shift towards the paired frequency, changing the tuning curve of the said neuron. This shift is more pronounced and more likely to happen if the paired frequency is not too far away from the original preferred frequency (Weinberger, 2003).

Training experiments are the most widely used way of triggering plasticity of the adult auditory cortex in the current research (Polley, 2006; Reed et al., 2011; Letzkus et al., 2011; Takahashi et al., 2011; Znamenskiy and Zador, 2013; Xiong et al., 2015). They are most likely favored because of their very physiological aspect, as they deal with living intact animals performing in tasks that are trying to be as close as possible to the natural functioning of the animal. The list of different tasks available to teach animals and trigger plasticity is quite extensive. Among others, detection tasks, discrimination tasks, mazes, working memory tasks and mismatch detection tasks are the most commonly used.

Detection tasks are similar to conditioning experiments, except that the animal has to actively report the decision of whether or not he perceived the stimulus. Typically, a sound is presented to the animal and it should either actively avoid an aversive stimulus, for example by moving away, or

it should actively report its decision by licking a water reward port, press a lever or move to collect a reward. Fear conditioning tasks can also be related to some extent to this category if the animal can react to the aversive stimulus and try to avoid it.

Discrimination tasks are a more complex version of detection tasks as the animal is often not only presented with a single sound that it should detect, but it is also has to avoid reporting for some other sounds, referred to as *distractors*. Typical setups consist in a single *target* sound with a defined frequency, and which the animal should report as being relevant. This target sound is then accompanied by one or more distractor frequencies, which the animal should not report as relevant. This type of tasks can come in many variants with different rewards (water, sugary water, food pellets, soya milk or even drug administration), and different reporting mechanisms (licking ports, nose poke, level press, etc.).

The most typical form of discrimination task is the *go / no-go task*. In this variant, the animal is requested to act or report the go sound but ignore or not report the no-go sound or the no-go sounds. This way of using the discrimination task is a bit similar to the detection task, as the animal has basically only to detect the go frequency among many others. This version of the discrimination task is the one that was used in this thesis.

A slightly more sophisticated variant of this is the *two alternative forced choice task* (2AFC). In this paradigm, the animal is presented with two reporting options, typically two licking spouts, and has to report both sounds that it is presented with. Each sound is associated with one of the reporting option, for example sound A requires the animal to lick to the left, while sound B is rewarded when licking to the right.

Several auditory discrimination studies have also highlighted the interactions between auditory cortex and striatum (Znamenskiy and Zador, 2013; Xiong et al., 2015). These studies show that auditory cortex neurons projecting to the striatum are directly involved in the decision making process, as manipulating the activity of this corticostriatal population can bias the decision of the animal. This finding suggests that corticostriatal synapses made by neurons in the auditory cortex that are tuned to different features of the sound, like high or low frequency, are selectively potentiated to enable the learned transformation of sound into action.

Limits of the adult learning

Auditory discrimination task are as shown above widely used and a very useful way of triggering plasticity. Some limits to the adult learning in mice exist. Especially in the *go / no-go* paradigm, the effect of attention is critical. Indeed, in this task, the difference between the refraining decision of not reporting a sound as a *go* sound, and a lack of attention or engagement in the task cannot be told apart. The 2AFC task solves this problem by requiring a report on every sound.

Hearing loss is also an issue in adult mice. With ageing, some mouse strain have a dramatical hearing loss in the high frequency range (Trujillo and Razak, 2013). Therefore, prolonged learning paradigms have to be avoided in these mouse strains, as they might perturb the learning towards the end of the paradigm.

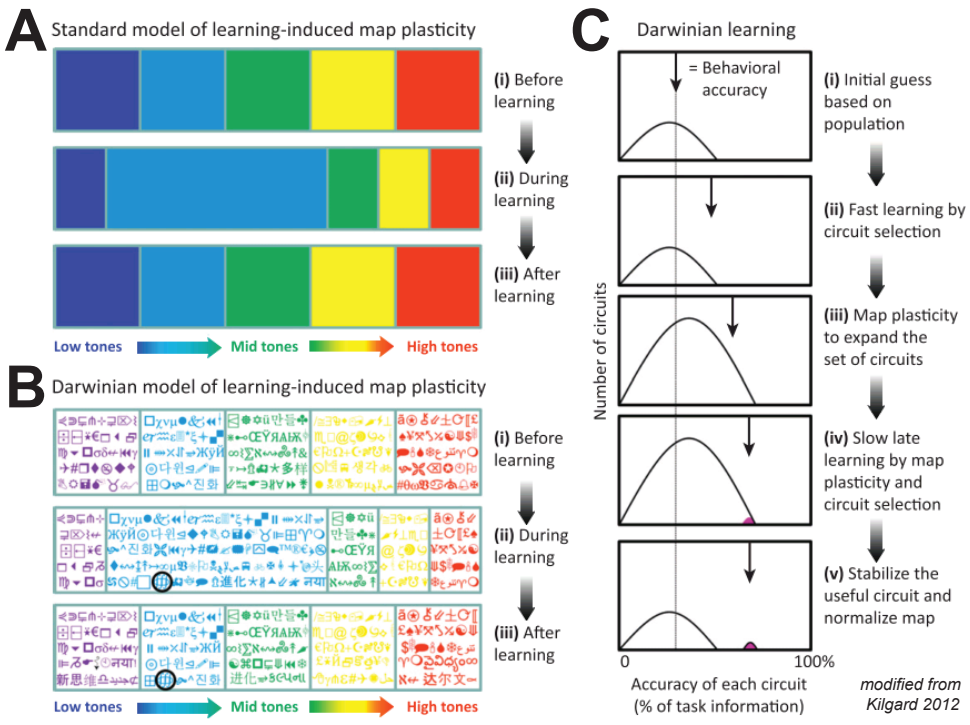

Figure 1.8: The Darwinian learning theory: (A) *Discrimination of low-frequency (light blue) tones increases the fraction of neurons that respond to these sounds, thus increasing the map-level representation of this frequency. Map plasticity usually renormalizes after learning without a decrease in performance (Reed et al., 2011).* ***(B)*** *Map plasticity is the* diversity *of neural circuits that could accomplish the task. Each symbol is a neural circuit encoding the task. In this view, an enhancement of the map is actually an increase in the number of circuits trying to solve the task. When the best circuit is selected and stabilized, maps could be returned to normal, while the new skill and memory of the task is maintained. The black circle denotes the new circuit that persists and supports the memory of the learned task. These circuits involve neurons from many brain regions.* ***(C)*** *The amount of information provided by neural circuits that respond to the task stimuli (like the light blue low-frequency neurons in (A) and (B)). Circuit effectiveness is represented as the percentage of task information provided by each circuit. The pink circuit corresponds to the circuit circled in black in (B).* From Kilgard (2012).

1.4.4 Map plasticity and Darwinian learning theory

The above mentioned ways to trigger plasticity can also work on the map level, by changing the shape of the tonotopic map. The expansions of cortical maps have been observed both in sensory cortices but also in motor cortices, in well-trained animals and even in humans. The enlarged region of the map always corresponds to sensory stimulus that was trained (Bieszczad and Weinberger, 2010). These map-level changes were blocked by NB lesions and cholinergic receptor antagonists (Conner et al., 2003). An overview of other tonotopy mapping studies and tonotopy

plasticity studies have been summarized in Figure 1.6 and Figure 1.7.

The map-level changes were also shown to be influenced by top-down effects (Polley, 2006). Indeed, animals were able to learn different discrimination tasks, based on loudness or frequency, with the very same set of stimuli, but with different reward association (rewarding once the loudness and once the frequency). This shows that the relevance of the stimuli (loudness or frequency) was more meaningful and influential on the map plasticity than just the stimuli themselves. Based on findings showing that this map expansion can be reversed without loss of function (Takahashi et al., 2011), a hypothesis regarding how this map plasticity can occur was developed by Kilgard (2012). In his *Darwinian learning* theory, he proposes a multi-step process that would explain how multiple tasks can be learned by the same population of neurons forming different networks, which specialize into solving a specific task. The theory is described in the following paragraph and with schematics in Figure 1.8.

Initially for a new task, the behavioral decision would be made by computing the average contribution of many circuits. Initial behavioral performance is therefore relatively low. With rewards, the brain could select the most effective circuit and have a first rapid improvement of the behavioral performance. The number of responsive circuits to the task would increase and a map expansion would be seen as consequence. This expansion could result in the selection of a new, more effective circuit with a better behavioral performance. If that circuit is stabilized, the rest of the circuits could return to the initial silent state to support future learning. The expansion phase of the map therefore corresponds to the recruitment of many neuronal circuits to better represent the task, and the proposed re-normalization would correspond to the stabilization of an expert circuit accompanied by the return to silent state of the rest of the recruited circuits.

The extent to which plasticity can occur at the map level was addressed in a few studies (Takahashi et al., 2011) but the time course of the reverting to the original state still remains unclear. Moreover, only area surfaces were quantified without clear description of the entire tonotopy map. Finally, the changes happening in the expanded region of the map were never studied on the cellular level.

1.5 Specific aims of the thesis

This section presents the specific aims and unanswered questions that I addressed during my thesis, as well as the reasons why these questions are relevant. Overall, the goal of this thesis was to explore the neuronal properties and neuronal activity pattern changes happening in the auditory cortex during and after the learning discrimination task. Establishing two-photon calcium imaging in the auditory cortex combined with behavior, and creating analysis and visualization tools for these experiments were two additional required goals to achieve this.

1. **Explore the oddball effect and SSA with supra-threshold recording techniques**. The oddball project was a small exploratory part of my thesis, with more limited goals. It was shown previously that stimulus specific adaptation (SSA) could be seen using *sub-threshold*, intra-cellular recording techniques (Chen et al., 2015). The main aim here was to examine whether the oddball effect and the stimulus specific adaptation (SSA) could be seen in the auditory cortex using *supra-threshold* recording techniques, namely two-photon calcium imaging and cell-attached electrophysiology.
2. **Measure frequency tuning and tuning stability of single neurons**. Frequency tuning is a very well studied and major property of auditory neurons. It is only in the recent years that genetically encoded calcium indicators combined with two-photon imaging through a cranial window opened up possibilities to study these properties on a population level and in a chronic repeated manner. The main questions were therefore related to stability of neuronal properties and examined at the circuit level in neuronal populations. A first aim was to examine the homogeneity of the responsiveness and the frequency tuning of single neurons in the same sub-region of auditory cortex. Furthermore, the stability of the frequency tuning of a single neuron over consecutive days was also examined. Establishing chronic recording of the same neurons over several days and weeks was a pre-requisite for this aim.
3. **Explore mapping techniques for the tonotopy in the auditory cortex**. Mapping of the tonotopy in the auditory cortex with different methods has already been done many times. However, when defining precise functional regions within the auditory cortex, the literature is still not yet fully consistent. Therefore, the aim was to define the boundaries of the sub-regions of the auditory cortex (AI / AAF / AII) using tonotopic maps.
4. **Establishment of chronic two-photon imaging in auditory cortex during a discrimination task**. Learning and plasticity were the main focus of this thesis. On the neuronal level, it was examined to which extent the responses of neurons in auditory cortex represent behavioral information and whether tuning of neurons is changing upon learning a discrimination task. It was further studied how the response of a population evolves throughout learning

a discrimination task, by comparing different *epochs* (stages) of the learning (naïve, expert, late expert). These aims required to establish chronic two-photon imaging of the same neurons in the auditory cortex, with the challenge of the lateral location of the auditory cortex.

5. **Measure learning-related changes in the auditory cortex at the at the map level**. The *Darwinian learning* hypothesis was studied on the map level. It was examined if an expansion and subsequent reduction of the surface area of the auditory cortex following the learning of a sound discrimination task can be seen. These map-level changes were assessed using wide-field calcium imaging with different mapping approaches: *standard* and *Fourier* imaging.
6. **Cortical dynamics during a sensory discrimination task**. To study the learning-related changes on the cortical level and to avoid movement artefact related limitations, chronic wide-field imaging in auditory cortex during a *delayed* discrimination task had to be established. The cortical dynamics related to the behavior of mice in this *delayed* discrimination task were explored. Specifically, the dynamics of different cortical regions, including auditory cortex, were studied during such a delayed sensory discrimination task. It was examined how the behavior decision is kept in memory during the delay period.
7. **Develop visualization and analysis tools**. In order to deal with the complexity and size of the data sets produced by the previously described aims, a major goal of this thesis was to develop visualization and analysis tools. These tool would help for the data management by organizing, sorting, and filtering data. They would also enable faster and easier processing and analysis via batch-processing and automation functions for the data analysis. Finally, as complex data sets needed to be visualized in order to get a "*feeling*" for the data and to do the necessary data mining for the data-driven part of the project, the visualization tool needed to be made interactive. Ideally, all these tools would fit in a common integrated framework.

2 | Methods

2.1 Recording methods

All experimental procedures were carried out following the guidelines of the Veterinary Office of Switzerland and were approved by the Cantonal Veterinary Office in Zurich.

2.1.1 Cell-attached electrophysiology

For the oddball and cellular frequency tuning experiments, cell-attached electrophysiological recordings were performed. SST-IRES-Cre mice (Jackson Laboratories, no. 013044); Taniguchi et al. (2011)) were crossed with a tdTomato reporter line (Jackson Laboratories, no. 007914; Madisen et al. (2010)). Somatostatin (SST) positive interneurons of layer 2/3 of the auditory cortex were recorded in cell-attached mode, with two-photon imaging guidance. The two-photon imaging was done as described in the later section. Animals were anaesthetized with isoflurane (~4.5% induction, ~1% afterwards). Patch pipettes of borosilicate glass capillaries (1.5 mm O.D. x 0.86 mm I.D., GCl50F-7.5, Harvard Apparatus) were fabricated using a flaming micropipette puller (P-87, Sutter Instrument). The internal solution contained 135 mM potassium gluconate, 10 mM HEPES, 10 mM sodium phosphocreatine, 4 mM MgATP, and 0.3 mM Na_3GTP. Glass pipettes were in addition filled with 20 µM Alexa-488. Voltage recordings in current clamp mode were performed with an Axoclamp 2B amplifier (Molecular Devices). The patch pipette was controlled with a micro-manipulator (Luigs & Neumann). A custom-written Igor (WaveMetrics) software controlled data acquisition and current injection through an ITC-18 board (InstruTECH). The analysis of the recorded traces (filtering, binning, averaging) was then later performed using custom MATLAB scripts.

2.1.2 Intrinsic signal optical imaging

Intrinsic signal optical imaging (ISOI) was used for two different purposes in this thesis. It was used to localize the auditory cortex and to create tonotopic maps of the auditory cortex. In both purposes, the following protocol and methods were identical. A blood vessel pattern image was taken before each session to use as reference. The reference was used to determine the measured intrinsic signal's location on the brain. The skull or the brain were illuminated by either a red LED light or a green LED light (Thorlabs). The red light (~620 nm) was used for the functional recording and the green light (~510 nm) was used for the reference image. All ISOI experiments were carried out in lightly (~1%) isoflurane-anaesthetized animals. Images were acquired with a high-resolution camera from the cortical surface by a ORCA-Flash4.0 digital CMOS camera (Hamamatsu, 2.3 x 2.3 mm^2 image area, 256 x 256 pixels after 4-by-4 spatial temporal binning, 30 frames per second imaging rate) and were stored after acquisition using custom MATLAB and LabVIEW software. Sound stimulation was presented to the animal as described later.

Standard **intrinsic signal optical imaging**

ISOI was used before chronic cranial window implantation to localize the auditory cortex and therefore better position the chronic cranial window. This was done through the exposed skull of the animals during the window implantation surgery described later. ISOI was also performed after window implantation to locate the auditory cortex more precisely within the window. In the *standard* paradigm, 2 second long band-limited noises (5 - 15 kHz) or pure tones (4 and 16 kHz) were used to stimulate the auditory cortex in a non-specific manner. The number of repetitions was usually 20 to 30 repetitions with an inter-trial interval of 15 to 30 seconds. The activation was measured using the $\Delta R/R$ formula described before (see Introduction) and averaged across all repetitions.

Fourier **intrinsic signal optical imaging**

The *Fourier* paradigm was used to obtain tonotopic maps of the auditory cortex (see Introduction, Kalatsky and Stryker (2003); Kalatsky et al. (2005)). Briefly, a temporally periodic stimulus was presented and the component of the response at the frequency of stimulation is extracted, analysed using a Fourier transform and corrected for hemodynamic delay using the stimulus reversal method (see Introduction). Forward and reverse presentation recordings were typically 4 - 10 minutes long each. Each stimulus cycle was either 1, 4, 8 or 16 second long (stimulus frequency between 0.0625 Hz and 1 Hz). The number of stimulus cycle used was between 40 and 150 loops.

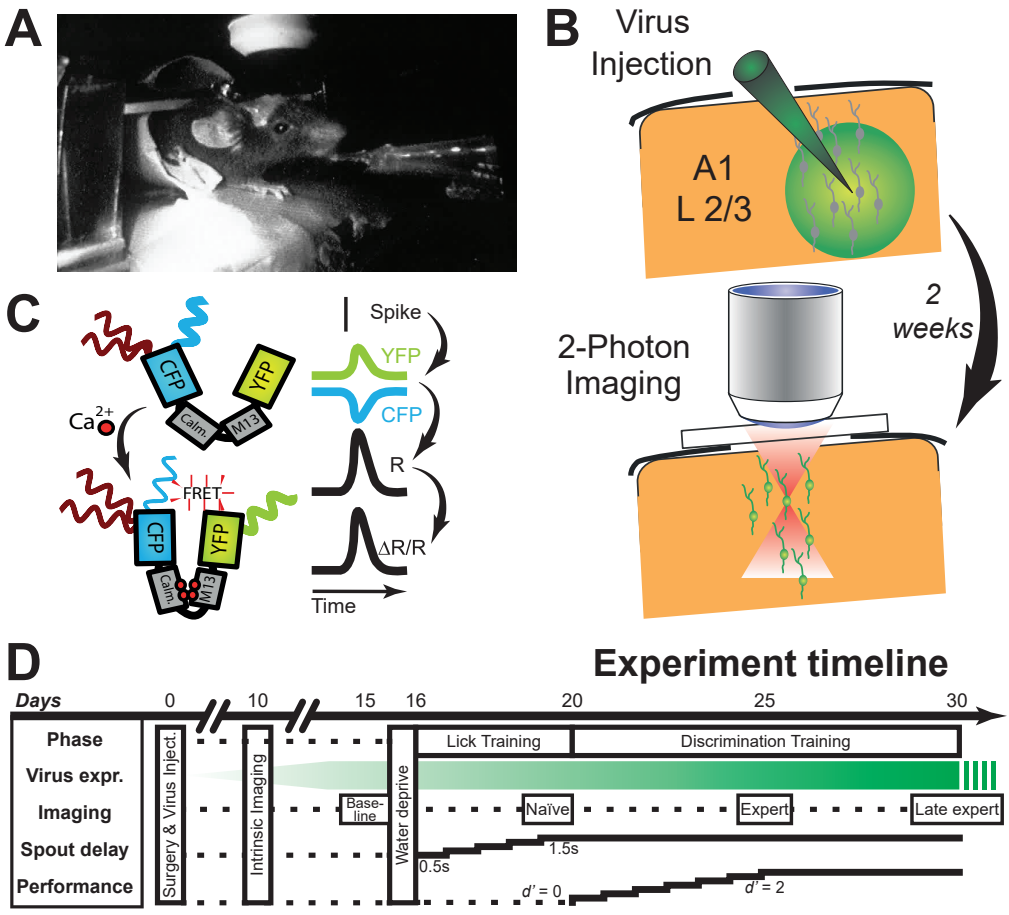

Figure 2.1: Calcium indicators and experiment timeline for the go / no-go behavior: ***(A)*** *View of a mouse performing in the discrimination task while being imaged with a two-photon microscope.* ***(B)*** *Scheme explaining the virus injection protocol. Virus was bulk-injected through a small craniotomy to infect neurons with a virus coding for the genetically encoded calcium indicator protein. After ~2 weeks, the activity of neurons was measured through a cranial window with a two-photon microscope.* ***(C)*** YC-Nano140 *is composed of two fluorescent sub-units,* YFP *and* CFP*. When neurons spike, calcium enters the cell and binds to the indicator. This changes the conformation of the protein and enables* FRET*, which leads to a decrease in* CFP *emission and an increase of* YFP *emission. Calculating the ratio between the two time-series* R *and normalizing it by the baseline* ΔR/R *provides a motion-artefact-free robust measurement of neuronal activity.* ***(D)*** *Experimental timeline. After surgery (virus injection and window implantation), an intrinsic signal optical imaging session was performed to confirm the overlap between the virus expression and the primary auditory cortex location. After a* baseline *imaging session, the animal was moved to the training protocol.* Naïve*,* expert *and* late expert *epochs were defined according to the animal's performance.*

2.1.3 Two-photon calcium imaging

Two-photon microscopy was used in combination with calcium imaging (see Introduction). For the two-photon calcium imaging experiments described in this thesis, the *YC-Nano140* (Horikawa et al., 2010) and *GCaMP6m* (Chen et al., 2013b) genetically encoded calcium indicators were used. The indicators were introduced in neurons using viral vectors. Two-photon microscopy was performed through chronic cranial windows (for the preparation, see below). A Mai Tai DeepSee

(Spectra-Physics) or a Tsunami (Spectra-Physics) laser were used at 840 nm or 920 nm emission wavelength (YC-Nano140 and GCaMP6m respectively). The laser beam was sent through a custom built microscope into a water immersion 16X objective (Nikon, 0.8 NA) to image the cortex of living animals. Laser intensity was adjusted by a Pockels cell (M302RM, Conoptics) and light was collected using photomultiplier tubes (E850-13, Hamamatsu). Scanning frame rate was either 10 Hz (galvanometric scanners) or 77.67 Hz (resonant scanners). The `Helioscan` software was used to acquire images during experiments (Langer et al., 2013).

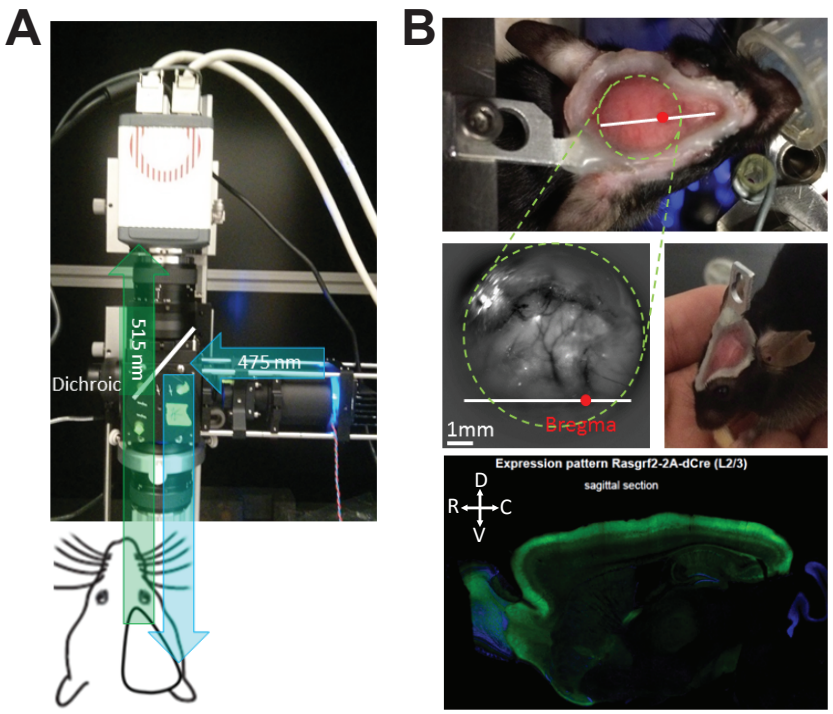

Figure 2.2: Wide-field imaging in transgenic animals: (A) *Schematic of the wide-field imaging setup. The light source (475 nm LED, right) emits collimated light deflected downwards by the dichroic (center). Excitation light (515 nm) from the calcium indicator is passing through the dichroic and recorded by the camera (top).* ***(B)*** *Top and middle: view of wide-field preparation. Bregma (red dot) and midline (white line) are marked. Bottom: sagital section showing the layer-specific expression of the calcium indicator (bottom image from Lazar Sumanovski). Abbreviations:* R *rostral;* C *caudal;* D *dorsal;* V *ventral.*

2.1.4 Wide-field calcium imaging

Wide-field imaging was done through the exposed skulls of mice (for the preparation, see below). The usage of transgenic mouse lines was critical to get homogeneous expression in the whole cortex in a layer-specific manner. For the wide-field experiments, the *Camk2a-tTA;Rasgrf2-2A-dCre;Ai93(TITL-GCaMP6f)* transgenic mouse line was used, which combines the layer 2/3 specificity (Figure 2.2, B bottom; Madisen et al. (2015)), the GCaMP6f calcium indicator (Chen et al., 2013b) and inducibility via Trimethothoprim (*TMP*, Sando et al. (2013)). An ORCA-Flash4.0 digital CMOS camera (Hamamatsu) was used to record calcium indicator fluorescence, with 2-by-2 spatial binning to 512 x 512 pixels and 20 Hz frame rate. Excitation light was done at 475 nm wavelength using LED (Thorlabs). A 515 nm emission filter was used before collecting light with the camera (Figure 2.2, A). Wide-field imaging was used both for the anaesthetized mapping

experiments (tonotopy and cortical sensory regions) and for the awake behaving experiments.

2.1.5 Auditory stimulation

Sound playing system

The auditory stimuli were generated using a Tucker-Davis System processor (RZ6) as described in Chen et al. (2015). All stimuli were either generated or played by the Tucker-Davis software RPvdsEx. A 5 ms rise/fall time was used to avoid sound artefacts. Sounds were presented in the free-field configuration by using an electrostatic loudspeaker (ES1, Tucker-Davis) or a magnetostatic loudspeaker (MF-1, Tucker-Davis). The loud speaker was placed at about 5 cm from the contralateral ear of the animal. Sound shielding was surrounding the experiment chamber to reduce the ambient noise.

Frequency mapping for single neurons

For the electrophysiology experiments, mapping of the neuron's tuning was performed as described in Chen et al. (2015), in order to choose the F_1 and F_2 frequencies for the oddball experiments. Pseudo-random blocks of pure tones ranging from 4.00 to 45.26 kHz (0.25 octave apart, 15 frequencies, 100 ms duration, 800 ms onset-to-onset inter-stimulus interval) presented with 0, 10, and 20 dB attenuation levels (corresponding to 90, 80, 70 dB). Each block contained 60 tones (4 repetitions per frequency). The spiking response were then analysed to extract the best frequency.

Oddball paradigm

The oddball stimulation and paradigm was the same as used in Chen et al. (2015). Two pure tones (F_1 and F_2) with frequencies around the best frequency of the neuron and separated by 0.5 octave were pseudo-randomly assigned as either *oddball* or *standard* tone in alternate blocks. The probability of the *oddball* tone was either 0.1 (100 oddball trials and 900 standard trials in 10 stimulation blocks, at least 6 standard tones between oddballs), 0.3 (120 oddball trials and 240 standard trials in 4 stimulation blocks) or 0.5 (100 oddball trials and 100 standard trials in 2 stimulation blocks, control condition). All tones were presented at 80 dB (10 dB attenuation level) with 100 ms duration and 500 ms ISI.

Cloud-of-tones for discrimination task

As pure tones only evoked limited firing in pyramidal neurons of auditory cortex (due to the *sparse* coding in auditory cortex, see Hromádka and Zador (2009)) and therefore responses were not

easy to pick up *in vivo* with calcium imaging, a more complex stimulus was used that would potentially evoke bigger responses: *cloud-of-tones* (Znamenskiy and Zador, 2013). A *cloud-of-tone* is a stream of 30-ms overlapping pure tones presented with 10 ms between the tone onsets (Figure 2.3, B). The frequency for the tones were chosen from a list of 18 possible tone frequencies, logarithmically spaced between 4 and 20 kHz.

The cloud-of-tones were used for the discrimination task combined with the two-photon recordings. For each trial either the low cloud (~5.2 to ~7.3 kHz) or the high cloud (~13.4 to ~19.0 kHz) was presented. The high or the low cloud was randomly assigned as target sound for each mouse.

Fourier imaging sweeps

To do the Fourier imaging for the tonotopy mapping experiments, continuous periodic stimulation of the auditory cortex was used, as described in Kalatsky et al. (2005). This consisted in ramps of short tones played in relative quick succession. Several different settings were explored in order to obtain the best stimulation possible. The key parameters were the frequency range of the stimulus, the stimulation frequency, the number of tones and the tone duration. Frequency range was typically between 4 and 32 kHz, and usually 25-35 tones were used with a duration 50 to 150 ms. Stimulation frequency was key as it was the frequency at which the response was extracted using the Fourier transform. Values between 0.0625 Hz up to 4 Hz were used, but best results were achieve using 0.125 or 0.5 Hz.

2.2 Preparations and surgeries

2.2.1 Optical access with chronic windows

In order to get an optical access and to implant a cranial window, the auditory cortex was exposed with a surgery and preparation of a cranial window (Holtmaat et al. (2009)). Animal were anaesthetized with a general isoflurane anaesthesia (4% induction, 3% afterwards). The head was sterilized with betadine and shaved. An about 1-cm long cut was made in the skin and the skull cleaned. Muscles were bluntly detached to get a better access to the lateral part of the skull, where the auditory cortex is located. A small cranial window (3-5 mm on side) was then prepared above the auditory cortex using a drill. Following gentle removal of the bone, a chronic cranial glass window was prepared and a small metal head post was attached to the skull. The cover glass was secured in place with a rim of dental cement (light curing Tetric Evoflow). A period of 5 - 10 days was waited before doing any imaging experiments, in order to let the brain recover and the window clear up.

2.2.2 Virus injection

For labelling cell populations, the expression of genetically-encoded indicators was induced using viral transfections (Figure 2.1, B). One advantage of labelling via viral transfections is that no re-labelling in subsequent imaging sessions is required, which in particular makes it unnecessary to re-open a cranial window with the associated potential risks of damage. Viral constructs coding for fluorescent protein based calcium indicators were used (*YC-Nano140* or *GCaMP6m*, see above). Virus injections were performed in brief (0.5 h) surgical sessions under isoflurane anaesthesia, using a stereotactic apparatus to guide the pipette tip to the target region. Virus-containing solution (maximally several hundred nanoliter) was injected through a small hole in the skull directly into the target brain regions using a very thin glass capillary tip. Depending on the virus and the protein, sufficient levels of expression were reached within 1-3 weeks after the virus injection. Adeno-associated viral (AAV) vectors or lentiviral vectors were used, which yield good results with stable protein expression over the period of weeks and months and are well tolerated by the animals. All procedures are carried out in accordance with the biosafety guidelines.

2.2.3 Wide-field preparation

For chronic imaging of large parts of the neocortex in mice an exposed skull preparation was used (Guo et al., 2014). This preparation was used for the wide-field calcium imaging experiments. It was easier to prepare compared to the cranial windows, durable for months and did not require a craniotomy (making it less invasive). Preparation started with removing the skin and exposing the skull over large parts of the hemisphere (see above). Next a thin layer of clear dental cement was applied to the intact skull (light curing Tetric Evoflow). Finally, a wall of dental cement was built along the edges of the preparation. This preparation was stable for several months and enabled longitudinal studies in behaving animals (Figure 2.2, B).

2.3 Behavior paradigms

2.3.1 Head-fixed behavior in water-scheduled animals

In order to perform imaging in awake animals that performed in a discrimination task, animals had to be habituated to head immobilization using the implanted head post (see above) while sitting still inside a tube. The animals were handled for two days and subsequently, they were progressively habituated to sit in the tube with their forepaws resting on a bar while their head was immobilized by holding the head-post with a clamp.

Training included an initial handling phase (~1 week), a 6-10 day-period during which the duration of head fixation was slowly increased in a step-by-step procedure, and an adaptation period to the experimental setup (Figure 2.1, A). An extended initial handling period was important for the build-up of trust between experimenter and animal because mice that had been extensively handled showed more cooperative behavior later. The step-by-step approach involved first adapting the mouse to the tube, stopping the mouse when exiting the tube, holding the head post shortly to the fixation-bar and finally extending the fixation duration over the days from 1 s to 15 min. Care was always taken that stress level remained low. During the training period the animal's health and well-being was carefully monitored.

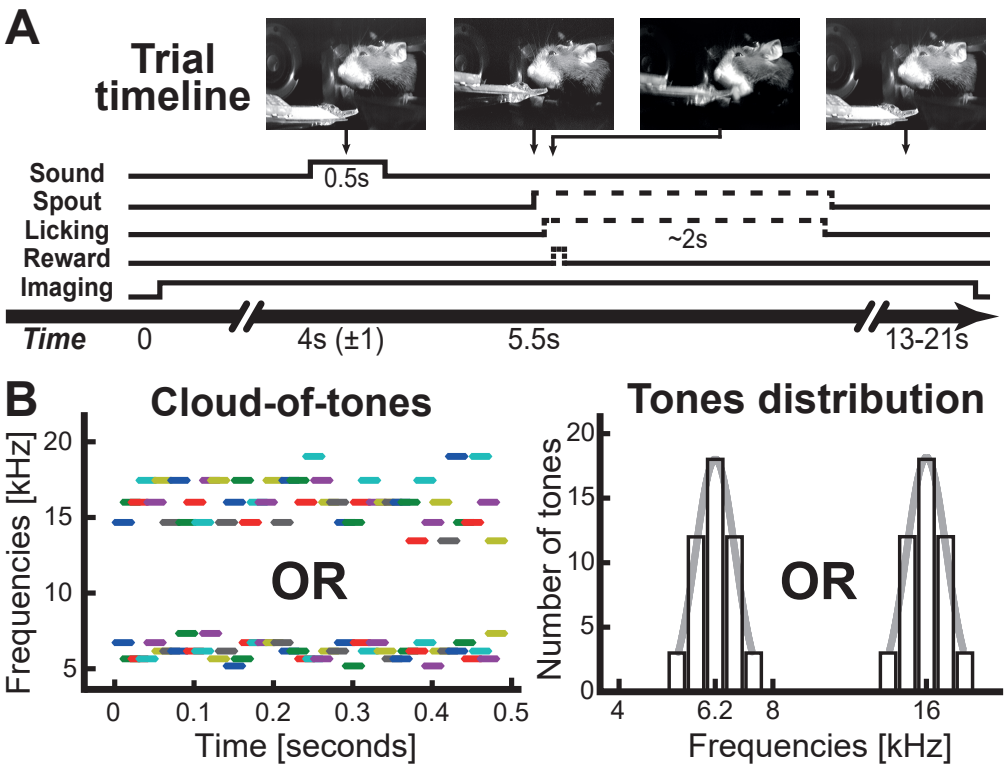

Figure 2.3: Trial structure and cloud-of-tones for the go / no-go behavior: (A) *Timeline of a single trial for the* go/no-go *sound discrimination task. The 4 main epochs are shown: sound presentation, short delay, decision (lick or not) and outcome (reward or delay).* ***(B)*** *The sound stimulation used for the* go/no-go *sound discrimination task. Left: cloud of tones are mixtures of overlapping short pure tone pips. Only one cloud is played at a time (either low or high cloud). Right: the tones are chosen from a Gaussian centered on either a low or a high central frequency.*

Mice were trained on a reward-based model (see below), which requires water scheduling to increase motivation levels, improve performance, and accelerate learning curves. Water scheduling of mice is widely used for this purpose (Mayrhofer et al., 2013). Animals undergoing a reward-based behavioral paradigm were water deprived on a 5/2 schedule, i.e. water restriction for 5 days a week with water obtained only during imaging sessions once a day and *ad libitum* access to

water over the weekend. The water intake during each experiment session was measured and a minimum daily water intake was assured, if required by supplementing at the end of the day. Before the start of water scheduling the animal's weight was determined for reference.

2.3.2 Training protocols

Different training protocols have been used in the work described in this thesis. All of them are based on a sound discrimination task, with the type of sound and the exact trial structure varying. The common principle was the following: the mouse was receiving an auditory stimulus and was required to learn to associate it to a reward, which was a droplet of water. To report their decision, mice had to lick a water spout, which was detected with a mechanosensitive piezoelectric-film and electrically recorded. All the behavior paradigms used were *go* / *no-go* discrimination tasks, in which mice had to lick for reward following presentation of a target sound but refrain from licking for non-target sounds (Figure 3.10, B). The outcome of the trial depended on the correct or erroneous behavior of the mouse (Figure 3.10, B, bottom).

Simple sound-frequency discrimination task

A simple version of a frequency discrimination task was used for the first part of the thesis. Mice had to discriminate pure tones with a single frequency for each tone. The frequencies used for the target sound was either 8 kHz or 12 kHz, and the distractor was either 4, 8, 12 or 16 kHz. Either a single or multiple distractor sounds were used. The use of multiple distractor sounds was always introduced only after the mouse already performed well with a single distractor sound. In later experiments, the pure tones were replaced by 2 *cloud-of-tones* (one target and one distractor) as described above.

The overall timeline of the experiments addressing the *Darwinian learning* theory is shown in Figure 2.1 (D). The goal was to see the change across different learning epochs, therefore the surgery, virus injection and training times had to be timed accordingly.

Delayed response discrimination task

In order to avoid movement artefacts in the measurement of neural or cortical activity during the sensation period of each trial, a delayed version of the discrimination task described above was used. This delayed version was implemented in two different ways.

First, a moving licking spout approach was used for the two-photon imaging experiments. A movable licking spout was installed and put into licking range only when animals already waited a little delay after the sensation period. Figure 2.3 (A) shows the trial timeline for these experiments.

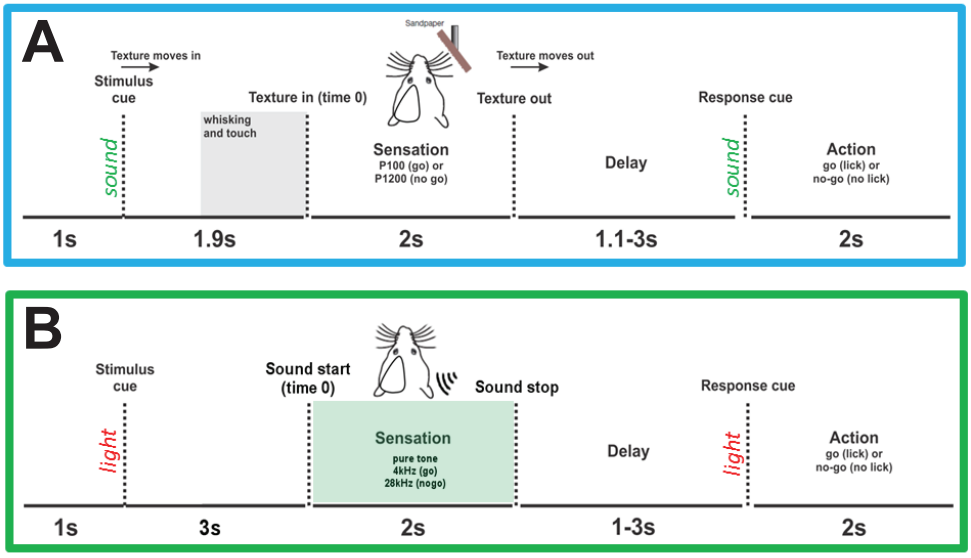

Figure 2.4: Wide-field imaging in transgenic animals: ***(A)*** *Schematic of the original delayed texture discrimination task.* ***(B)*** *Auditory version of the delayed discrimination task.*

This version used no visual cues for the different events during the trial.

Another version of this delayed discrimination task was used for the wide-field imaging experiments. The aim was also to avoid movement artefacts during sensation but furthermore a longer delay period was used to see working memory or licking refraining related activity in the cortex. This version of the auditory discrimination task was made very similar to an existing texture discrimination task used previously (Figure 2.4, A sensory, B auditory). This allowed the possibility to compare the tasks as only the sensory modalities were different. For this version, light cues were used to signal the stimulus and the response periods, helping the animal to match events with sensory inputs. The visual modality was used for the cues in order to avoid disturbing the main discrimination modality (auditory). Additionally, a 2 second long punishment white-noise sound was used for miss and false alarm trials. These correspond to when the animal had to lick and did not (target sound with no response, miss) or when the animal had to refrain from licking and did not refrain (distractor sound with response, false alarm). These trial types are described in Figure 3.10 (B) (bottom).

2.3.3 Performance analysis

Performance of mice were analysed with several criterion. Primarily, the *hit* and *correct rejection* (CR) rates were always calculated. They respectively correspond to the fraction of trials where the animal had to lick and did so correctly (target sound with response, hit) or to the fraction of trials where the animal had to refrain from licking and did refrain correctly (distractor sound with no response, correct rejection). These rates were also good indicators to monitor motivation level or

engagement in the task (high *hit*) and impulsiveness (high *CR*).

A performance index was also calculated using the d' sensitivity index, commonly used to assess performance of mice. Sensitivity index d' was calculated using the hit rate and the false alarm rate with the following formula:

$$d' = \frac{\mu_{hit} - \mu_{false\ alarm}}{\sqrt{\frac{1}{2}\sigma^2_{hit} + \sigma^2_{false\ alarm}}}$$

where μ and σ are the mean and the standard deviation of each rate, respectively. d' is commonly used for behavior performance quantification. The threshold of $d' = 2$ is often used to define expert performance in discrimination tasks.

Additionally, for the delayed discrimination protocols, the early lick rate was also monitored. Early licks correspond to the lick events happening before the response cue was shown. These results in the termination of the trial and no further sound or reward being given for the aborted trial.

2.4 Data processing and data analysis

All data analysis for the calcium imaging experiments was performed using the analysis framework that is extensively described at the end of the results section. The precise methods of data analysis are described there, at the same time as the analysis tool itself.

3 | Results

3.1 Detection of the oddball effect in the auditory cortex

The oddball effect and stimulus-specific adaptation (SSA) were examined using supra-threshold recording techniques. To quantify the oddball effect in the auditory cortex, two different methods of recording were used in combination with the oddball stimulation paradigm: electrophysiology and two-photon. The following sections present the results obtained in defining whether or not SSA can be observed in the layer 2/3 neurons of primary auditory cortex in an anaesthetized mouse using supra-threshold recording techniques. The general oddball paradigm was fairly similar for both methods but differed in some properties of the sound presentation.

3.1.1 The oddball effect assessed by single-cell electrophysiology

To quantify the oddball effect for a single neuron, cell-attached recordings of somatostatin (SST^+) positive layer 2/3 interneurons were performed. A total of 24 SST^+ neurons from 17 SST-IRES-Cre-tdTomato mice were recorded. Spiking activity was extracted and quantified for both the *oddball* stimulation and the *standard* sound preceding the oddball, in order to have similar number of trials for both conditions. An example trace of such recording is shown in Figure 3.1 (A). The 90% standard, 10% oddball paradigm is shown, which was the condition with the rarest amount of oddball. The example only shows one block, corresponding to 10% of a recording session for one condition for a neuron, as typical recording sessions for one paradigm contain 100 oddball presentations.

Panel (B) shows the peri-stimulus time histograms for 3 paradigms: the 90%/10% paradigm described above (top), a control condition were the oddball is presented at the same probability as the standard (50%/50%, middle) and a frequency control paradigm were frequency preference can be assessed. Indeed, in the two first paradigms, both frequencies F1 and F2 are used for the oddball in different experimental blocks, in order to cancel out the frequency-specific effect and only highlight the oddball effect. In other words, the oddball sound can be either F1 or F2 in

different experimental blocks. Therefore the response seen in the oddball condition cannot be due to a frequency preference from the neuron to one frequency. Due to the low success rate of the recordings, no pooled analysis of the 17 recorded neurons were done, but the example neuron shown in Figure 3.1 suggests that SSA can be seen in the supra-threshold spiking activity of SST$^+$ interneurons in the auditory cortex of mice.

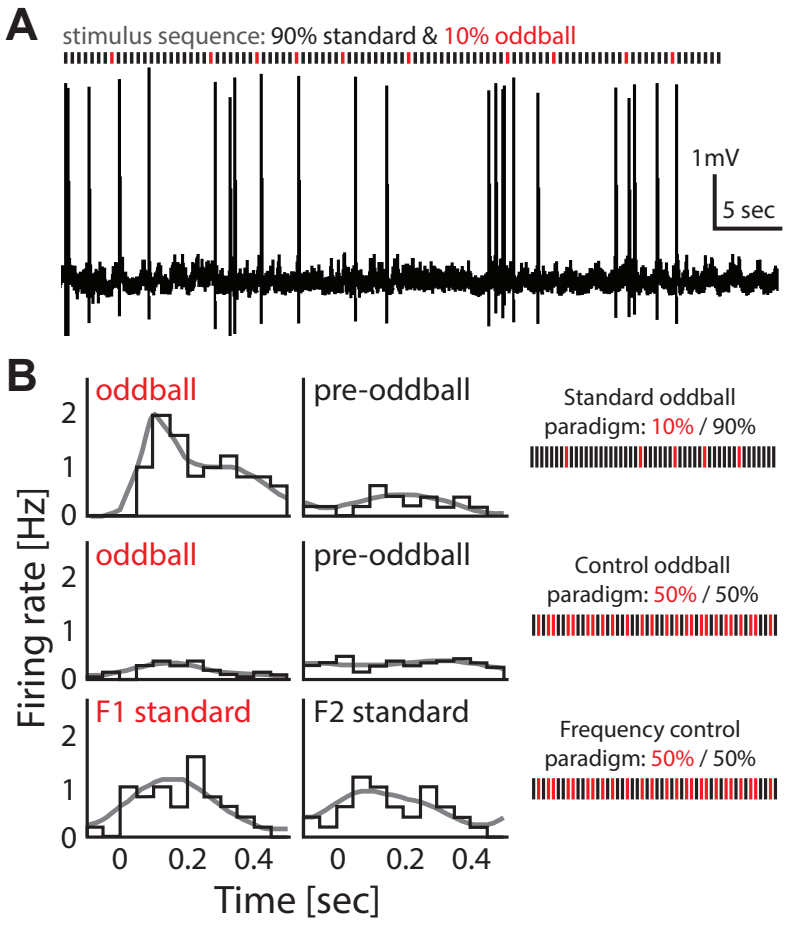

Figure 3.1: Oddball effect in the auditory cortex assessed by single-cell electrophysiology: ***(A)*** *Part of an example trace of an oddball experiment for a single neuron recorded in cell-attached mode. Stimuli are presented at 1 Hz. The neuron was located in layer 2/3 of the auditory cortex and was recorded with the animal in anaesthetized condition.* ***(B)*** *Peri-stimulus time histograms for the example in (A). Top: comparison between the oddball stimulus (*odball*) and the standard stimulus just before the oddball (*pre-oddball*) in a 90% standard frequency, 10% oddball frequency configuration. Middle: control comparison between odball and pre-oddball in a 50% standard, 50% oddball frequency configuration. Bottom: control comparison of each frequency separately in a 50% standard, 50% oddball frequency configuration.*

3.1.2 The oddball effect assessed by two-photon calcium imaging

To quantify the oddball effect for several neurons at the same time, two-photon calcium imaging in layer 2/3 of the primary auditory cortex was performed. A total of 7 animals were injected with the GCaMP6m calcium indicator and implanted with a chronic cranial window. Usually, a single imaging region containing 25-40 neurons was sampled from each animal. A 90%/10% oddball paradigm was used as in the previous section, but the interval between the stimuli was extended to 1.5 seconds in order to accommodate for the slower response dynamics of the calcium signal compared to the electrophysiological recordings. An example experiment with the response of 9 example neurons from a single animal is shown in Figure 3.2 (A). To minimize the continuous

laser exposure on the sample, blocks of 5 oddball with 45 standards have been used, instead of the 100 oddball blocks used in the electrophysiology experiments. The peri-stimulus time average for oddball and standard for 2 example neurons is shown in panel (B). Only few neurons were driven by the sound stimulation (Figure 3.2, A, data not quantified). Among these, several neurons showed an increase in evoked response for the oddball but not the standard (Figure 3.2, B, data not quantified). This suggests that SSA can be seen in layer 2/3 neurons in the auditory cortex of mice using two-photon calcium imaging with the GCaMP6 calcium indicator.

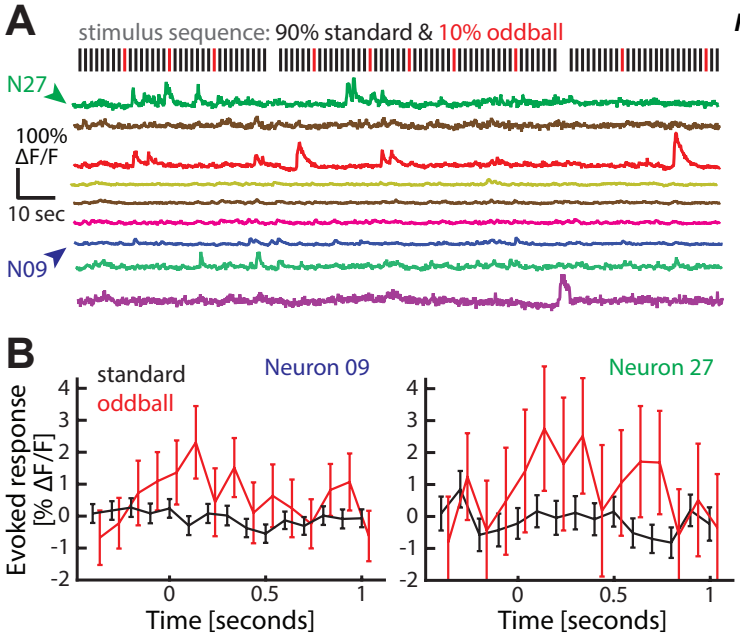

Figure 3.2: Oddball effect in the auditory cortex assessed by two-photon calcium imaging: (A) *Example calcium traces recorded in an anaesthetized auditory cortex from layer 2/3 neurons during an oddball experiment using GCaMP6 calcium indicator. Stimulus sound onset is shown above the traces. Stimulus sounds were short 100 ms pure frequency sound pips of two different frequencies, either* oddball *(in red) or* standard *(in black), presented every 1.5 seconds. Two example neurons are colored in blue (neuron 09) and green (neuron 27).* ***(B)*** *Peri-stimulus time histograms for the two example neurons. The average for all the oddball sounds (in red) and for all the standard sounds (in black) is shown (N = 100 for the oddball, N = 900 for the standard, error bars represent standard error of the mean (SEM)).*

3.2 Exploration of different approaches to functionally map the auditory cortex

Different methods were used to map the auditory cortex on different scales. This section shows the result of establishing these methods in the auditory cortex and the data collected using these methods.

3.2.1 Locating the auditory cortex with intrinsic signal optical imaging

A first requirement of recording functionally relevant data in any defined brain region is to precisely locate the targeted brain region. In the case of a sensory cortex like auditory cortex, one can combine the traditional approach of coordinate-based targeting with a functional mapping strategy. *Intrinsic signal optical imaging* (ISOI) is a very convenient and easy method to get a functional

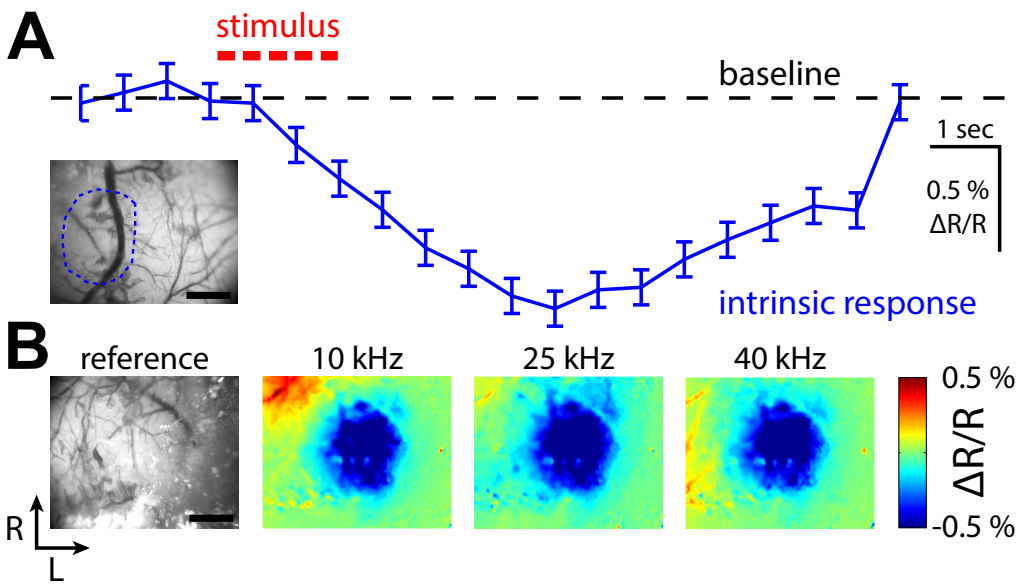

Figure 3.3: Basic mapping of the auditory cortex using intrinsic signal optical imaging: (A) *Mean time course of response to a band-limited white noise (11 - 13 kHz) recorded in the auditory cortex using intrinsic signal optical imaging through (ISOI) a cranial window (N = 10 repetitions, error bars represent standard error of the mean (SEM)). The mouse was anaesthetized during the recording. The inset shows the blood vessel pattern and the Region-Of-Interest selected for the averaging. Scale bar: 1 mm.* ***(B)*** *Average maps of the response to pure tones pips of 10, 25 and 40 kHz recorded in the auditory cortex using ISOI through the skull. The reference image (left) shows the blood vessel pattern. Scale bar: 1 mm. Abbreviations:* R *rostral;* L *lateral.*

response from any sensory cortical region. Although this method has relatively poor spatial and temporal resolution as the measured signal is originating from a blood oxygen level change of reflectance, it can nevertheless be used to roughly locate the target sensory cortex.

ISOI was used mainly for locating the rough position of the auditory cortex, either before implanting a chronic window or afterwards to locate the auditory cortex within the window. In the first scenario, the location of the auditory cortex was approximated using a set of coordinates relative to the *bregma*. Then, during the surgery but before the chronic window implantation, a more precise location was determined by recording the intrinsic response of the auditory cortex to a relatively strong auditory stimulus. This enables reliable and precise positioning of the window. In the second case, a 3-5 mm diameter glass window was implanted centered on a set of coordinates and the intrinsic recording was performed only after the surgery, to better locate the auditory cortex within the window. This approach could lead to misplaced windows as the initial positioning cannot be changed and relies solely on the coordinates. In both cases, the recordings were done in an anaesthetized mouse.

Figure 3.3 shows an example of both of these approaches. In the upper panel (A), an example response time course of the auditory cortex to a band-limited noise (11 - 13 kHz) is shown. The response was recorded using ISOI through a cranial window of an anaesthetized mouse. The re-

sponse is negative, very slow, and of small amplitude, which is characteristic of ISOI. The example trace is the average response of 10 repetitions of the same stimulus. In the lower panel (B), average maps of the response for 3 different frequencies are shown, along with the reference image showing the surface of the brain. The lower panel shows recordings performed during surgery to better locate the auditory cortex. All 3 frequencies show similar activation patterns and similar amplitudes. In conclusion, auditory cortex could reliably be located using ISOI in mice. This procedure was used in all subsequent experiments to locate auditory cortex before and after chronic window implantations.

3.2.2 Assessment of neuronal frequency tuning with electrophysiology

Electrophysiology is a precise and direct method to assess the frequency tuning of neurons in the auditory cortex. It differs from ISOI by giving single neuron resolution. A total of 24 SST^+ neurons from 17 SST-IRES-Cre-tdTomato mice were recorded in cell-attached mode (same data set as oddball experiments described above). This mode enables to record action potentials (or spikes) from neurons without having access to the sub-threshold variations of the neuron's membrane potential. It is a fair trade-off between the difficulty of setting up the recording and the value of the output (spiking activity). All electrophysiology results shown are from anaesthetized animals.

To perform the oddball experiments described before, it was necessary to measure the frequency tuning of each recorded neuron, as the frequency preference of neurons can bias the results obtained in an oddball protocol. Therefore, before presenting the oddball stimulation protocol, a frequency characterization protocol was first used. The frequency characterization is done by playing series of pure tones with different frequencies in quick succession in order to gather enough repetitions for each frequency. Figure 3.4 shows the result of such a characterization protocol. In the upper panel (A), part of an example recording run is shown with the presented frequencies marked in red (above). Black vertical lines within the recording are spikes generated by the neuron. These spikes are composed of both spontaneous firing and by sound-evoked firing. A view of the recorded example neuron (in red, marked with the *tdTomato* fluorescent protein) and of the recording pipette (in green, filled with the Alexa-488) is shown in (B). The pipette is pressed against the neuron without actually having an opening in the neuron, in which case the neuron would be filled in green.

The responses to each stimulus frequency is summarized in the peri-stimulus histograms in (C). Most of the frequencies evoke at least a low level of spiking in the neurons but the profile for each frequency is usually not similar. Mainly two groups can be seen: either sharp responses in the early phase (16.0 kHz, 22.6 kHz, 38.5 kHz, etc.) or a longer, less sharp evoked response (6.7 kHz, 8.0 kHz, 9.5 kHz). The evoked response for each frequency can be extracted and quantified

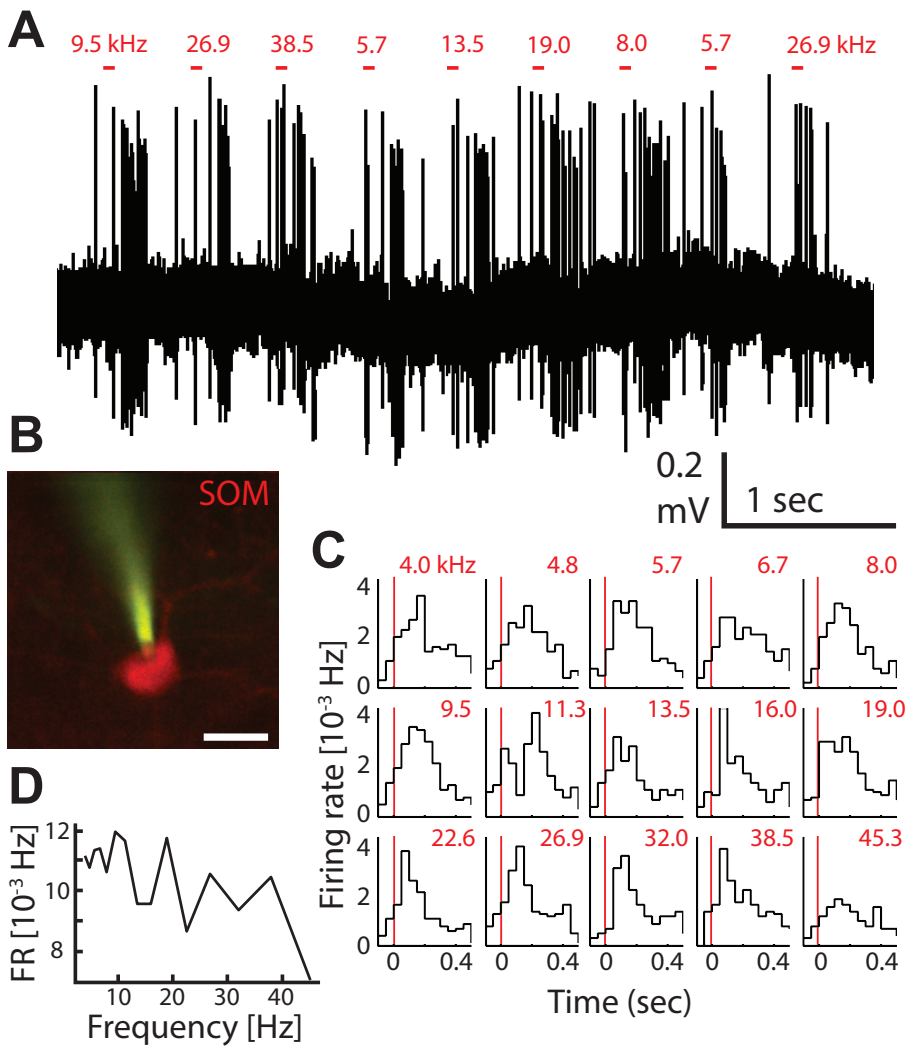

Figure 3.4: Frequency tuning assessed by electrophysiology: ***(A)*** *Part of an example trace of frequency tuning characterization experiment for a single neuron recorded in cell-attached mode. The neuron was located in layer 2/3 of the auditory cortex and was recorded with the animal in anaesthetized condition.* ***(B)*** *Two-photon view of the recorded example neuron (red) and of the recording pipette (green), scale bar:* 20 µm. ***(C)*** *Peri-stimulus histograms quantification of the firing rate in Hz for each frequency of the example neuron. Red bar indicates the stimulus sound onset. Stimulus sounds were randomized short 100 millisecond pure frequency sound pips, with the frequency indicated in red. Binning: 50 milliseconds.* ***(D)*** *Tuning curve for the example neuron, quantified as the sum of the early evoked response for each frequency. The absence of clear peak suggests that this example neuron is relatively broadly tuned.*

as a single value. This gives rise to the frequency tuning curve shown in (D), where the sum of the early evoked response is plotted for each frequency. This curve has often several peaks and can be relatively different from one neuron to the next, even for neurons in the same vicinity. In the example neuron shown in Figure 3.4, the tuning curve does not contain any clearly visible peak that would be higher for a specific frequency. This suggests that this example neuron has broad tuning, which was representative for most of the neurons recorded (data not quantified).

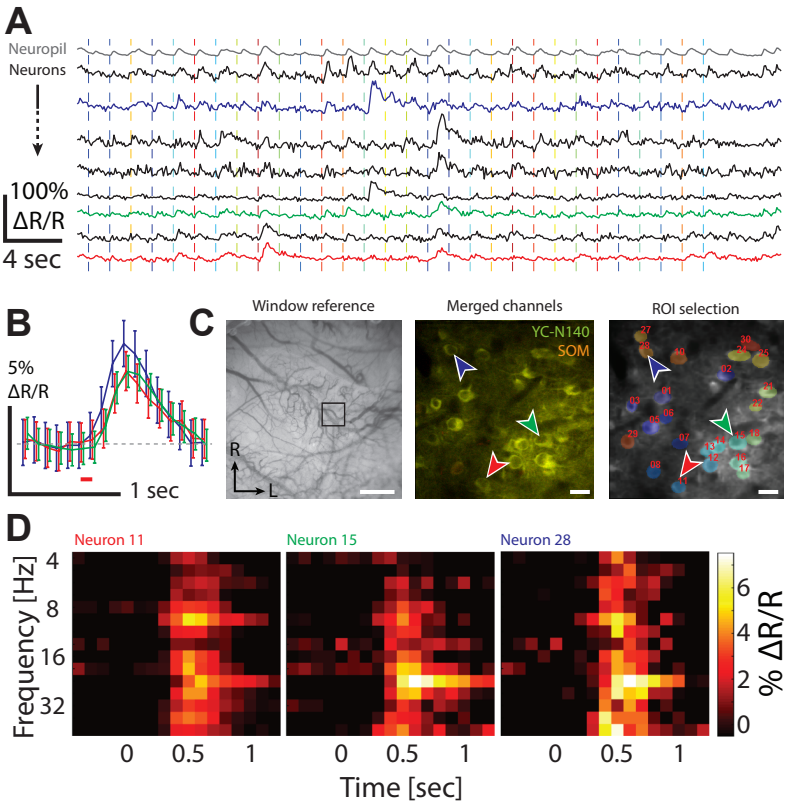

Figure 3.5: Frequency tuning assessed by 2-photon calcium imaging: (A) *Example calcium traces recorded in an anaesthetized auditory cortex from layer 2/3 neurons (~280 µm deep) using the YC-Nano140 calcium indicator. The first trace in gray is for the neuropil (top). Vertical dashed bars indicate the stimulus sound onset. Stimulus sounds were randomized short 100 ms pure frequency sound pips. 3 example neurons are colored in red (neuron 11), green (neuron 15) and blue (neuron 28).* ***(B)*** *Peri-stimulus average for the 3 example neurons (N = 20 repetitions, error bars represent standard error of the mean (SEM)). Red horizontal bar: sound stimulus (100 ms).* ***(C)*** *Left: Zoomed out view of the imaged region (indicated with the black box). Scale bar:* 200 µm. *Middle: Two-photon view of the imaged region with the example neurons labelled with the arrows. The image is a merge of the green and blue channels, from the calcium indicator YC-Nano140, and the red channel, used for the SST⁺ interneuron labelling. Scale bar:* 25 µm. *Right: Two-photon view of the imaged region with the Region-Of-Interest labelling of each neuron. Scale bar:* 25 µm. ***(D)*** *Peri-stimulus average heat maps for the 3 example neurons for every frequency. Stimulus onset is at time 0. Abbreviations:* R *rostral;* L *lateral.*

3.2.3 Assessment of tuning with two-photon calcium imaging

Assessing tuning in single neurons

Another method to quantify the frequency tuning of neurons is to measure their evoked response to pure frequency stimulation using two-photon calcium imaging. Two-photon calcium imaging provides an optical assessment of the neuron's activity, and when combined with a frequency characterization protocol, the evoked response for each frequency can be measured. Moreover, two-photon imaging allows the measurement of several neurons at the same time, while maintaining a single cell resolution. All recordings shown in this section were made on layer 2/3 neurons

from an anaesthetized auditory cortex. In total, 7 mice were injected with the viral vector for YC-Nano140 calcium indicator and implanted with a cranial window, out of which 2 mice were also used for behavior experiments, after assessment of the frequency tuning described in this section.

Figure 3.5 (A) shows example traces recorded with two-photon calcium imaging. Each trace shown is a different neuron and the top row (in gray) shows the neuropil. Typical stimulus-evoked transients can be seen, which usually have an amplitude from 10% to 50% $\Delta R/R$. Three neurons have been selected as example neurons, marked in red, green and blue. The peri-stimulus average (B) shows the time course of the average response of the neurons for 20 repetitions of the same frequency. A typical shape of calcium transient with a faster rise time and a slower decay time can be observed for all 3 neurons. The location of the imaging field (C, left) and the two-photon field-of-view (C, right) give an overview of the number of neurons recorded.

The peri-stimulus average is extracted for each stimulus frequency for the 3 example neurons in the heat maps of panel (D). The 3 example neurons show a higher evoked response for the stimulation frequency at 19.6 kHz, suggesting that they might be tuned for this specific frequency. Neuron 11 also shows a secondary peak around 8 kHz. Furthermore, only a few frequencies do not evoke visible response in the selected example neurons. All 3 neurons have their response onset around 0.5 seconds after stimulus onset. These evoked response are further analysed in the following figures.

Exploration of different methods for extracting frequency tuning curves

Different analysis methods can be used to establish the frequency tuning of single neurons. Figure 3.6 shows different approaches to quantify tuning using the recorded calcium traces. The presented approaches are not an extensive list, but give an overview of the types of analysis that can be done on such data. All the approaches presented are made to characterize the tuning of a single neuron at a time. Also note that all of the approaches presented here have been implemented using the analysis framework presented at the end of this result chapter (see `Analyser` module section).

Generalized Linear Model (*GLM*) is the first approach presented in Figure 3.6 (A). In a simplified summary, a GLM is trying to predict a *response* vector from the linear combination of a set of *predictor* vectors, with each predictor having a *coefficient* describing how much it contributes to the response vector. In other words, it is combining the *weighted* predictor vectors into the response vector. In the case of predicting the frequency tuning of a single neuron, the *response* vector is the measured calcium trace, the *predictors* are the convolved stimulus vector for each frequency and the *coefficients* are the tuning value for each frequency. The convoluted stimulus vector are obtained by convolving the stimulus vector of each frequency with a kernel, in this case the average

neuropil transient. Then the GLM will optimize each coefficient in order to predict as good as possible the calcium trace from the convoluted stimulus vectors. The output of the GLM is on one side the coefficients, which are directly used as a measure of tuning for each frequency, and on the other side the model, which can be compared to the actual trace to see if the prediction is good or not.

Another simpler approach is presented in Figure 3.6 (B). Using the known stimulus times for each frequency, it is possible to generate a peri-stimulus average of the calcium trace for each frequency for a single neuron. The average traces usually shows a typical response transient, with an increase in measured amplitude after the stimulus. A time window where the transient is peaking is determined as the *evoked response*. The data points from this evoked response should then be reduced to a single value in order to build the frequency tuning curve for the neuron. At this stage, several methods can be used to reduce the dimensionality of the evoked response data points into a single number. Here two approaches, the *mean* and the *maximum* are presented. Many other possibilities exist, like the sum, the 3-point-peak average, the 3-point-peak-maximum, etc. Nevertheless, taking the maximum or the average of the evoked response is usually a robust method to quantify the evoked response in a representative way.

The last approach presented in Figure 3.6 (C) is to quantify the *response probability* of a neuron for each frequency. Although this approach is a bit different as it disregards the variability of the response's amplitude, it can nevertheless be seen as a valid method to assess the preference of a neuron for one or another frequency. A simple test is run on each stimulus presentation (also called *trial*) for a single frequency and the determines whether that response is a *true* response or not. The test can either be a statistical test like a `t-test`, a d' sensitivity index with a threshold or even just a difference with a threshold. In the example from Figure 3.6 (C), a d' index was calculated for each trial and a threshold of 4 was chosen. Once every response is categorized as *true* or *false* response, the response probability can be calculated as the ratio between *true* responses and the total number of response. This ratio is then referred to as the response probability, and as it can be calculated for each frequency separately, it can be used to create a tuning curve for the neuron.

Figure 3.6 (D) shows the tuning curves obtained with the different methods. The tuning curves of each method has a different unit and range, therefore all curves where normalized to an interval between 0 and 1 (minimum and maximum). All the curves agree on the best frequency for this example neuron by having the highest peak at the 22.6 kHz frequency. The two curves that are the most similar are the *mean* and *max. evoked response* curves, which is not surprising given the similarity in the two approaches. The *Response probability* curve does not deviate very much in shape from the two previously mentioned curves, even though the response probability quantifies a moderately different aspect of the neuron's preference for frequencies. Finally, the GLM index

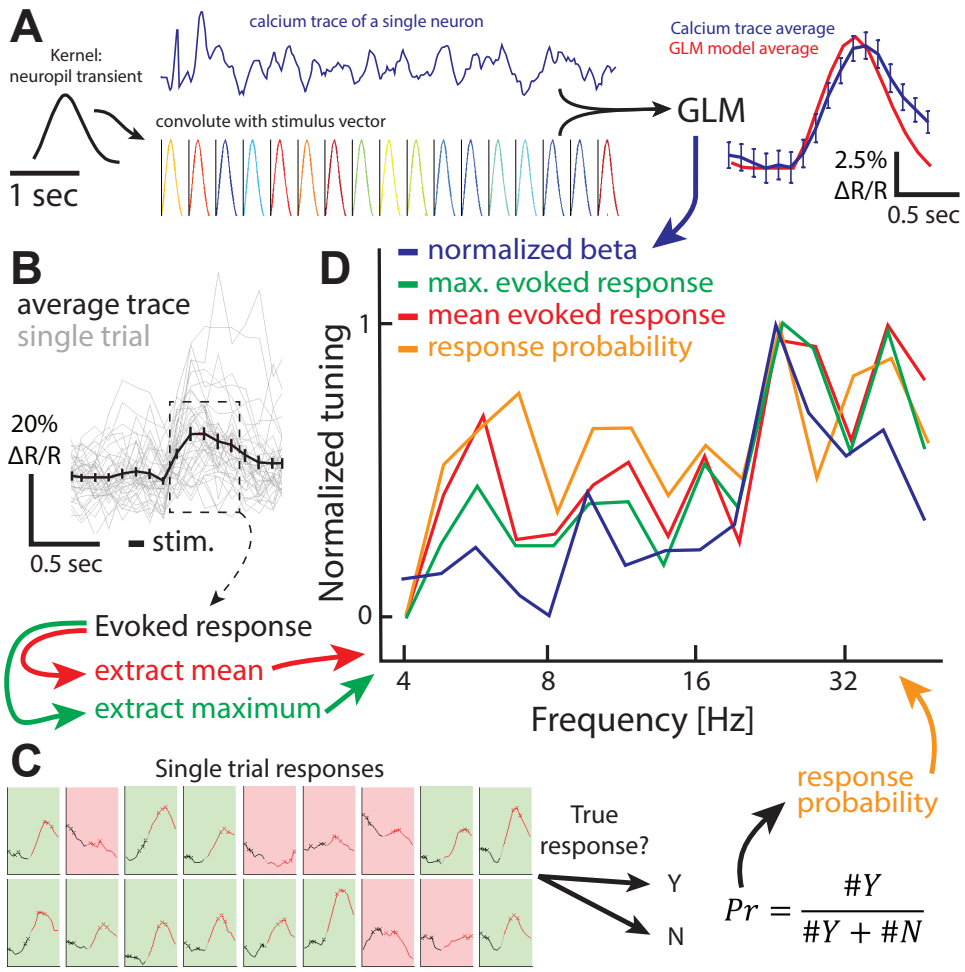

Figure 3.6: Frequency tuning analysis with different methods: (A) *Generalized Linear Model (GLM): a characteristic neuropil transient (left) is used as a kernel to convolve the stimulus onset time vector (middle). This convoluted vector is used in the GLM to fit the calcium trace for a single neuron. The GLM produces a fit that can be compared to the average of the actual data (right). The normalized coefficients of the GLM (one per frequency) are used to define a tuning curve for the neuron in d).* ***(B)*** *The single stimulus presentations (or trial, in gray) for one frequency are averaged (in black, error bars represent standard error of the mean (SEM)). The time points after the stimulus are referred to as the evoked response for that stimulus. The mean or the maximum of these evoked response time points can be extracted for each frequency and used to define a tuning curve for the neuron in d).* ***(C)*** *Each stimulus presentation (trial) can be tested for significance by comparing pre- and post-stimulus time points. The response probability is calculated as the ratio of true responses over the total number of responses. This response probability is used to define a tuning curve for the neuron in (D).* ***(D)*** *Normalized tuning curve for a single neuron using different methods. Each method's values are normalized to the [0, 1] range.*

also share similarities with the other curves, but it is the peak that differs the most. One of the main divergence is that the GLM-based curve, similarly to the maximum evoked response curve, only shows a single peak, meaning a single preferred frequency, whereas the other curves exhibit a first peak 6 kHz and then the main peak at 22.6 kHz. These peaks and mostly the main peak can ultimately be used to assign a frequency preference to a neuron. One should note here that this preferred frequency corresponds to the above described loose definition, as more commonly

used definitions exists, like the characteristic frequency *CF*, which is the frequency still responding to lowest stimulus intensity, or the best frequency *BF*, defined as the frequency eliciting the highest evoked response. Therefore, these approaches tend do describe a feature of the neuron similar to the best frequency. In conclusion, these different approaches provide a similar picture about the neuron's frequency tuning, although with some variability.

In the case were a clear peak can be seen, meaning that the neuron is relatively sharply tuned for a frequency, this tuning curve can be further analysed. The tuning width of the tuning curve can be assessed to obtain an information about the selectivity of the tuning for a specific frequency. This tuning width can for example be computed by fitting a Gaussian model to the tuning curve and extracting the full-width at half maximum amplitude. However for a good quality fitting, it is required that the neuron shows some degree of tuning, unlike the example data shown in the previous figures.

Spatial organization of tuning and responsiveness on the micro-scale

A great advantage of the two-photon imaging method over the electrophysiological methods is that two-photon imaging is an optical approach, therefore allowing to record simultaneously several tens or hundreds of neurons. These recordings can either be processed together to perform population analysis or as individual neurons. In the latter case, the output is the same as serially recording neurons with electrophysiology, but additional information can be gained as an *optical access* to the neuron exists. Therefore, the physical location of the neurons can be compared to either their firing activity, or the different tuning of the neurons, in order to detect any pattern in the spatial organization of these properties.

Each column of Figure 3.7 shows the spatial distribution of two different properties of neurons for a single day for two different imaging regions (also called *spots*). The two properties, *responsiveness* (A) and *tuning* (B), are color-coded and displayed in place of each neuron's location. The responsiveness for each neuron is quantified as the average evoked response for all frequency combined. The tuning for each neuron is quantified as the best frequency (frequency having the maximum responsiveness), which in this case corresponds to the frequency with the highest mean evoked response.

The next section will compare days to each other and see how these two properties evolve over time. First, let us consider each day separately (one column at a time). Neither of these properties show a clear pattern in their spatial distribution on this scale. Highly responsive neurons are not grouped together or distributed in an regular pattern (A). The tuning of all neurons is relatively similar on the first day but no visible gradient can be observed on this micro-scale. Each field-of-view is a square of about ~200 µm side.

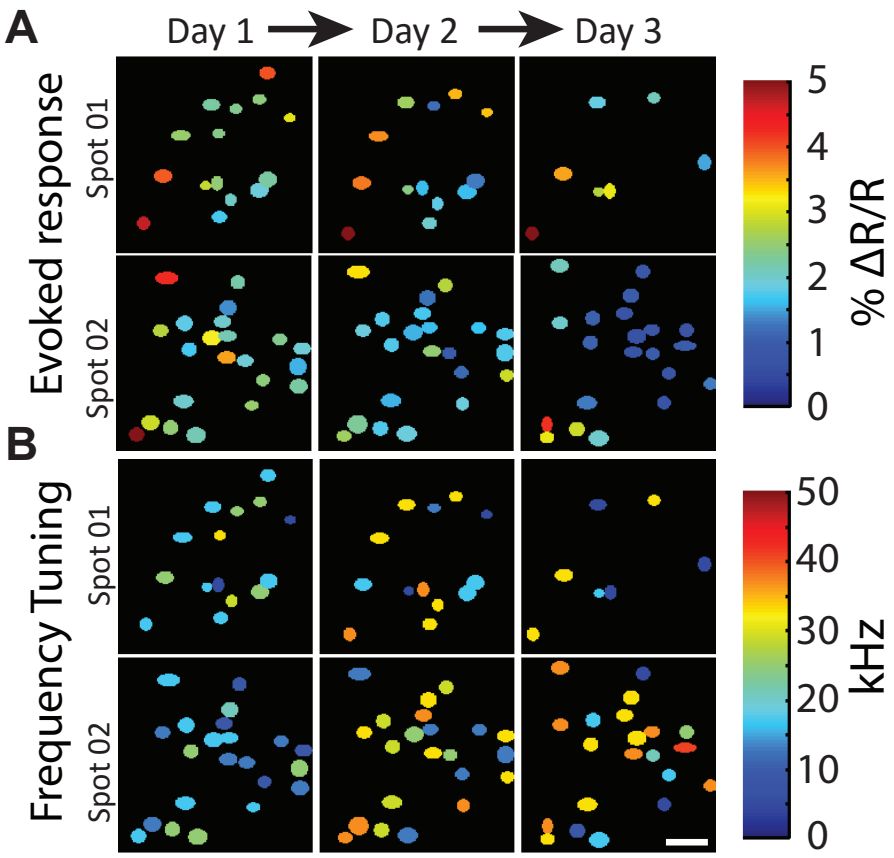

Figure 3.7: Spatial maps of responsiveness and tuning: ***(A)*** *The two top rows show the color-encoded responsiveness of each neuron from two different imaging regions (*Spot *01, top row and* Spot *02, bottom row) on 3 consecutive days of imaging. Evoked response for each neuron was assessed by two-photon calcium imaging across many different frequencies.* ***(B)*** *The two bottom rows show the color-encoded frequency tuning of each neuron from the same two imaging regions as in (A) on the same 3 consecutive days. Tuning for each neuron was assessed by two-photon calcium imaging. Scale bar:* 50 µm.

Stability of tuning and responsiveness over time

A great advantage of using two-photon microscopy with a chronic glass window implantation is that the *same* set of neurons can be imaged in a repeated manner over weeks or even months. Therefore, it is possible to record the activity of the same neurons for several time points and compare properties of neurons over time. An example of this method is shown in Figure 3.7. The same imaging region (or *spot*) was imaged over 3 consecutive days. The 2 example properties of neurons described above, responsiveness and tuning, were assessed on each day separately. It is then possible to compare these properties over these 3 days and assess their stability over time. Note that not every neuron could be found on every day and this leads to the picture not being exactly the same on each day for a given imaging region. Indeed, some neurons disappear from the field-of-view while other can be newly found. This is mainly due to the technical difficulty

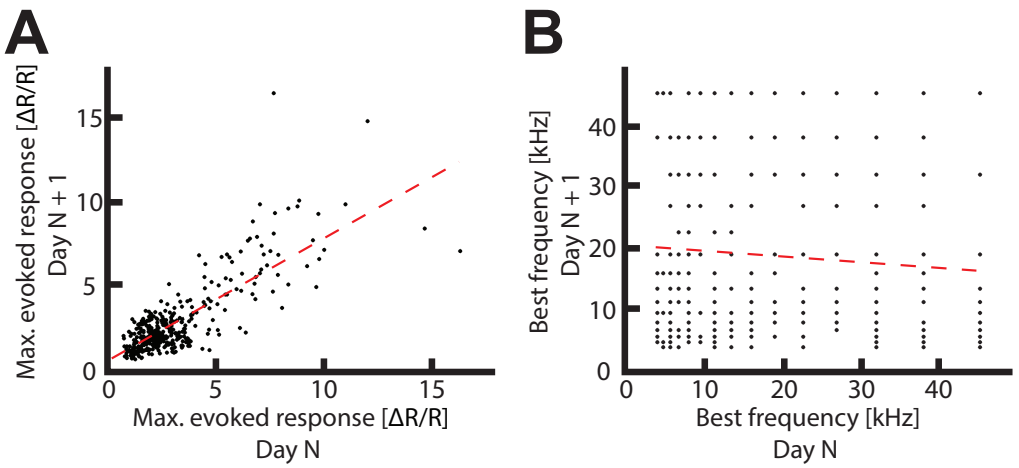

Figure 3.8: Stability of responsiveness and tuning across days: (A) *Relation between the maximum evoked response (amplitude of response) on one day and on the following day. Data is pooled across 9 days and for the same set of 20 neurons.* $r^2 = 0.582$. ***(B)*** *Relation between the frequency tuning (best frequency) on one day and on the following day for the same data set as in (A).* $r^2 = 0.008$.

of having exactly the same imaging view and focus plane on every day, as the brain is a relatively flexible tissue and perfect realignment can be challenging.

Regarding the responsiveness (A), it seems that for the first spot (top row), a number of neuron with similar responsiveness can be found on consecutive days, even though some neurons do change their responsiveness. Therefore the responsiveness property could be qualified as relatively stable over time. The second spot (second row) shows a slightly different picture as most of the neurons are lowly responsive. General responsiveness seems also to decrease over time in this spot.

Regarding the tuning (B), it seems that for both spots, almost each neuron changes its preferred frequency, sometimes in a dramatic way (from 10 kHz to 50 kHz in one day). Therefore one could conclude to a relative instability of the tuning property of these neurons. An alternative explanation is that the measure of the tuning was too noisy to be compared across days. It must be noted here that all neurons have been selected to display, even the neurons with lower overall responsiveness. By comparing selected neurons, it does not seem that highly responsive neurons would have a more stable tuning, although this was not quantified.

To better compare the stability and change over days of the neurons' tuning and responsiveness properties, a so called *N versus N + 1* analysis is shown in Figure 3.8. The responsiveness of a single neuron on one day (day *N*) is plotted against the responsiveness on the next day (day *N + 1*)(A). This shows the evolution of the responsiveness over time for the whole population pooled together. The same is done for the tuning property (B). Regarding the responsiveness, a relative high stability can be seen over time, as the data points fall close to the diagonal line and the slope

of the fitted line is close to 1, with an r^2 of 0.582 (A). In other words, neurons that had a low responsiveness on one day mostly kept being lowly responsive on the next day, and the same is true for highly responsive neuron that mostly remained highly responsive on the next day. This is quite different for the tuning property of the neurons (B). The data points are mostly arranged in a random way, showing no correlation between the tuning on one day compared to the next day. The slope of the fitting curve is almost 0 and the r^2 is 0.008. In conclusion, no or little stability could be seen for the tuning of neurons at this scale and in these recording conditions. However such a lack of stability could also be seen in the case where the recording method is not sensitive enough. It should be noted that lowly responsive neurons might also be actually silent, with the responsiveness coming from noise in the recording method.

3.2.4 Mapping tonotopy in auditory cortex with wide-field calcium imaging

As mentioned earlier, topographical features of the auditory cortex have been quite extensively described before in the literature. Most importantly, a tonotopic map was described to exist in the different parts of the auditory cortex. This tonotopic map consists of several gradients in the tuning preference of neurons, each gradient along a defined axis, from a low-frequency tuned to a high-frequency tuned region. The position of these gradients compared to each other can also be of use to locate the different parts of the auditory cortex, like the anterior auditory field (*AAF*), the primary auditory cortex (*A1*) or the secondary auditory cortex (*AII*). These gradients were however described to exist mainly on a meso- or macro-scale, and be absent on smaller scales, like the one measured in the previous section with two-photon imaging. Therefore, in order to measure tonotopy on larger scales than what can be achieved using two-photon imaging, another approach is required to assess the meso-scale spatial organization of the auditory cortex in terms of frequency tuning. The method I used to access to the meso-/macro-scale view of auditory cortex was wide-field calcium imaging, using a simple camera and one-photon excitation. The results of two different paradigms combined to this recording technique are presented in the current section: the *standard* mapping approach and the *Fourier imaging* technique.

The *standard* mapping approach

Standard mapping consists of a basic sequential stimulus presentation with long inter-stimulus intervals, followed by simple averaging for each frequency separately. This approach is similar to the paradigms used for the two-photon calcium imaging or the electrophysiology as described earlier. However in the case of calcium imaging, decay times of the measured calcium signals are much slower compared to electrophysiology. Therefore, longer inter-stimulus times are required to

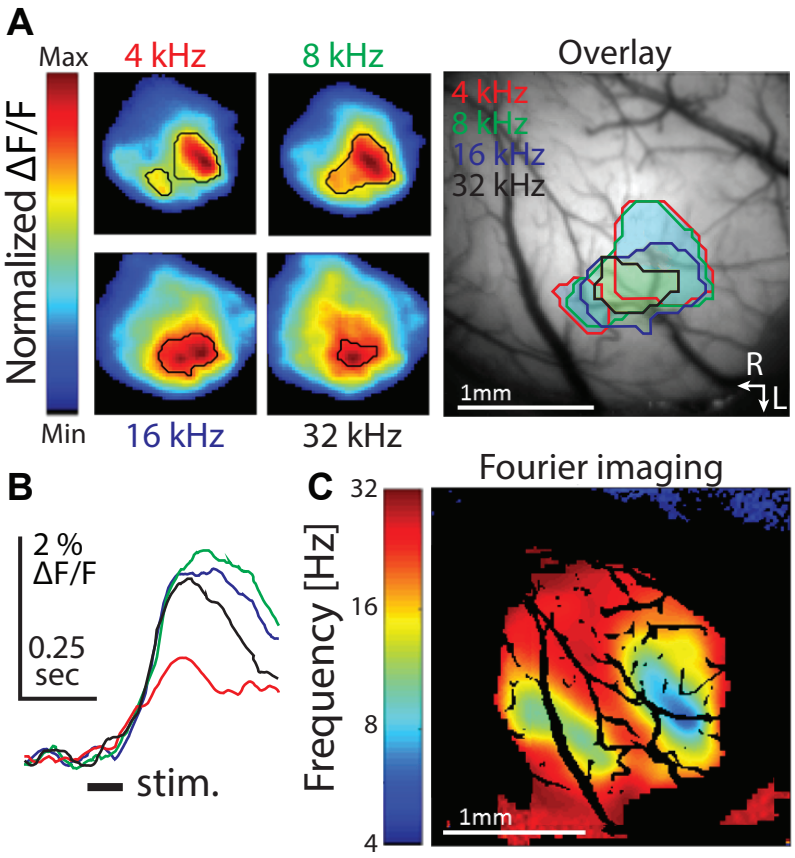

Figure 3.9: Mapping the auditory cortex using wide-field calcium imaging: (A) *Left: Average response maps for 4 different frequencies recorded with wide-field calcium imaging (N = 30 repetitions, each map is normalized independently). Right: overlay of the thresholded response maps on the blood vessel pattern. Scale bar:* 1 mm*; **(B)** Peri-stimulus average time course for the thresholded Region-Of-Interest of each frequency (N = 30 repetitions). **(C)** Frequency map derived from the phase map of the Fourier imaging method. Field-of-view and scale are the same as the overlay in (A). Abbreviations:* R *rostral;* L *lateral.*

avoid overlap between stimulus responses.

The upper panel (A) of Figure 3.9 shows the typical frequency maps that can be obtained with the standard paradigm. In the presented example, 4 different frequencies were used to create a rather coarse tonotopic map of the auditory cortex. The left side shows the activation response maps for the 4 different frequencies. Response maps were recorded from anaesthetized mice (N = 4 animals), through a cranial window that was centered on auditory cortex's coordinates. Each frequency's response was normalized to compare activation patterns and location rather than absolute activation amplitudes. Contours have been defined for each frequency by thresholding the maps to extract the peak activation regions. By comparing the contours of each frequency, a gradual displacement of the activation can be seen towards the location of the highest frequency contour (32 kHz) when increasing the frequency. Moreover, the two activation zones defined with the two contours on the lower frequencies seem to merge back into a single activation region for

the higher frequencies.

In the overlay picture on the right side, the overlap and relative position of each contour can be seen. The activation patterns shows the presence of two low-frequency regions and a single high-frequency region. This suggests the presence of two gradients, each going from the center of a 4 kHz region to the center of the 32 kHz region. This tonotopic map defined as two gradients going from anterior to posterior and from posterior to anterior is consistent with the tonotopic maps described before (Stiebler et al., 1997). The two gradients would then correspond to AI's (caudal, right) and AAF's (rostral, left) tonotopic gradient. The tonotopic map defined by these activation patterns will be compared in the next section with the tonotopic map obtained with the Fourier imaging. The extended high-frequency region (Figure 3.9, C, in red) is possibly an artefact of the Fourier imaging. It should be noted here that the color-code association is based on the *phase* of the response component at the stimulation frequency, irrespective of the *power* at this frequency. Therefore it is possible that the region in red is responding at the same *phase* as the high frequency sound presentation, but with a very lower *power*.

In the the panel (B) of Figure 3.9, the time profile of the response for each frequency is shown. Although the frequencies show different evoked response amplitude, the time courses are relatively similar. The activation for the 4 kHz sound is smaller (~1.5% ΔF/F) compared to the other frequencies (~2.2% ΔF/F) but its peak time is very similar (~0.25 seconds from stimulus onset). The amplitude of these calcium signals are typically smaller than the calcium signals that can be recorded from single neurons using two-photon imaging, as the region that is averaged is very large compared to a single neuron's somata. However, the temporal dynamics are relatively similar, even though many neurons' response is averaged in one wide-field contour, therefore *blurring* the signal to some extent.

Extracting continuous maps with *Fourier imaging*

As described before, Fourier imaging is a different paradigm of stimulus presentation, where the stimuli are presented in a relative quick succession, and with a specific stimulus feature being cycled through. A Fourier transform is then performed on the measured signal to extract the relevant response at the stimulation frequency. By looking at the phase of the signal at the stimulation frequency, one can extract the response for each stimulus feature separately. In the case of tonotopy mapping, the stimulus feature that is cycled through is the sound frequency. Therefore, by looking at the phase at the stimulus frequency, the sound frequency (in kHz) can be extracted.

An example result of such an extracted phase map is shown in Figure 3.9 (C). The phase map shown was converted to a sound frequency map in order to relate the phase measured and the sound frequency presented. The field-of-view presented is the same as the one shown in (A), in

order to be able to compare the two paradigms (*standard* versus *Fourier* imaging). Blood vessels and non-responsive regions are labelled in black. Non-responsive regions where defined using a threshold on the Fourier extraction's power at the stimulus frequency.

A very useful property of the Fourier imaging's phase-map based output is the continuous aspect of the extracted tonotopic map in terms of sound frequency. Indeed, since the sound frequencies where presented in a continuous fashion, there is virtually no limit in the number of discrete sound frequencies that can be used. This is translated to a smooth map going without noticeable '*steps*' from the low-frequency to the high-frequency region.

The example tonotopic map obtained via the Fourier imaging shows 2 or maybe 3 low-frequency regions, and a central high-frequency regions in the middle of these, creating therefore tonotopic gradients (axes) from the low to the high-frequency regions. When comparing this map with the one obtained with the standard imaging, the two low-frequency regions seem to be matching in their location, although the left low-frequency region (rostral) seems to be more extended with the Fourier imaging. In both maps, there is a high-frequency region in between the two low-frequency regions. The similarities between the two maps tend to confirm the shape and location of the tonotopic map from this animal. Furthermore and as mentioned before, the shape of this map shows some level of consistency with the maps described in the literature, where the two low-to-high gradients would correspond to AAF (rostral) and to A1 (caudal).

3.3 Learning-related changes in the auditory cortex

A good fraction of the results described above are relatively exploratory. They were however helpful and to some extent necessary to achieve the main goal of this thesis, which was to establish the two-photon calcium imaging in the auditory cortex in behaving animals. Following that, the aim was to study the learning-related changes in the auditory cortex of awake behaving mice. The mapping experiments were required to functionally locate the auditory cortex and for the choice of the sound frequencies to discriminate. The analysis framework was the main tool used to analyse all the different complex data that resulted in the learning experiments described below.

I performed several rounds of behavior experiments during my thesis with different training paradigms and brain activity techniques. The results for each of these are summarized in the following sections.

3.3.1 Establishment of a simple frequency discrimination task

The first step to study the learning-related changes in the auditory cortex was to establish an auditory discrimination learning task with head-fixed mice (Figure 3.10, A). This was successfully

achieved using at first a simple learning paradigm with a single target sound frequency (12 kHz) and 4 different distractor frequencies (4, 8, 16, 20 kHz), in a go / no-go task with water rewards. The number of distractor frequencies was gradually increased from 0 to 1, and then from 1 to 4. Behavior output variables were measured for each animal that underwent this basic discrimination task. Two animals were trained for this simple frequency discrimination task, which were also used for the two-photon calcium imaging frequency tuning experiments described above.

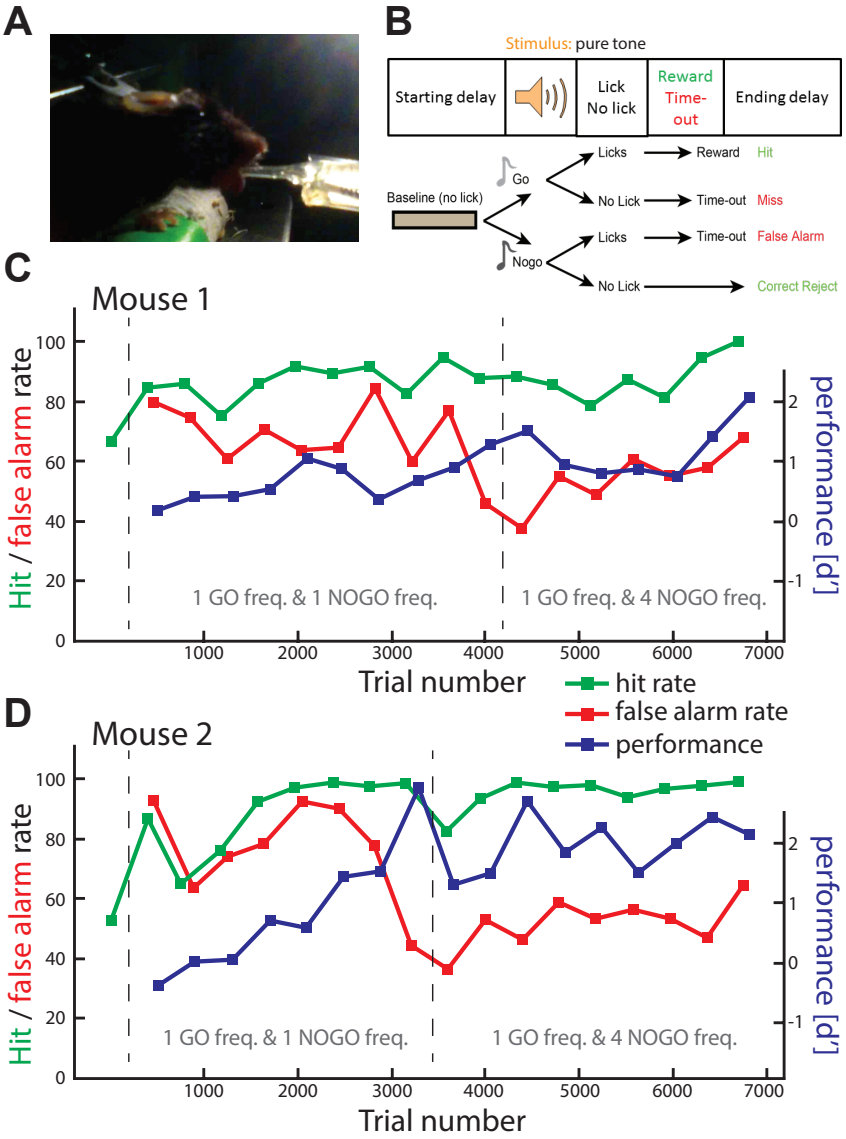

Figure 3.10: Behavior quantification for a simple auditory discrimination task: ***(A)*** *View of the head-fixed animal performing the discrimination task. Licking spout with licking sensor on the right.* ***(B)*** *Scheme of the stimulus paradigm and animal decision outcomes.* ***(C-D)*** *Behavior output quantification for the two animals. Left Y axis: hit rate (in green) and false alarm rate (in red). Right Y axis: performance as the* d' *selectivity index. Training paradigm: 1-frequency* go *detection task (left), 1-frequency* go *and 1-frequency* no-go *discrimination task (middle) and 1-frequency* go *and 4-frequencies* no-go *discrimination task. Sound stimuli were short 0.5 second long pure tones (target: 12 kHz, distractor: 4, 8, 12, 16, 20).*

To quantify the learning state of mice in the discrimination experiments and to get an understanding of their performance and behavior output, 3 main variables were quantified: the hit rate, the false alarm rate and the sensitivity index *d'*. They are all based on the outcome of each trial, which are categorized as hit, miss, false alarm and correct rejections (Figure 3.10, B).

The summary of the entire learning period for the two animals is shown in Figure 3.10 (C-D).

Mice typically achieved stable expert performance (*d'* >= 2) after ~6'000 - 7'000 trials over 5 - 10 days of training (2 sessions per day). A common feature of all trained animals was a high hit and false alarm rate at the training start, followed by a continued high hit rate but a progressive decrease in the false alarm rate as the animals reached expert levels. Typically, these animals were very motivated by the water reward and had to learn to refrain from licking.

The performance, measured as the sensitivity index *d'*, is steadily increasing, although with some fluctuation. It is a common feature in all animals that performance levels are not perfectly stable and animals can perform significantly worse in a session compared to the performance of the previous sessions. Moreover, changes in the training paradigm can temporarily decrease the performance. For example, switching from 1 to 4 distractor sound frequencies perturb the animals and performance drops until they adapt to the new conditions (Figure 3.10, D). Both trained mice reached expert performance level (d' >= 2.0, final d': 2.08 and 2.15) in this simple discrimination paradigm, showing that mice can promptly learn a simple goal-directed water rewarded discrimination task.

3.3.2 Chronic measurement of neural activity in awake behaving mice

Having successfully established that mice can learn simple sound discrimination tasks in a reasonable amount of time, the next step was to combine behavior and learning with neural activity measurement. The hypothesis was that it is possible to finds sets of neurons that change their representation of the sound during the learning. More specifically, the *Darwinian learning theory* states that most of the neurons should first be relatively unresponsive. In a second stage, many neurons would be recruited for the task by the learning process until a set of highly responsive neurons emerges, forming a network that can efficiently solve the task. This set of neuron would gain a higher information content as the learning happens, however the overall population would go back to a more silent state, to allow further tasks to be learned.

The previous learning paradigm was slightly modified to include only two sounds to discriminate. These sounds were *cloud-of-tones*, which provide a better control of the sensory discrimination difficulty and can potentially evoke higher responses in the auditory cortex. In addition, to address the *Darwinian learning theory* hypothesis described above, the learning period was divided in three main learning epochs: *naïve*, when the animal knows the task and the setup, but not the sensory discrimination, *expert*, when it just reached an expert level (*d'* >= 2), and *late expert*, when the animal is an stable expert level for a longer period of time and performance reached a stable level (no more sensory learning). Another set of 2 mice was trained on this task. Both animals readily learned the discrimination task in 10 - 15 days, after performing in 4'500 - 5'000 trials (final d': 3.88 and 3.90, Figure 3.11, A).

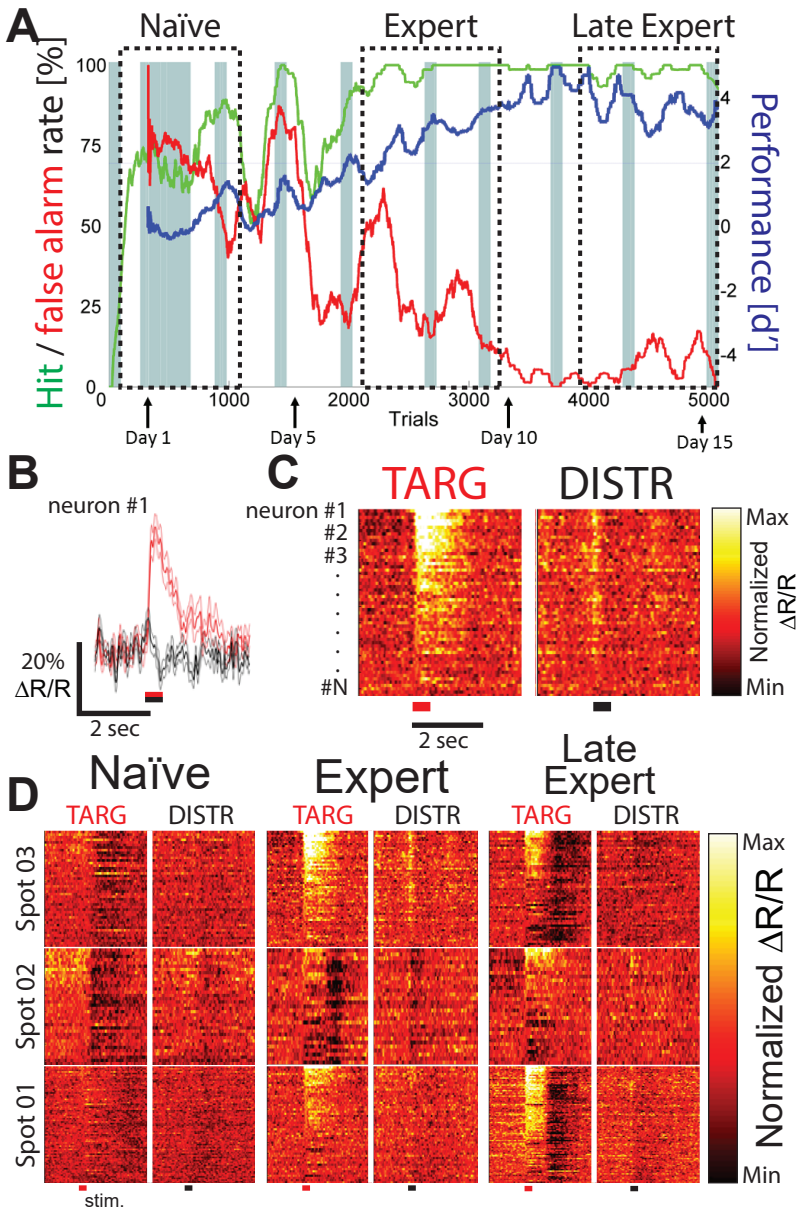

Figure 3.11: Chronic two-photon calcium imaging combined with frequency discrimination task: ***(A)*** *Behavior output quantification for an animal performing in a frequency discrimination task in combination with two-photon calcium imaging. The 3 parameters (hit rate in green, false alarm rate in red, and performance as d' in blue) are represented as running averages. Three epochs of learning are defined: naïve, expert and late expert. Blue background rectangles represent trials with combined two-photon imaging.* ***(B)*** *Example peri-stimulus time average for both sound (target, red; distractor black) for a single neuron recorded in layer 2/3 during the expert epoch. Cloud-of-tones sound stimulus time and duration (0.5 seconds) are shown at the bottom (red and black bars).* ***(C)*** *Peri-stimulus time heat maps for an example imaging region (spot 01) during the expert epoch. The trials of each epoch are divided in 2 types: target sound (TARG, left) and distractor sound (DISTR, right). Each row of the heat map represents a single neuron.* ***(D)*** *Peri-stimulus time heat maps for 3 different imaging regions (spot 01-03) in a single animal for 3 imaging sessions, one in each learning epoch (naive, expert, late expert).*

The activity of the neural networks in auditory cortex was assessed by two-photon calcium imaging, as it is the technique of choice to measure the individual activity of a large number of neurons simultaneously. Imaging was performed in several sessions during the training paradigm, and regrouped in the three learning epochs described above. In each imaging session, the neuronal activity was measured in the same set of neurons for each mouse. The measured neurons were always located in the 2/3 of the auditory cortex. Activity was averaged for all the correct trials of a session and separated into hit and correct rejection conditions, corresponding to the target and distractor sound respectively (Figure 3.11, B).

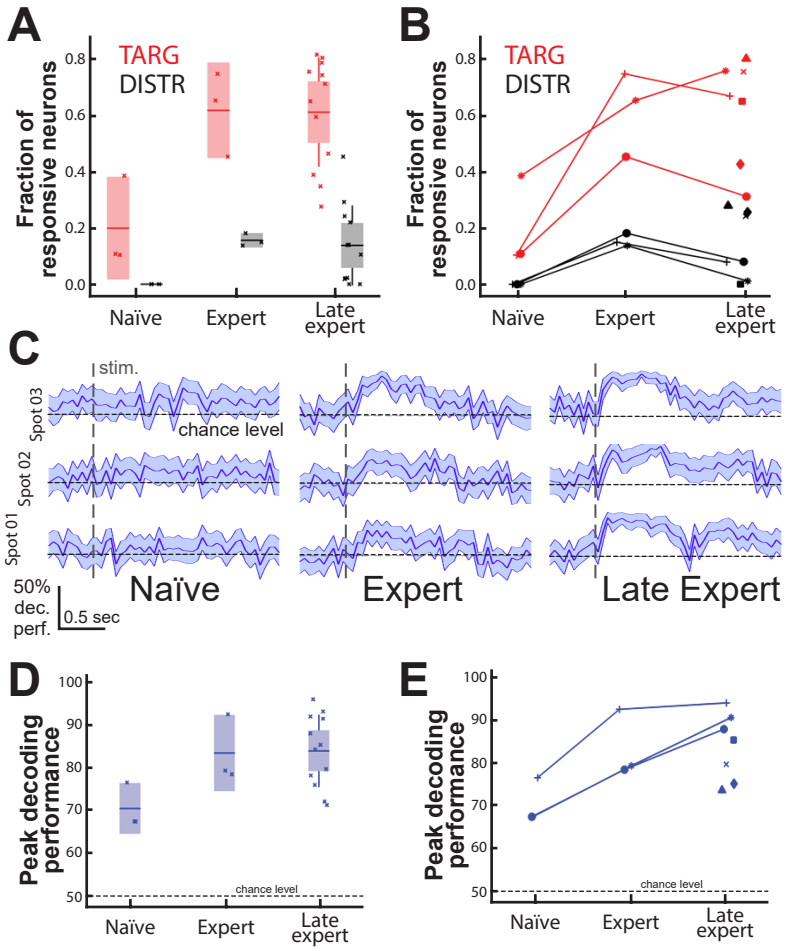

Figure 3.12: Population response fraction and population decoding: ***(A)*** *Fraction of responsive neuron for a same imaging regions recorded during the 3 epochs (N = 12 regions, 3 recorded at all epochs), quantified separately for target (red) and distractor sound. All imaging regions belong to the same example mouse* ***(B)*** *Same data as (A), highlighting the chronically imaged regions. Data points linked by a line are from the same imaging region (same neurons).* ***(C)*** *Decoding performance of a Bayesian classifier separating target from distractor trials. 3 imaging regions and 3 epochs are shown. Horizontal dashed line marks chance level (50%), vertical dashed line marks stimulus sound onset.* ***(D)*** *Peak decoding performance for the imaging regions in (A).* ***(E)*** *Same as (D), highlighting the chronically imaged regions. Data points linked by a line are from the same imaging region (same neurons)*

In the *naïve* condition, both sounds, target and distractor, evoked very little activation or even in some cases a suppression of activity (Figure 3.11, B left). After learning the sensory task (*expert* epoch, Figure 3.11, B middle) a large response for the target fraction appears in a good fraction of the neurons. The distractor sound also shows a response that is bigger than in the *naïve* condition, but much smaller than the response of the target sound. Some variability exist between the different imaging regions (*Spots*), Spot 02 being less responsive overall compared to Spot 01 and 03. Finally in the *late expert* epoch, the fraction of neurons still showing a large response to the target sound decreased compared to the *expert* condition in Spot 03 (Figure 3.11, B right). Additionally, responses to the distractor sound seems to have disappeared. Both Spot 01 and 03

show a relatively large suppression of activity after the initial activation in response to the target sound.

The results of the 3 example imaging regions described above are summarized together with additional data points in Figure 3.12. Pooled data analysis confirms that the fraction of responsive neurons increases from *naïve* to *expert* both for the target and the distractor sound (Figure 3.12, A). The fraction of responsive neurons does not show an average decrease between the *expert* and *late expert* epochs (Figure 3.12, A). However, individual spots show a tendency to decrease in the fraction of responsive neurons in the *late expert* epoch compared to their *expert* epoch fraction (Figure 3.12, B). This temporary increase trend is more visible in the fraction of responsive neurons for the distractor sound (Figure 3.12, B in black).

To better describe the learning-related changes happening in the measured neuronal networks, information content of the measured populations was assessed by using a Bayesian decoding approach. A Bayesian classifier was created using all the measured neurons for one imaging region. The classifier was then trained on a subset of trials to predict whether each trial was a target or distractor trial. The classifier was then used to classify the remaining trials and a classification performance was calculated by comparing the prediction with the actual trial type. Classification was done either on the whole trial or for each time point.

Decoding performance improved for all 3 example imaging regions over the 3 learning epochs, with the decoding performance improving only after stimulus onset (Figure 3.12, C). The same classification analysis was performed on all the recorded imaging regions. Pooled data analysis shows a similar increase between *naïve* and *expert* epochs and a stable classification performance between *expert* and *late expert* (Figure 3.12, D). Analysis of individual imaging regions reveals that even though the fraction of responsive neurons decreased in the later epoch of learning (Figure 3.12, B *late expert*), the information content remained high as the decoder's performance remained stable (Figure 3.12, E). Taken together, these results suggest the emergence of a smaller number of highly informative neurons.

3.3.3 A delayed discrimination task to control for movement artefacts

A potential problem of the previous behavior paradigm was that expert mice learned to report their response very quickly, almost immediately after the sound onset. Their licking behavior for reporting a target sound interfered with the sensation period during which they were hearing the sound. Movement artefacts could be seen during the sensation period, interfering with the measurement of the auditory cortex's response to the sound.

To avoid this problem, the trial time-line was modified and a short delay period introduced after the sound onset. In addition, the licking spout was removed from the licking range and only

approached after the delay period, forcing the animals to wait before being able to report their decision. A set of 4 mice was trained on this task. All mice could learn this task in 10 to 15 days and became expert after ~1500 to ~3000 trials (final d': 2.49, 3.55, 2.93 and 3.04; Figure 3.13).

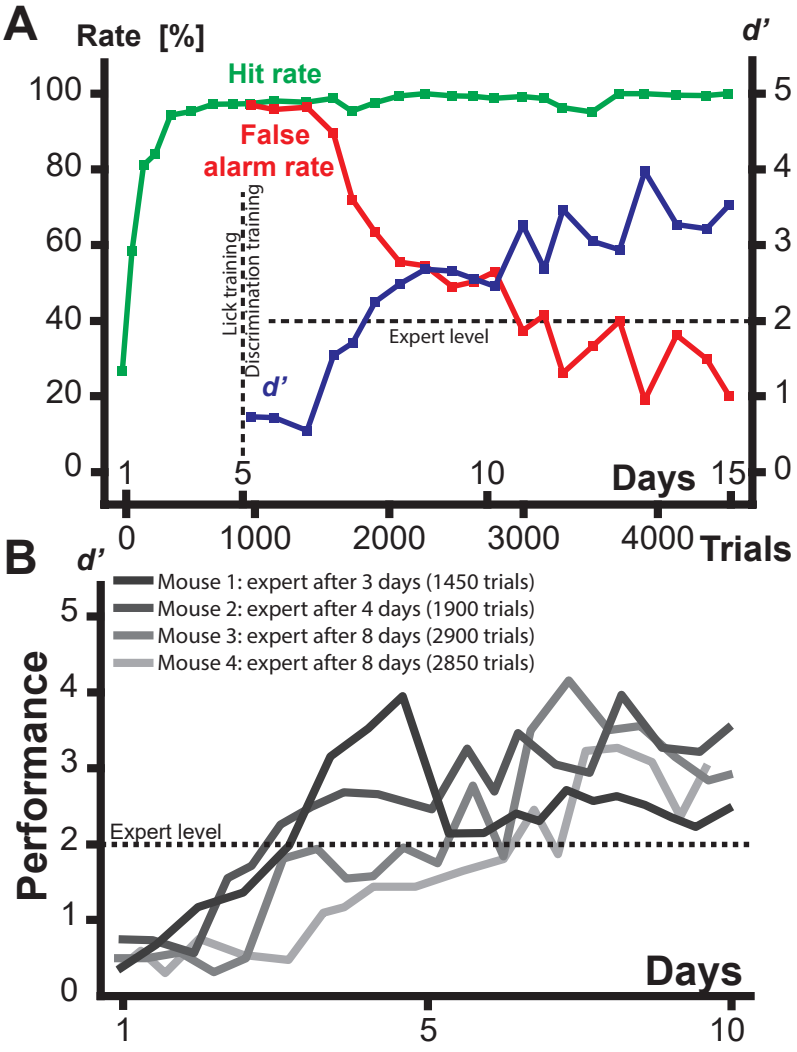

Figure 3.13: Behavior performance quantification for the go / no-go behavior: (A) *Behavior output quantification for an example animal that performed in the delayed go / no-go behavior combined with two-photon calcium imaging. Hit rate (green) and false alarm rate (red) as percent of total trials and performance as sensitivity index (*d'*, blue) are shown for mouse 2. After 7 days of discrimination training (12 total days), discrimination performances reaches* d' *= 4, with sessions containing more than 60 trials without a single mistake.* ***(B)*** *Performance is shown for the 4 animals used in this experiment. Animals 1 and 3 had the low cloud-of-tone as target sound, whereas animals 2 and 4 had the high cloud-of-tone as target sound.*

The previously described learning epochs were also analysed to address the *Darwinian learning* hypothesis, with an additional *baseline* epoch, measured before the animals were ever exposed to the task (non-engaged condition). A batch of 4 mice was trained, combined with two-photon calcium imaging measurements in layer 2/3 neurons of the auditory cortex. The same set of neurons were monitored for each animal over the whole learning period (Figure 3.14, A). Raw traces and peri-stimulus time averages were extracted for each neuron and analysed on a per-neuron basis (Figure 3.14, B and C). Neurons showed a great range of variability in their response compared to each other, but also when compared across different days. Neurons could either gain or lose in

response amplitude to either the distractor or the target sound without any particular trend observable on the single neuron level.

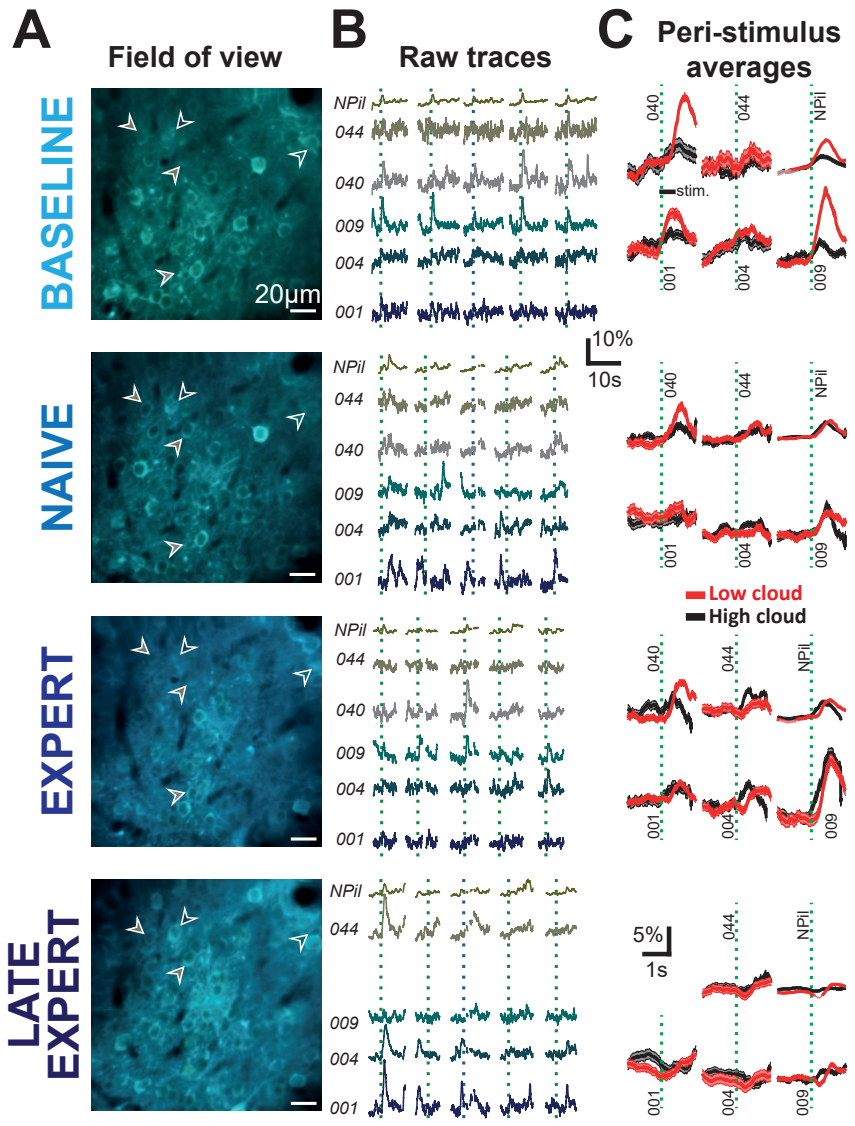

Figure 3.14: Calcium traces and averages for neurons from the go / no-go behavior: (A) *The same example field-of-view, at the 4 different learning epochs, located in layer 2/3 of A1.* ***(B)*** *Example traces from the same neurons imaged chronically throughout the 4 learning epochs. Savitzky-Golay filtering for display.* ***(C)*** *Peri-stimulus time averages for the neurons in (B), averaged either for the response to the low or to the high cloud-of-tones sound stimulation (N = 15-30 trials). Low cloud (in red) is the target sound in this example.*

To see whether the combination of all neurons' response showed some consistent change over days, peri-stimulus time averages for all neurons within an imaging region were pooled together for each sounds (target and distractor) separately (Figure 3.15, A). Sound-evoked responses were visible in almost every neuron, however with some expected variability in the amplitude of the responses. The first observable change over the learning period was a reduction in the response amplitude and in the fraction of responsive neurons. Indeed, a reduction in the number of responsive neurons and in the responsiveness of the neurons could be seen between the *expert* and *late expert* epochs (Figure 3.15, A). Moreover, the neuronal response onset time to the auditory

stimulation also increased over the learning period, changing from ~0.1 second after sound onset in the *baseline* and *naïve* epochs to almost 0.7 seconds after sound onset in the *late expert* epoch. This shift in response time is further examined further below.

Peri-stimulus time average responses were also separated according to the behavior outcome (hit versus correct rejection and correct versus false decision, Figure 3.15, B). The same reduction of responsiveness between *expert* and *late expert* was visible, irrespective of the grouping of the trials. These observations were quantified as distributions for the responsiveness of the neurons (Figure 3.15, C top). As described before, responsiveness decreased over the time course of the learning, reaching very low levels at the late expert state.

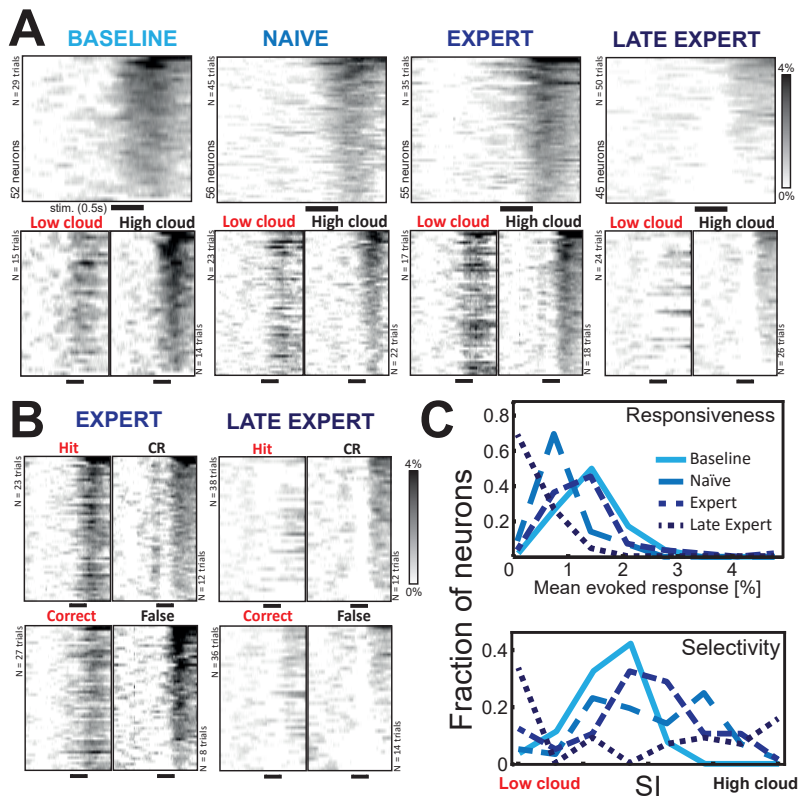

Figure 3.15: Responsiveness and selectivity of neurons during a go / no-go behavior: ***(A)*** *Peri-stimulus average responses for a population of neurons, grouped according to the sound type: low vs. high cloud-of-tones) Each line represents the trial-averaged response for one neuron. Neurons are sorted according to the mean evoked response for the high cloud response. Black bars show the sound stimulation (0.5 seconds duration).* ***(B)*** *Same as (A) but trials are grouped according to the behavioral decision: response (go vs. no-go) or outcome (correct vs. false). Low cloud (in red) is the target sound in this example.* ***(C)*** *Quantification of the responsiveness and sound preference for the neuronal population shown in (A) and (C) at all 4 learning epochs. Responsiveness is defined as the mean evoked response and sound preference as selectivity index (*SI*).*

The preference for either the target or the distractor sound was also examined using the selectivity index `SI` (Figure 3.15, C bottom). Neurons as a population showed very little preference at the start of the training for either sound (SI curves centred close to 0). In the *late expert* epoch however, the selectivity index shifts largely to the target sound's direction.

The *Darwinian learning* hypothesis predicts that after the formation of a stable circuit of neuron that can represent the task in a reliable way, unused neurons should revert to a more silent state.

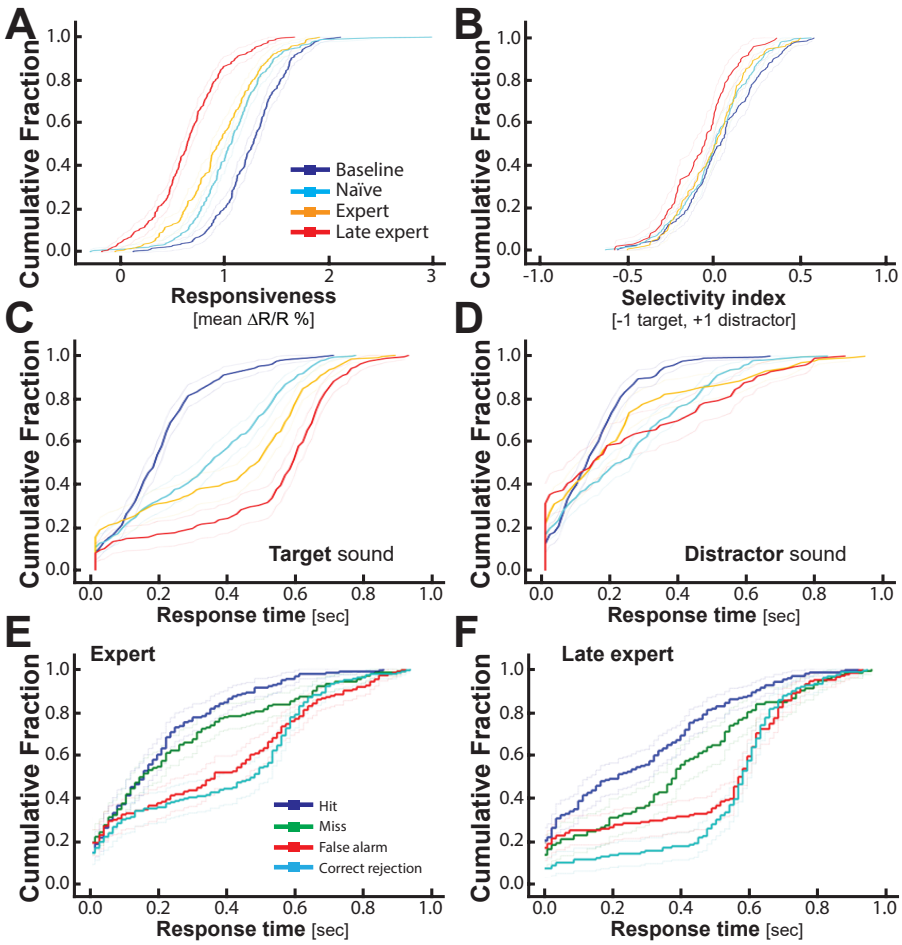

Figure 3.16: Pooled population analysis for all mice of the go / no-go behavior: (A) *Cumulative distribution of responsiveness of all neurons for the 4 learning epochs (N = ~990 neurons, N = ~800 trials, N = 4 mice, responsiveness as the mean evoked response).* ***(B)*** *Cumulative distribution of sound preference as the selectivity index for either the target or the distractor sound. Same data set as (A).* ***(C)*** *Cumulative distribution of neuronal response time for the response to the target sound. Neuronal response is defined as the time to reach half of the maximum evoked response. Same data as (A).* ***(D)*** *Cumulative distribution of neuronal response time for the distractor sound. Same data set as (A).* ***(E)*** *Cumulative distribution of neuronal response time in the* expert *phase for the 4 different trial types. Same data set as (A).* ***(F)*** *Cumulative distribution of neuronal response time in the* late expert *phase for the 4 different trial types. Same data set as (A).*

To test this hypothesis, the overall responsiveness of all measured neurons was pooled together and examined (N = 4 mice, ~990 neurons). Cumulative distribution shows that there is a reduction in the fraction of responsive neurons in the *late expert* epoch (Figure 3.16, A).

To determine what stimulus the neurons preferentially responded to, selectivity index (`SI`) was calculated for the target versus distractor sound conditions. Neurons did not generally show a great preference, but over the course of the learning, neurons showed a tendency to prefer the target sound over the distractor sound (Figure 3.16, B).

A unexpected effect of the learning was the delaying of the neuronal response time. Neuronal response time was defined as the time to reach half of the maximum response amplitude. Pooling

together the individual response time of each neuron, a strong shift towards longer response time can be observed over the course of the learning. This effect is however only present for the target sound (Figure 3.16, C) but not for the distractor sound (Figure 3.16, D).

The response time was also analysed more precisely in the *expert* and *late expert* epochs (Figure 3.16, E and F). Neuronal response times were separated according the trial's outcome. In the *expert* epoch, a shorter response time can be seen for *hit* and *miss* trials (target sounds) compared to the *false alarm* and *correct rejection* trials (distractor sounds). The same can be observed in the *late expert* epoch, although the differences are not as clear and the overall response time is shifted to longer response times.

3.3.4 Long-term calcium imaging caveats

To further confirm the previously described results, another set of 5 mice were trained on the same task with the same conditions. In addition, the aim was to prolong the experiment for a longer time in order to potentially see a further diminution of the responsiveness described above.

In this batch, 5 animals were trained for the same sound discrimination task. Animals were trained in shorter training sessions (less trials) and the protocol was changed from a continuous training to a *5/2* schedule with 5 days of water scheduling followed by 2 days of *ad libidum* water. These changes prolonged the time required for the animals to successfully learn the task (from ~25 days to almost 50 days) and 3 out of 5 mice never learned the task (final d': 2.20, 3.44, 0.58, 1.00, 0.70; Figure 3.17, A-C).

Unfortunately a major problem appeared in this data set, which prohibited to examine the neuronal responsiveness. Due to the prolonged training time, neurons showed signs of toxicity or photo-damage. As many imaging sessions were performed to continuously monitor the activity in the neurons, it is possible that the neurons suffered from the prolonged laser exposition time. Another possibility is that the viral injection used for the introduction of the calcium indicators showed its limit in terms of the possible duration of imaging. Since the virus was present in the neurons for a very long time (almost 2 months), it is possible that the neurons suffered unrepairable damage.

The damages to the neurons described above resulted in the slow disappearing of the neurons over the time course of the learning, either from apoptosis or from the disappearing of the calcium indicators from the cells. The overall number of neurons that could be measured and the conserved number of neurons decreased dramatically until only an extremely reduced number remained (Figure 3.17, D and E). These problems prohibited the proper analysis of this data set, which then could not be used to confirm or repeat the previously described findings.

In summary, several mice could learn different variations of discrimination. The learning paradigms were changed to adapt to the potential problems that arose in each batch of mice. First, move-

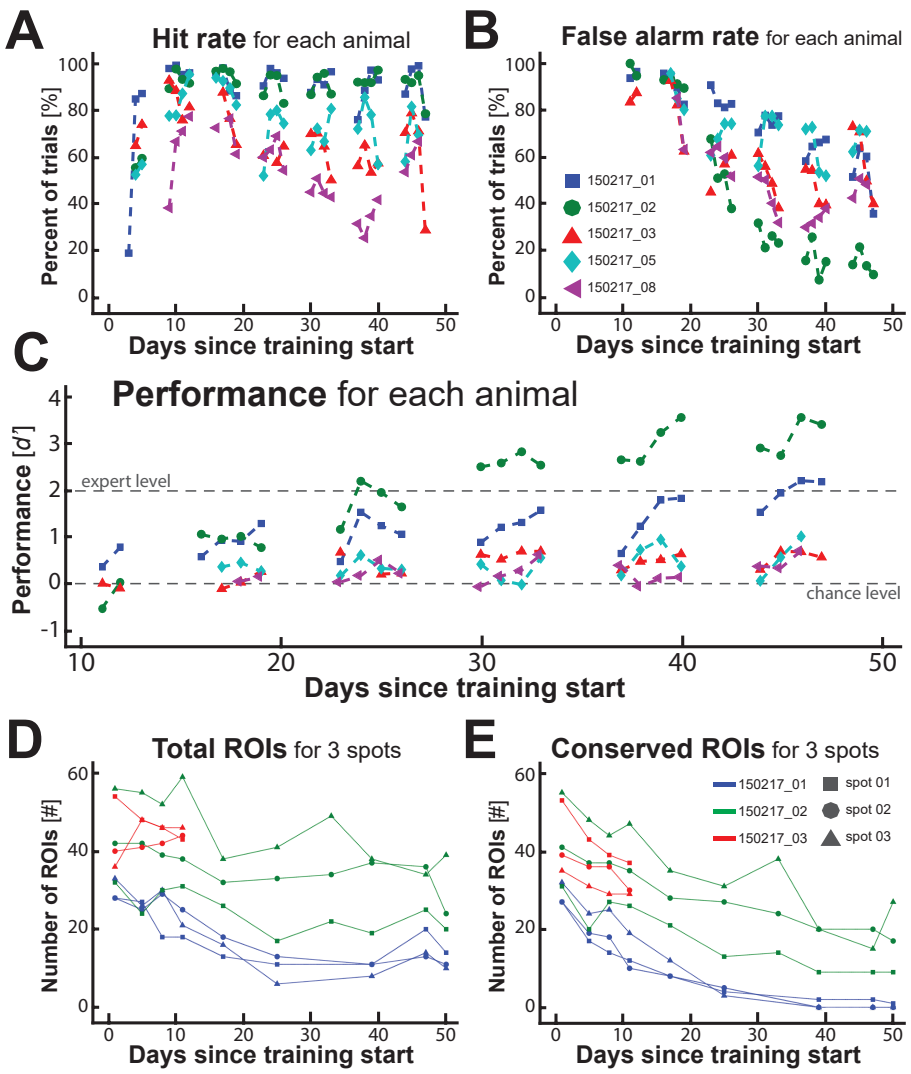

Figure 3.17: Prolonged go / no-go behavior and imaging limitations: (A-C) *Hit rate as percent (A), false alarm as percent (B) and performance as* d' *selectivity (C) for 5 animals that performed in an extended duration go / no-go sound discrimination task (N = 5 animals, ~50 days).* ***(D-E)*** *Total number of Region-Of-Interests (*ROI*) (D) and conserved number of ROIs (E) for each imaging session in 9 imaging regions for 3 animals shown in (A-C). Conserved ROIs are defined as ROIs that are present in both the first and the current day's imaging session. Animals are labelled with colors, imaging regions with symbols.*

ment artefacts due to the reporting of the mice had to be avoided. This was implemented through the introduction of a delay period and a moveable licking spout. This strategy helped reducing the movement artefacts. However, in a second round of experiments performed to consolidate the preliminary findings of reduction of responsiveness in the expert mice, another experimental limitation was met. As the training time increased due to the introduction of a delay, viral toxicity and photo damage induced irreversible damage in the neurons and therefore impaired imaging conditions. A possible solution to this would be the usage of transgenic animals, where viral toxicity is avoided, as the calcium indicator's expression is better controlled through the expression via a transgene.

3.4 Assessing learning-related changes on a larger scale

3.4.1 Combining wide-field calcium imaging and transgenic mouse lines

Recent advances in genetically encoded calcium indicators allowed to replace viral injections with transgenic mouse lines in calcium imaging experiments. To avoid the caveats of viral injection and photo-bleaching, the same discrimination behavior was combined with wide-field calcium imaging. Wide-field calcium imaging can record the activity of almost half of the cortex (see Methods section and Figure 2.2). The mouse line used for this experiment was expressing the GCaMP6f calcium indicator specifically in the layer 2/3 in the entire cortex. The aim of this part was to establish a chronic wide-field imaging experiment in auditory cortex during a *delayed* discrimination task.

The data presented for this section was collected from a single animal only, due to time constraint reasons. However, several other mice are currently being trained on the exact same protocol as this is written and their data is already starting to be analysed (a continued work from Yasir Gallero Sallas, member of the group of Prof. Fritjof Helmchen). Therefore, the presented results are only from one animal, which is only partially analysed (only 5 / 100 sessions, 2 / 18 days), and thus they still need to be replicated and confirmed. The mouse presented was trained to performance well above standard expert level (usually set at *d'* >= 2), as it reached a *d'* of 4 and above in several session (Figure 3.18).

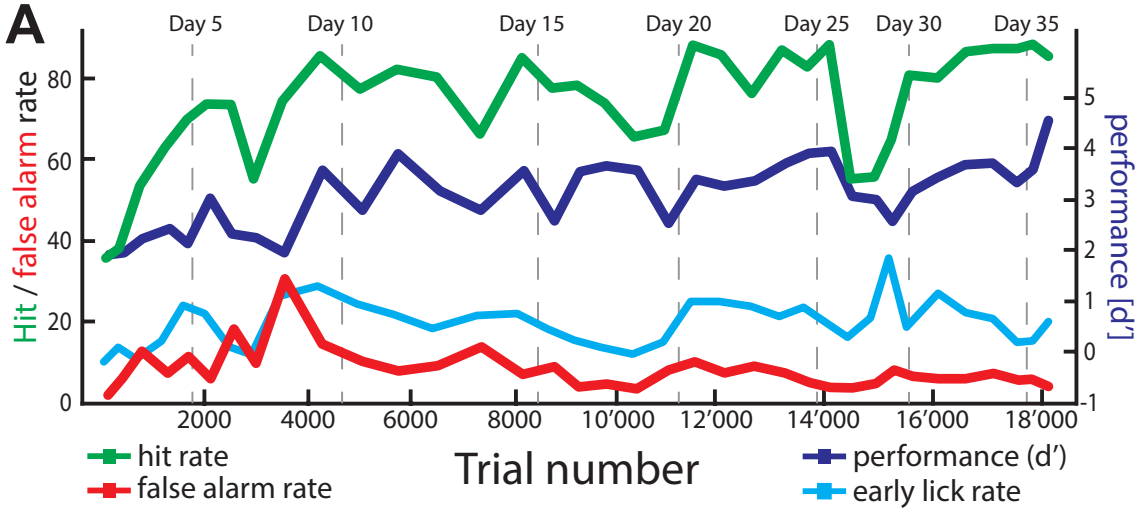

Figure 3.18: Behavior performance quantification for the delayed discrimination with wide-field calcium imaging: (A) *Behavior output quantification for the animal that performed in the delayed go / no-go behavior combined with wide-field imaging. Hit rate (green), false alarm rate (red) and early lick rate (cyan) as percent of total trials, and performance as sensitivity index (*d'*, blue) are shown for a period of ~35 days (~18'000 trials). Gray dashed bar show the day count of the training. The mouse was trained on a 4 kHz pure tone target (go) sound stimulus and a 28 kHz pure tone distractor (no-go) sound stimulus.*

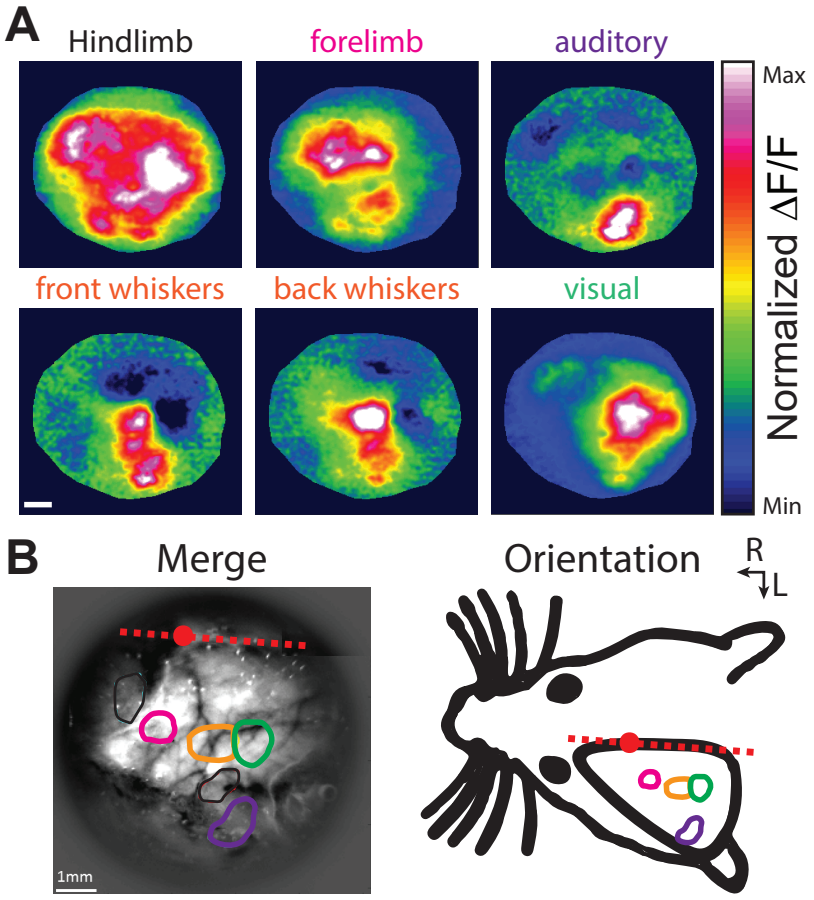

Figure 3.19: Mapping sensory cortices using wide-field imaging: (A) *Normalized response map for 6 different sensory stimulation. Scale bar: 1 mm.* ***(B)*** *Left: merged view of the ROIs defined using the response maps in (A), overlayed on a blood vessel pattern of the same field-of-view. Red dashed line represents the midline. Red dot represents bregma. Scale bar: 1 mm. Right: schematic of the mouse's head for orientation. Abbreviations:* R *rostral;* L *lateral.*

Despite the data set size limitation stated above, the goal of this part was to explore the cortical dynamics related to the behavior of mice in this *delayed* discrimination task. Specifically, the dynamics of the auditory cortex and of other cortical regions was studied during the different time periods of the discrimination trials, mainly the sensation period and the delay period.

3.4.2 Identification of sensory cortical regions and single trial analysis

As mentioned above, wide-field imaging can provided activity measurement for a large portion of the cortex, but the cortex has to be however functionally mapped to identify the cortical regions. To identify the cortical regions, sensory stimulation of different modalities were presented to the anaesthetized animal. Responses of the cortex were recorded using wide-field calcium imaging. A set of 6 different sensory stimulation were presented, evoking responses in different regions of

the cortex (Figure 3.19, A). The evoked responses were thresholded to define putative sensory cortical regions, according to the modality of the presented stimulation (Figure 3.19, B). These putative regions are matched with stereotaxic coordinates and with the activity patterns emerging during the awake behavior sessions.

A great attention was brought to the single trial analysis and to the animals body movements during the behavior sessions using a special module of the analysis framework described later (see Figure 3.35). A major concern was to use trials where the body movement of the animals were minimal or ideally even absent. This was necessary as it was observed that even small posture changes or body movements of the animal could elicit large activity changes in large parts of the recorded cortex, especially in the motor regions (Dr. Ariel Gilad, personal communication, observed in the texture discrimination task). Therefore, a great care was taken to monitor the animal with a video recording and to examine trials individually, either manually or semi-automatically using the `TrialView` module, to have a good measure of the animals body movement during each trial.

3.4.3 Measuring the body movement is critical to explain cortical activity

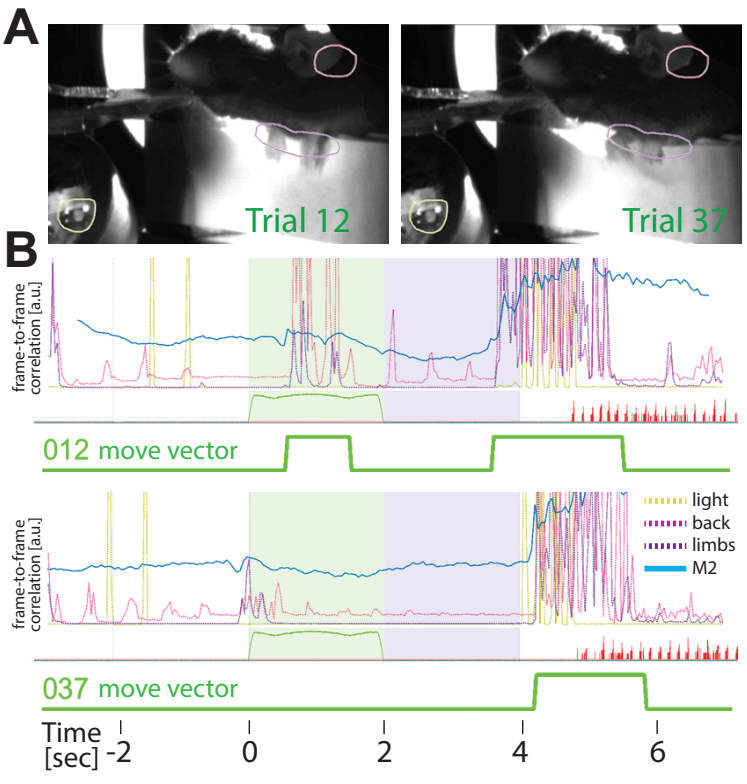

Figure 3.20: Behavior movement identification and extraction: ***(A)*** *Still frame from the monitoring video of an animal performing in the delayed auditory discrimination task for 2 selected hit trials. Regions-of-Interest are labelled around the light cue (bottom left, yellow), the limbs (middle, purple) and the back/ear (top right, pink). The two latter are used to quantify the animal's movements.* ***(B)*** *Time course of the behavioral variables for the 2 trials in (A). Behavioral variables are either recorded during experiment (bottom: licking rate in red and sound stimulation in green) or extracted from the behavioral movie shown in (A) using frame-to-frame correlations ($F2F_{corr}$, dashed lines, middle: light in yellow, limbs in purple and back/ear in pink). $F2F_{corr}$ traces are obtained by correlating each frame of the behavior movie with the next frame for a given region of the movie. The activation of the motor cortex (plain line labelled M2) is overlayed on these behavioral variables. The obtained move vector is displayed below each trial (green).*

To quantify the body movements, frame-to-frame correlations were calculated from defined

regions of the behavior monitoring movie (Figure 3.20, A). Typically, the forelimbs and the back regions were selected as they were the parts of the frame that most reliably reported general movements. These frame-to-frame correlations were thresholded to define *move vectors* (Figure 3.20, B). Move vectors are binary vectors telling for each time point whether the animal was moving or not. The threshold at which a time point is declared as "not moving" is not absolutely zero, meaning some very minor movements are not taken into account (amplitude on the level of the breathing for example).

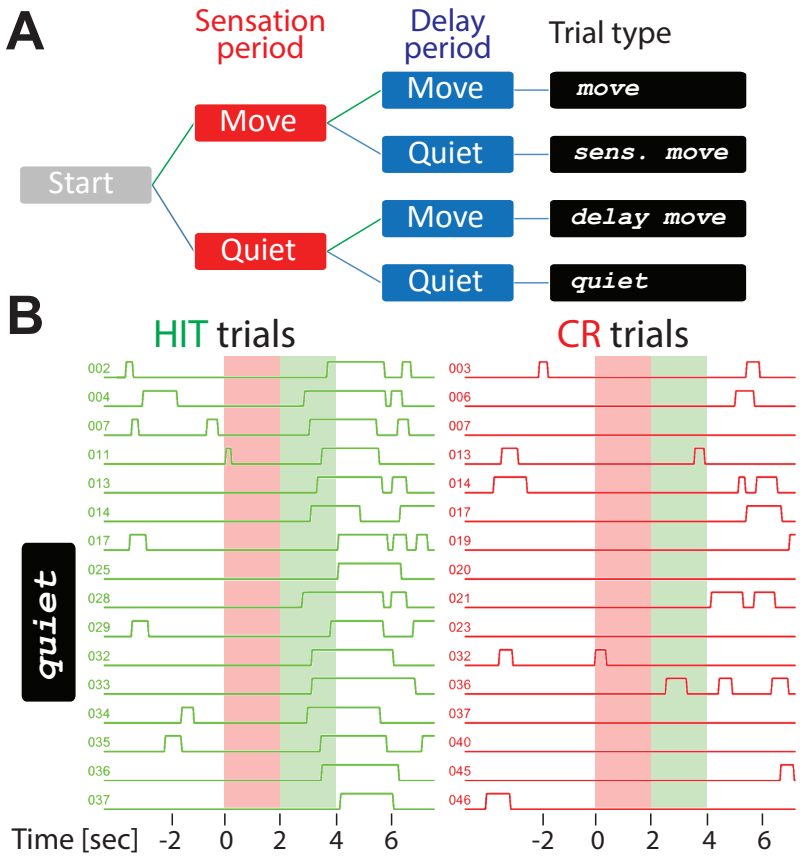

Figure 3.21: Trial classification according to the behavior reactions: (A) *Scheme of the classification logic for the trials. Trial types are defined based on the animals movement during both the sensation (red) and the delay (blue) period.* ***(B)*** *Example move vectors created using the behavioral variables extracted from the monitoring video. Only* `quiet` *trials are shown, corresponding to no movement during sensation and no movement at the start of the delay period. Very short periods of movement are not considered as movement (threshold: 0.45 sec). Left column: hit trials, right column: correct rejection trials.*

3.4.4 Defining *move vectors* and trial types based on the body movement

The move vectors are used to define different trial types, based on when movement occurred during the trial. Two main periods are taken into account for this trial classification: the *sensation* period, corresponding to the time during which the sound is played, and the *delay* period, corresponding to the time when the animal has to wait and retain the information before reporting its decision. Combining the *move* / *no-move* state in both of these periods, 4 different trial types are defined: `move`, `sens. move`, `delay move`, `quiet` (Figure 3.21, A). The most quiet and therefore *clean* trial type is the `quiet` condition, as this is the trial type that has neither movement

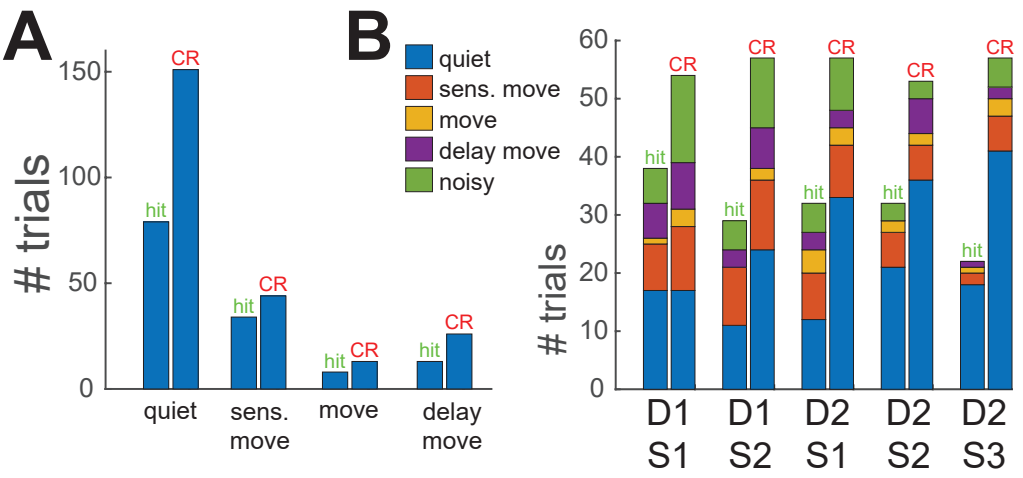

Figure 3.22: Quantification of trial numbers for each type: (A) *Quantification of the number of trials for each trial type for 5 sessions.* ***(B)*** *Same as (A) but separately for each of the 5 session (day 1 and 2 (D1, D2) and session 1, 2 and 3 (S1, S2, S3)).*

during the sensation period nor during the delay period. This is the trial type that is retained for the following steps of the analysis.

As said, the mouse presented in this section was trained until it reached an expert performance level. This was required in order to minimize the body movements as the mouse became more and more quiet as the training went on. Longer training time was not problematic here compared to the previous two-photon experiments as the photo-damage is nearly non-existent with wide-field imaging (single photon excitation through the skull) and no virus was involved as transgenic mouse line is used to express the calcium indicator. The analysis described further below only uses the correct trials of the animal (*hit* and *correct rejection*) as in such an expert state, the amount of mistakes is extremely reduced and therefore cannot be interpreted too confidently.

Most of the trials recorded in this expert state were quiet trials (`quiet` category), even though all trial types were present (Figure 3.22, A). The trials were also more often categorized as quiet in the correct rejection outcome compared to the hit outcome. Amount of trials and trial types were fairly constant across sessions and days (Figure 3.22, B).

The probability of movement for each of trial type was quantified using the previously described move vectors (Figure 3.23, A). Prominent movements occurred during the reporting period in all trial types in the *hit* condition, usually starting before the reporting cue comes in (at T = +4 seconds). Very little number of trials can be observed where the mouse quietly waited for the reporting cue during the whole delay period. In the *correct rejection* condition, movement is comparable before the stimulus (-3 to 0 seconds) as the animal does not know yet what sound is going to come. After the stimulus, movement is reduced in the *correct rejection* compared to the *hit* trials. In general, the `quiet` trial type contains less movement, confirming that the classification is consistent.

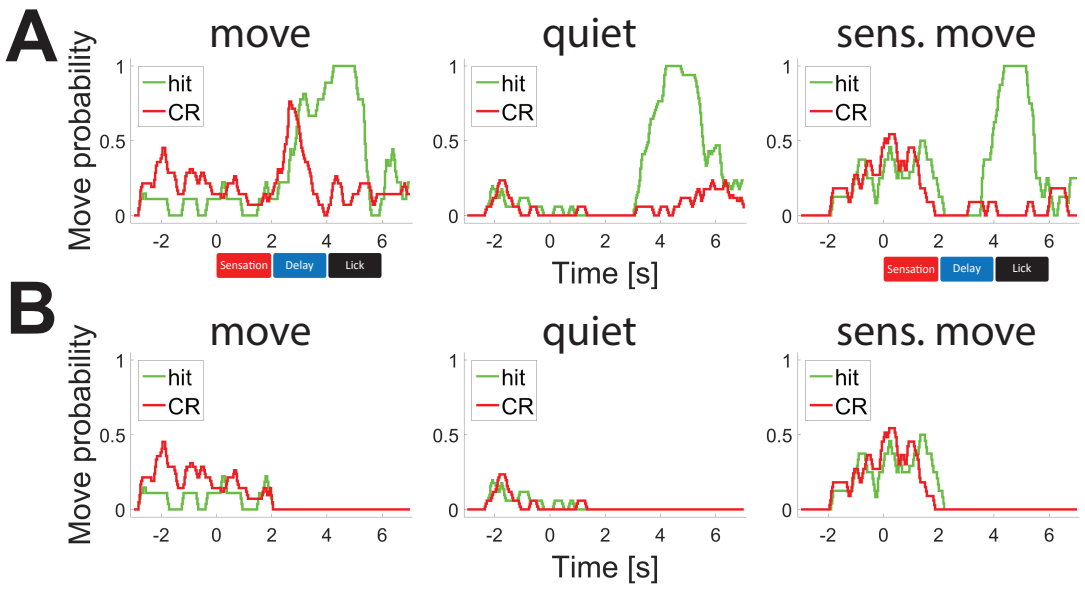

Figure 3.23: Behavior movement quantification for the different trial types: (A) *Peri-stimulus time histograms of the move vectors for 3 trial types, separated between hit (green) and correct rejection (red) trials for a single session (between 10-20 trials for each trial type). Sensation period spans from 0 to +2 seconds, delay period is from +2 to +4 seconds and lick period is from +4 to +6 seconds. The prominent movement observed in the end of the trial is due to the licking of the mouse.* ***(B)*** *Same as (A) but after filtering for movement onset. Time points after movement onset are excluded, resulting in clean and quiet trials only. Abbreviations:* CR *correct rejection.*

In order to exclude all possible movement contamination from the analysed data, only `quiet` trials were used. Moreover, move vectors were used to truncate the calcium imaging data to exclude the movement part of each trial individually. By detecting movement onset on the move vectors and truncating the rest of the trial from there, a truncated data set could be created (Figure 3.23, B). Only truncated (cleaned) quiet trials were used for further analysis. Two main trial epochs were examined for spatio-temporal activation patterns: the *sensation period* and the *delay* period. The other trial epochs either contained no relevant information (no stimulus during baseline period for example) or were excluded because of the movement artefacts (reporting period excluded because of licking and movements). The goal was to observe whether or not differences between target and distractor conditions (hit versus correct rejection) exist in the activation patterns of the recorded cortical regions.

Average response maps were computed for three different periods within the trial: light cue period (-2 to 0 second), sensation period (0 to +2 second), delay period (+2 to +4 second) Figure 3.24. The two later maps, the sensation and the delay maps, are further examined in the next sections.

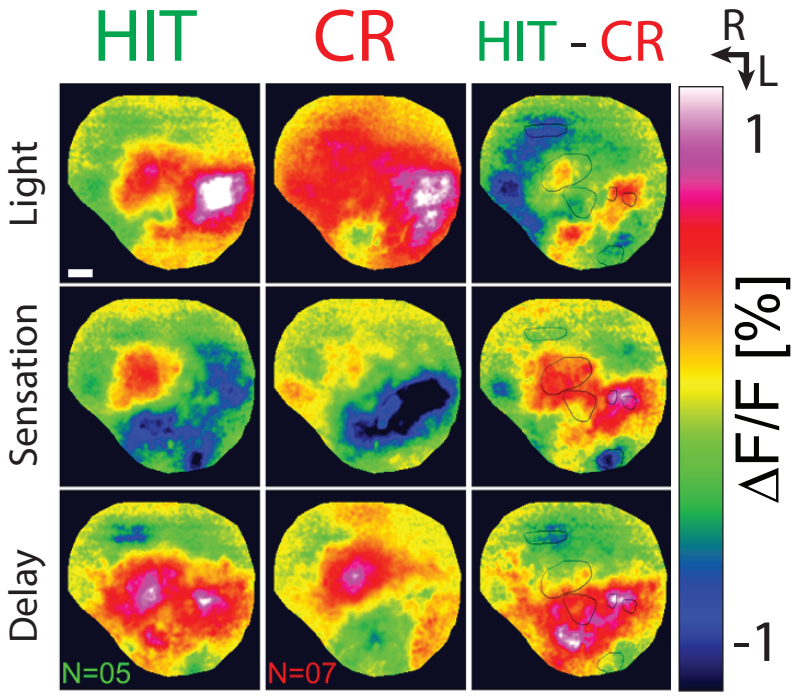

Figure 3.24: Activation maps during different periods of the trial: *Average response maps were computed for three different periods within the trial:* light cue *period (-2 to 0 second),* sensation *period (0 to +2 second),* delay *period (+2 to +4 second). The maps shown are the average of the* `quiet` *trial types from an example session of the trained animal. Trial numbers are indicated at the bottom for each condition. Scale bar: 1 mm. Abbreviations:* CR *correct rejection;* R *rostral;* L *lateral. The maps are normalized (F_0) to the beginning of each trial.*

3.4.5 Auditory activations during the *sensation* period

During the sensation period, either a *go* sound stimulus or a *no-go* sound stimulus is presented. These sounds are two different pure tones with different frequencies (4 kHz *go* and 28 kHz *no-go*, 2 second duration). The first hypothesis was that both these sounds would evoke distinct activation in the auditory regions during the sensation period. To show this, average response maps of the sensation period were extracted from all trials for the *hit* (corresponds to the *go* sound) and the *correct rejection* (*CR*, correspond to the *no-go* sound) trials separately (Figure 3.25, A, top and middle rows). To compare the two conditions, difference maps were computed for the example 5 sessions (Figure 3.25, A, bottom row).

Activation patterns looked relatively similar across days and sessions within a condition. A unexpected major difference between the *hit* and the *CR* trials was the direction of the change upon auditory stimulation. Indeed, whereas the *CR* trials show a moderate auditory activation (Figure 3.25, A middle row: yellow spot at the bottom of each map, corresponding to the purple ROI shown in B), the *hit* trials show a reduction of activity in the same region (Figure 3.25, A top row: blue roundish spot at the bottom of each map). This difference is more visible in the difference map, where the deactivation in the auditory cortex of the *hit* trials compared to *CR* trials is enhanced (Figure 3.25, A bottom row: blue roundish spot at the bottom of each map).

Other dissimilarities between the two conditions include the general deactivation in the visual regions (labelled V1 in the B panel) for the *CR* condition but not the *hit* trials, showing a positivity

in the difference maps. Moreover, in some cases activation in the frontal regions in the *hit* trials can be seen but rarely in the *CR* trials. This results in the frontal regions being positive in the difference maps.

To examine the temporal aspect of these activations, the time course of 3 example ROIs have been extracted for all trials and averaged for each condition (Figure 3.25, B). The 3 regions were the auditory cortex (A1), the visual cortex (V1) and the posterior parietal cortex, as these regions show particular activation patterns, either in the sensation or in the delay periods (see next subsection).

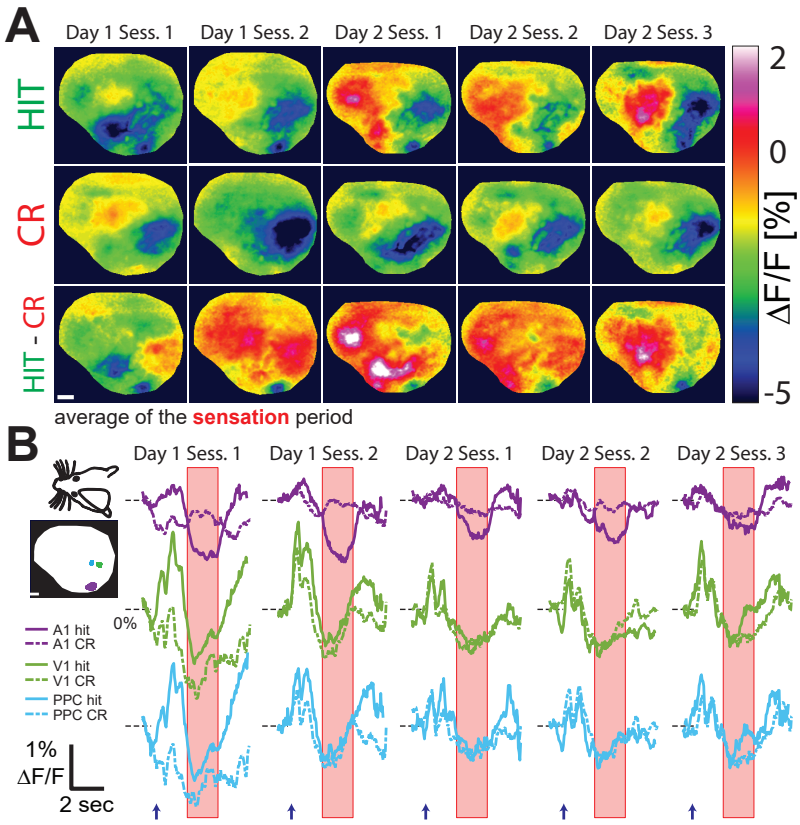

Figure 3.25: Activation pattern and time course during the* sensation *period: ***(A)*** *Average response maps of the sensation period for 5 sessions of the same animal for two consecutive days (N = 5 sessions, average of 10-30 trials for each session). Only quiet trials are shown. Top row: hit trials, middle: correct rejection trials, bottom: difference map. Scale bar: 1 mm.* ***(B)*** *Time profiles of 3 selected Region-of-Interest: primary auditory cortex A1 (purple), primary visual cortex V1 (green) and posterior parietal cortex PPC (cyan). The traces correspond to the sessions shown in (A), red rectangle indicates the sensation period averaged in (A). Blue arrow indicates stimulus light cue (0.5 sec). Dashed black bar shows baseline (0% ΔF/F). Scale bar: 1 mm. Abbreviations:* CR *correct rejection.*

Time courses in the visual and PPC region both show a prominent activation at the start of the trial, due to the presentation of the trial start cue, which was a light flash (Figure 3.25, B). During the sensation period, all ROIs show a decrease in activity, however the auditory cortex is showing a relatively large difference between the *hit* and the *CR* average trace, confirming the difference visible on the spatial average maps. These results suggests that activity in the auditory cortex is suppressed during the perception of a sound specifically during the *hit* trials.

3.4.6 Posterior sustained activity during the *delay* period

The *delay* period was examined with the same methods as the *sensation* period (see previous subsection). The hypothesis was that there exists some cortical regions that show a sustained activity during the delay period. Indeed, the animal must hold the sensory information from the moment it knows which trial type he is in (*go* vs *no-go*). The sensory information must transit from the sensory cortex (here the auditory cortex) to an information retaining region where it is held during the delay period. Only after the end of the delay period can a signal be sent further to initiate the motor execution (lick).

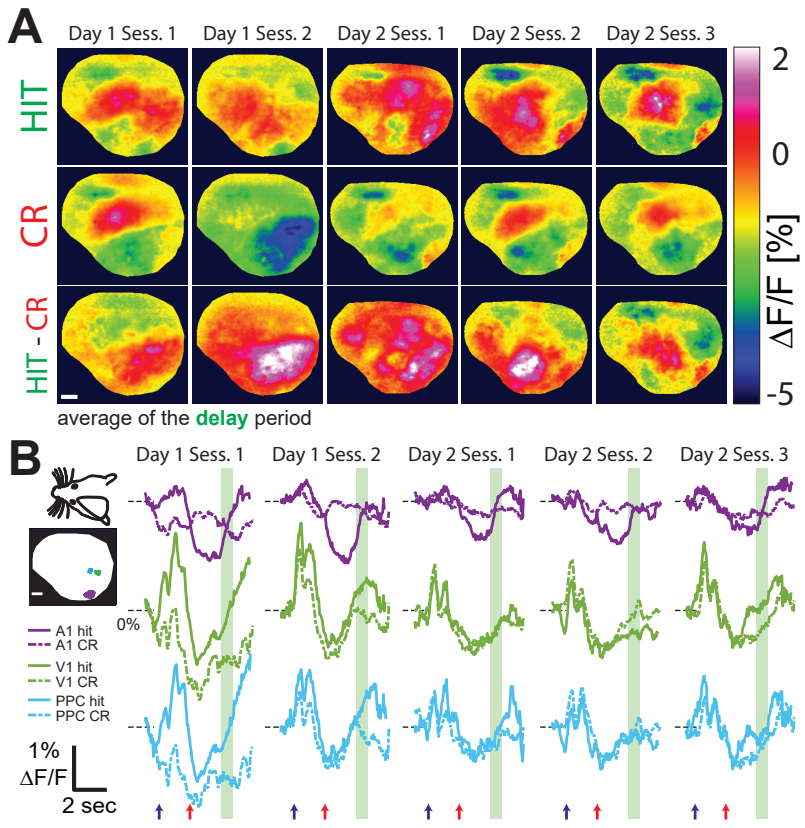

Figure 3.26: Activation pattern and time course during the delay period: ***(A)*** *Average response maps of the delay period for 5 sessions of the same animal for two consecutive days (N = 5 sessions, average of 10-30 trials for each session). Only quiet trials are shown. Top row: hit trials, middle: correct rejection trials, bottom: difference map. Scale bar: 1 mm.* ***(B)*** *Time profiles of 3 selected Region-of-Interest: primary auditory cortex A1 (purple), primary visual cortex V1 (green) and posterior parietal cortex PPC (cyan). The traces correspond to the sessions shown in (A), green rectangle indicates the delay period averaged in (A). Blue arrow indicates stimulus light cue (0.5 sec), red arrow indicates auditory stimulus onset time (duration: 2 sec). Dashed black bar shows baseline (0% ΔF/F). Scale bar: 1 mm. Abbreviations:* CR *correct rejection.*

Average maps in both trial conditions (*hit* and *CR*) have been extracted for the delay period (Figure 3.26, A). They show frontal activations that are similar in size and shape for both conditions as they do not form a clear positivity or negativity on the difference maps. Some posterior regions showed higher activation in the *hit* compared to the *CR* condition, leading to a positivity in the difference maps (Figure 3.26, A, bottom row). These activated regions are corresponding to visual and PPC areas, according to the mapping experiments and to the stereotaxic coordinates.

The time course of the 3 selected regions were also analysed for an increase during the delay

period (Figure 3.26, B). In all but one session, the V1 activation is higher in the *hit* condition compared to the *CR* during the delay period. The same is true for the PPC region, although the difference is smaller and seems to appear only at the beginning of the delay period.

Taken together, these results show that different activation patterns exist in the layer 2/3 neurons of the cortex of animals performing in the discrimination task, and that these differences are depending on the trial type. Some of these activation patterns could suggest that sounds are encoded differently depending on their relevance (see previous subsection), or that some cortical regions hold or transmit trial type identity during the delay period until the reward collection time (see above).

3.4.7 Motor activation and auditory suppression

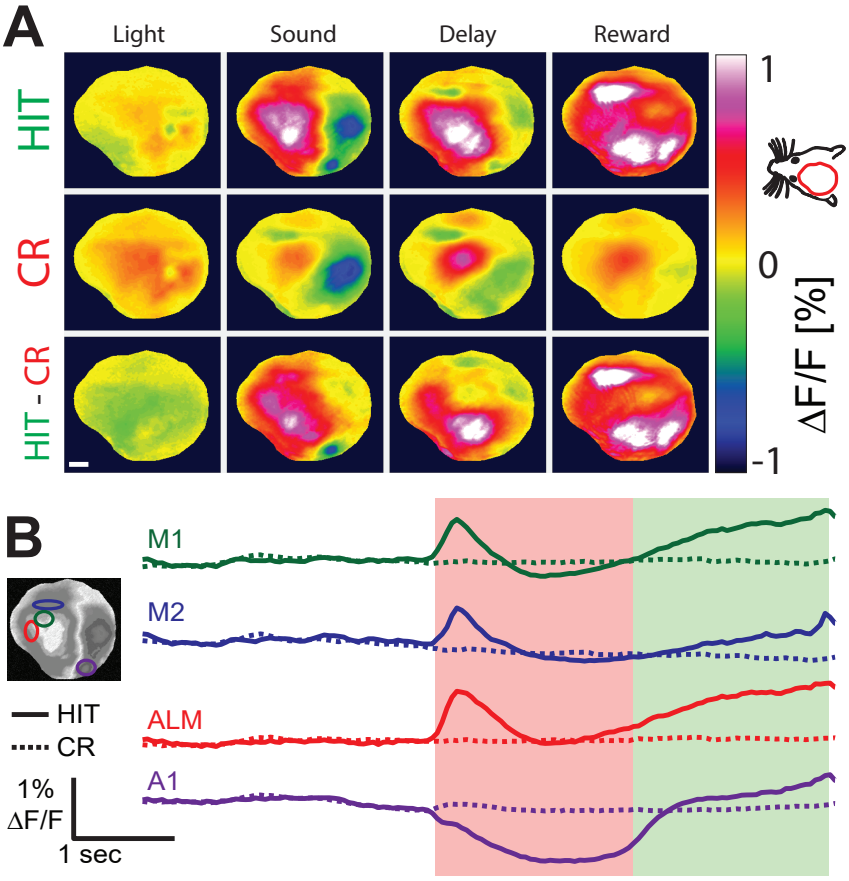

Figure 3.27: Motor activation and the auditory suppression: ***(A)*** *Average response maps of all trial period for all sessions of the same animal (N = 14 sessions, N = 474 HIT trials, 961 CR trials). Only quiet trials are shown. Top row: hit trials, middle: correct rejection trials, bottom: difference map. Scale bar: 1 mm.* ***(B)*** *Time profiles of 4 selected putative cortical regions: primary motor cortex M1 (green), secondary motor cortex M2 (blue), anterior lateral motor cortex ALM (red) and primary auditory cortex A1 (purple). The traces correspond to the grand averages shown in (A), red rectangle indicates the sensation period, green rectangle indicates the delay period. Abbreviations:* CR *correct rejection.*

Average maps in both trial conditions (*hit* and *CR*) have been extracted for all time periods for all sessions (Figure 3.27, A). They show the same lateral spot of suppression visible in single sessions, corresponding to the auditory cortex. In addition, frontal activation in the motor regions are visible during the sound presentation for the hit but not for the correct rejection trial condition.

The activity of selected regions were further examined in the time dimension by extracting the average time course for 4 cortical regions: primary motor cortex M1, secondary motor cortex M2, anterior lateral motor cortex ALM and primary auditory cortex A1 (Figure 3.27, B). As previously described, the exact identification of these regions is not yet finished, therefore these regions are only putatively labelled as M1, M2, ALM and A1, respectively. During the delay period, all the motor regions, particularly M1 and ALM, show a rising activity, starting after the end of the initial activation peak during the sensation period. As previously described, the time course for the A1 region shows a striking suppression during the entire sensation period, after which the activity level return to baseline level and follows a similar rising trend during the delay period.

A potential relationship between the observed motor activation and the auditory suppression is discussed later. It is interesting to notice already here that the motor activation happens in trials carefully selected for absence of movement in the body camera recording.

3.5 Creation of an *in vivo* data analysis framework

This section describes the result of my work of creating and improving analysis and visualization tools for the large amount of complex data produced during my PhD. This work ultimately lead to the creation of the analysis and visualization framework used during my thesis. This section gives a detailed description of the structure of the software with description of each module and of implementation strategies. Details about the methods used for data analysis of the previously described results are also described here.

3.5.1 The `OCIA` framework

The main tool I used for interacting with and analysing my data was a self-written analysis framework named `OCIA`. This framework will be described in the following sections. This software, written in MATLAB, is currently at version 5.1.10, as it had 5 major iterations where most of the code was re-written or re-organized. The core functions (without the external helper functions) are composed of 573 files and 65'874 lines of code. The entirety of the code is freely available on a public `GitHub` repository, that can be found at the following address:

`https://github.com/blaurenczy/OCIA.git`.

Best practices of programming have been used as much as possible, such as:

1. commenting: 21'094 of the above mentioned lines are commented either in-line or as full comment line, meaning that on average, roughly every 3rd line of code is commented.
2. separating large code into small files following the *MURDER* principle:
   - **M**aintainability: smaller, simpler functions are easier to maintain
   - **U**nderstandability: simpler functions are easier to understand
   - **R**euseability: encourages code reuse by regrouping operations to a separate function
   - **D**ebugability: it is easier to debug simple functions than complex ones
   - **E**xtensibility: code reuse and maintainability lead to functions to extend later
   - **R**egression: reuse and modularization lead to more effective regression testing.
3. modularity of code: there are no hard-coded values, variables or parameters since they would be very hard to find and change; everything that might be changed is a parameter
4. consistent syntax and spacing for an easier human-readability
5. consistent and explicit variable and function naming, as cryptic and/or shortened function and variable names for the sake of brevity can make a code impossible to maintain and understand

Finally, as the first law of programming says: '*Code is more read than written*', therefore sim-

ple solutions and explicit steps of programming have been used along with the mentioned best practices to help future readers of this code to understand it.

Origin and usage

The `OCIA` (pronounced *OKIA*) stands for ***O**nline **C**alcium **I**maging **A**nalysis*. It must be said here that this acronym is purely historical as the framework does not do this any online analysis any more. It originated from the need of an automated data processing pipeline for calcium imaging data. An existing processing pipeline from Dr. Henry Lütcke was originally used and then modified to perform the basic processing steps of calcium imaging analysis. These basic processing steps are described in more details in a later chapter.

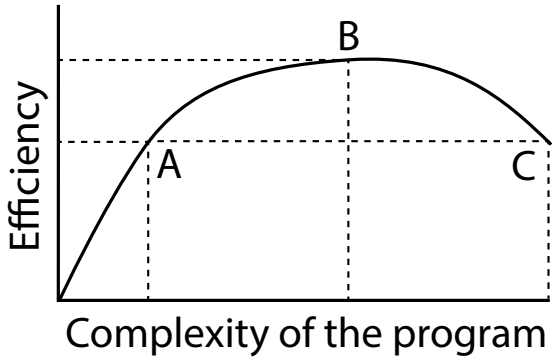

Figure 3.28: *Efficiency versus complexity*

However, it appeared that other parts of the whole analysis pipeline would benefit to be integrated with the automated processing pipeline, for example the non-automated steps of pre-processing and the post-processing analysis steps (see below). The benefit of an integrated analysis pipeline are mainly a gain of time, a better overview of each step, flexibility and increased consistency in the way the data is analysed. Moreover, having a fully automated pipeline leads to the data being processed at speeds allowing an *online* analysis during the experiment, and thus to have a feedback on the quality of the data currently being recorded while doing the experiment. This idea of an online analysis was the beginning of the `OCIA` as a processing tool with a Graphical User Interface (*GUI*) that I used to assess the quality of my recordings during the experiments. This first *quick and dirty* processing tool with a GUI then evolved step by step over four years and many revisions to do much more in a much more sophisticated way and became in its final form the framework described below. A constant worry of this evolution and sophistication, as well as for any task of my PhD, was not to fall on the right side of the *efficiency versus complexity* curve (Figure 3.28).

Efficiency and complexity are related to each other via an inverse U-shaped curve (original idea from Dr. Henry Lütcke). There is an initial fast gain of efficiency (Figure 3.28 A) by creating a program with some complexity, that can automatize sequences of tasks for the user. A more complex program has a gain in efficiency that begins to be smaller (Figure 3.28 B) due to overhead in maintaining and writing code that complies with the other existing features. Finally, creating an extremely complex program might even reduce the efficiency of it (Figure 3.28 C) compared to a simpler software, as staying consistent becomes harder due to the increased complexity and

number of the features. Therefore, one should always consider on which *side* of the curve a program is (or will be), and try to remain '*as complex as needed but not more complex*'.

The OCIA was mainly used by myself to process my own data. However since "*Sharing is caring*", I used the OCIA to process the data sets of several other members of the Helmchen group and some members also used it themselves to process their own data. Altogether and so far, around 10 members of the lab, including myself, used or benefited from at least one module of the framework, most of them by using the calcium imaging related modules.

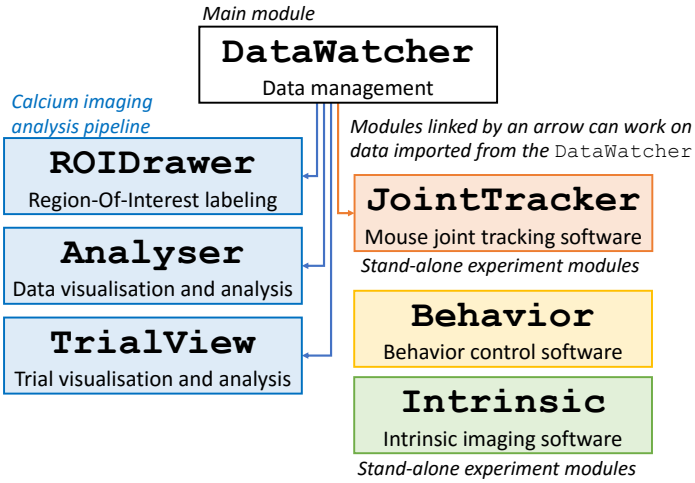

***Figure 3.29: Overview of the OCIA's module**: The DataWatcher is the main module. It handles data management, data saving and loading operations and serves as starting point for most of the other modules (marked by an arrow), including the calcium imaging analysis pipeline. The ROIDrawer, the Analyser and an in a lesser extent the TrialView, are all part of the calcium imaging analysis pipeline. The ROIDrawer is a module providing manual and semi-automatic labelling of neurons for the calcium imaging data analysis. The Analyser provides analysis, plotting and visualization capabilities for any data type using custom analysis functions. The TrialView module is used to analyse mouse behavior trials one-by-one and extract relevant features from behavior movies. The JointTracker is a module integrated with the DataWatcher to perform semi-automatic annotation of mouse joints. The Behavior module is a stand-alone software to control behavior experiments. The Intrinsic module is another stand-alone module, used for the intrinsic imaging experiments.*

3.5.2 An integrated framework with modularity

Given the advantages of the integration mentioned above (speed, flexibility and consistency), I created this framework to merge together these 3 steps of the calcium imaging analysis: the non-automated pre-processing, the automated processing itself and the post-processing analysis. The non-automated pre-processing includes the managing the calcium imaging data sets (see DataWatcher section) and drawing of the Regions-Of-Interest (*ROI*) to define the boundaries of neurons on the images (see ROIDrawer section). The post-processing analysis involves the visualization of the processed data and the actual analysis (sorting, averaging, etc.; see Analyser section).

This whole pipeline had to be implemented in a flexible and modular way, as not all the steps of processing are always required and also not always with the same parameters. Therefore, the pipeline was divided into modules and within each module the parameters to use for each processing steps and analysis were made flexible. Each module is independent but linked to the

others so that the data can be brought from one module to the next.

Since not all modules are always required, the OCIA comes in many different flavours, each with a personalized configuration that includes the required modules. This personalization of the framework is implemented through configuration files that list the requested modules and many other starting parameters, but all of the flavours run on the same core functions of the OCIA. This design allows users to change their configuration file without having to deal with the core functions. Moreover, updates to the core functions or additions of new modules do not disrupt the users, except in the case of major revisions.

3.5.3 The modules and the common features

All modules will be described individually in the following sections. Here is first a brief overview of how they are linked to each other, to complement the module overview (Figure 3.29). The core module, the DataWatcher, is present in all flavors of the OCIA. It serves as starting point for the calcium imaging pipeline but also provides overview of the data sets of any type. The other calcium imaging pipeline modules are the ROIDrawer, the Analyser and an in a less integrated way, the TrialView. The Analyser is also used in other flavors of the OCIA, as it provides plotting and visualization capabilities for any data type and not only calcium imaging. The TrialView module also deals with calcium imaging data but it does not fall in the *classic* calcium imaging analysis pipeline, as its purpose is to give mouse behavior trial visualization and analysis features. The Behavior module is a stand-alone software for the behavior experiments, by controlling and synchronizing the analog and digital inputs and outputs during the experiment; however the Behavior module still uses the common features of the OCIA, detailed further below. The Intrinsic module is similar to the Behavior module, as it is also a hardware controlling stand-alone module, used for the intrinsic imaging experiments. Finally, the JointTracker is also stand-alone modules, also integrated with the DataWatcher, but it performs a specific semi-automatic annotation task described below.

The advantage of having a module-based system is that it saves code, energy and time to implement new modules. The core OCIA has a flexible structure to implement additional modules. This flexible structure has the following features that enable creating new modules easily:

1. **Embedding in the common window**: each module does not need to re-implement the basic features of a window and user interface on its own, they all re-use the common window of the framework (see Figure 3.30).
2. **Easy custom GUI generation**: creating a custom GUI for each module is made easier by a set of common functions to create custom GUI elements (buttons, drop-down menus, check-boxes, tables, etc.). Modules only need to implement the

`OCIA_createWindow_[MODULE_NAME]` function to have a custom GUI created in the main window. Many GUI elements of the `OCIA` framework use the access to the Java properties underlying MATLAB's GUI. These properties allow to better customize the GUI by providing advanced display features or better user interaction capabilities, like mouse drag events.

3. **Mouse and keyboard events**: the common window captures the key press, mouse move, mouse click and mouse drag events, and forwards the actions to each module. Thus, modules only need to implement the actions to do upon the user interactions and not the whole capturing and handling of these interactions (see Figure 3.30).
4. **User feedback**: a common logging, warning and error system is present in all modules, making the handling of errors and warnings easier to code, but also clearer to the user. A *log bar* at the top of the GUI shows messages and warnings to the user. This log bar is common and available in all the modules (see Figure 3.30).
5. **Dynamic function calling**: the framework provides a system to dynamically call custom functions based on their name. This simplifies adding new modules, functions, configuration files, etc. For example, all analysis functions are using the convention `OCIA_analysis_[FUNCTION_NAME].m`. Adding new analysis functions is then easily done by creating a new file named using the same convention. For example a function to do trial averages, `OCIA_analysis_doTrialAvgs.m`, is easy called or referred to by calling the core function `OCIAGetCallCustomFile(this, 'analysis', 'doTrialAvgs')`. This way of referring to functions that have a convention of naming gives a layer of abstraction for the dynamic calling of these functions. In other words, one can then refer to any analysis function within a loop (or *dynamically* call it) without having to hard-code the list of the names of all functions in the code.
6. **Common GUI manipulation**: a set of core function enables to create GUI elements and interact with them in a module-independent way. For example, functions to temporarily disable or enable the whole GUI during data processing are available in any module, like: `OCIAToggleGUIEnableState(this, moduleName, stateOnOrOff)`. Another very useful function can dynamically create a parameter panel based on a customizable configuration (see Figure 3.30). This whole framework contains many configuration files with many parameters and having to write the code for each of the GUI element would be extremely tedious and difficult to maintain, as the configuration files and parameters are often created and modified. Therefore, a single core function, `OCIACreateParamPanelControls` creates a two or three column panel where each parameter from a defined configuration file has its own control GUI element (see Figure 3.30). Since each parameter can be of different type (text, numbers, true/false, lists, etc.) and can be set with different GUI elements (text

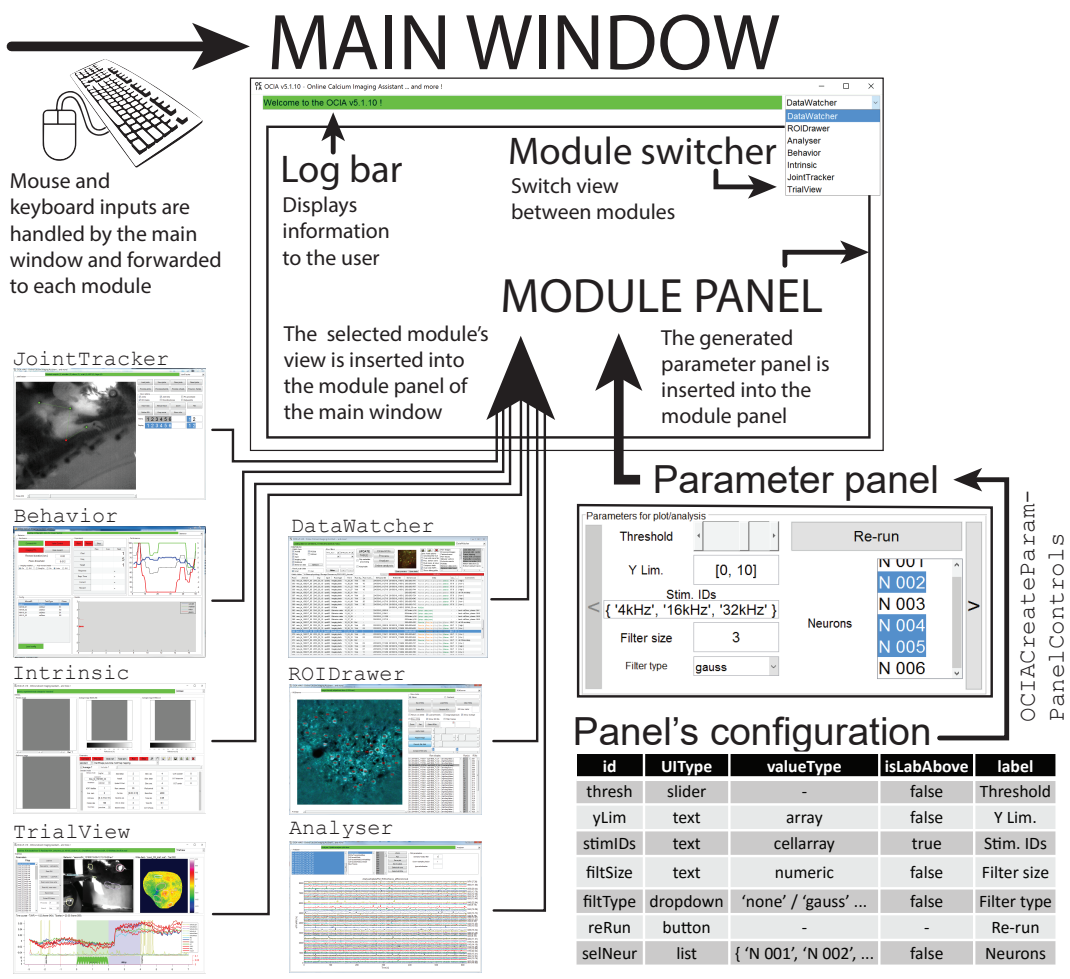

id	UIType	valueType	isLabAbove	label
thresh	slider	-	false	Threshold
yLim	text	array	false	Y Lim.
stimIDs	text	cellarray	true	Stim. IDs
filtSize	text	numeric	false	Filter size
filtType	dropdown	'none' / 'gauss' ...	false	Filter type
reRun	button	-	-	Re-run
selNeur	list	{ 'N 001', 'N 002', ...	false	Neurons

Figure 3.30: Overview of the `OCIA`'s GUI: **Main window:** *the main window contains the log bar, the module switcher and all the modules in a central panel. It also handles the keyboard and mouse events;* **Log bar:** *The log bar displays messages to the user about the computation happening in the software (green background). It can also display warnings (yellow) and errors (red).* **Module switcher:** *A drop-down menu to switch between the different modules. Upon change, the current module becomes invisible and the selected module is displayed.* **Modules:** *Each module only needs to take care of its own specific task, but they all have access to the core functions provided by the framework. All GUI elements have a text tool-tip to explain their function, appearing when hovered with the mouse.* **Parameter panel:** *An example of a core function accessible by all modules. Each module can define a parameter panel configuration, which will then be converted into a parameter panel inserted into the window's GUI, via the* `OCIACreateParamPanelControls` *core function. The configuration for the panel is defined in a dynamic way for each module, using the set of fields shown in the bottom-right table: a unique* id*, the User Interface type* UIType *(slider, text, drop-down, etc.), the input value type* valueType *(text, numeric, array, cell-array, etc.), whether the label should be above or not* isLabAbove*, and the* label *for this element.*

box, slider, buttons, drop-down menu, etc.), having this dynamic creation based on the configuration file rather than hard-coded for each module saves a great amount of code, time and energy. To complement this, the `OCIAUpdateVariablesFromParamPanel` function updates the value of the variable associated with each parameter when the GUI control is used by the user.

3.5.4 Management of complex data with flexibility - `DataWatcher`

As already mentioned above, the amount of data is exploding both in neuroscience and in science in general. This leads to data storage and data transfer problems that better hardware and technology are trying to solve, by providing better data storage capacity and faster transfer rates. However, a very important aspect of this data amount increase is the difficulty to keep an overview of large data sets. Indeed, one of my typical imaging and behavior experiment contains about 9'800 files in about 540 directories or sub-directories. These high numbers of files and directories are simply impossible to overview and remember with a human mind, unless it is assisted by a computer and a good organization software. Such a data management and organization software is referred to as an information system software.

The `OCIA` provides such an information system via the `DataWatcher` module. Although other software for maintaining data organized exist, like `openBIS` (Bauch et al., 2011), I originally wanted a simple and specific system for calcium imaging data. But the `DataWatcher` module, similarly to the whole `OCIA` framework, ended up having a much broader use than originally designed, mainly because of the possibility to customize it. The ability to customize everything in it, led the `DataWatcher` module to be very useful in solving the data management problem, as it can be configured to display and manage any kind of data in a customizable table. The functioning of this module will be described in the sections that follow.

Navigation through hierarchically stored data sets

Data in biology and neuroscience experiments is typically stored in an organized hierarchical manner. Each of the multiple levels of this hierarchy is usually associated with one experimental condition or entity, creating therefore one folder to regrouping all the data related to a single animal, one for a single day, for a recorded region, a recording session, a sample, etc. This hierarchy and organization is most of the time different for each experimenter as very few common standards exist regarding the data storage strategies in neuroscience, or even within single research groups. Therefore, the information system should be made flexible regarding to which levels exist and how they are organized.

As mentioned above, even the data set for a single animal is too big to be viewed all at once (~10'000 files). Therefore, it is required that only a part of the whole data set is displayed at one time. This requires then that only selected parts of the hierarchy tree should be explored and displayed when viewing files. In the `DataWatcher`, users can define through configuration files how their data hierarchy is organized. A list of levels (`watchType` in the code) is defined for each user, where each level can be of two types: either the level is a generic folder, which

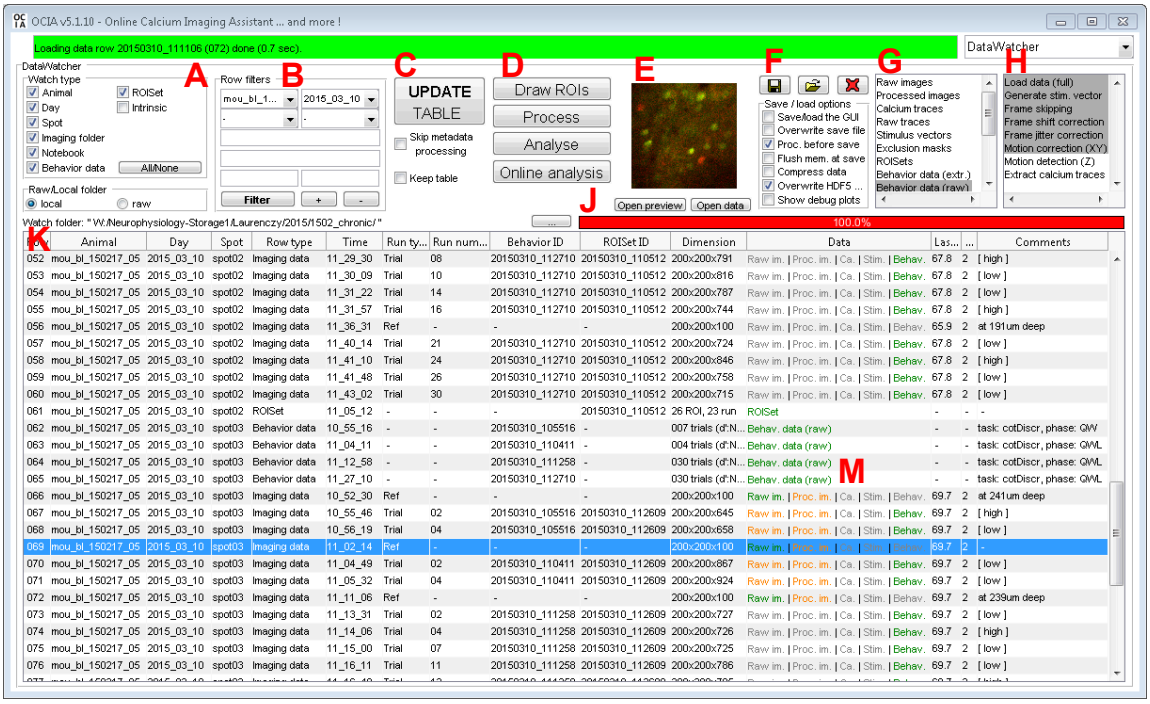

***Figure 3.31:* `DataWatcher` *module**: an information system to explore, display and manage any data file of any experiment. Selected data rows can be transferred to the other modules. **(A)** WatchType filter, used to select which levels of the file hierarchy and which file types should be displayed (see Figure 3.32 for more details). **(B)** Row filter, enabling the selection of a sub-part of the file hierarchy's tree for display (see Figure 3.32 for more details), but also selection of rows within the table using the Filter button. **(C)** the Update Table button triggers the searching in the file system using the row and WatchType filters and updates the table with the found files and folders. **(D)** A list of customizable buttons to do any kind of actions with the selected rows, including neuron labelling via the `ROIDrawer` (Draw ROIs), run an analysis pipeline (Process) or display and analyse the processed imaging rows in the `Analyser` module (Analyse). **(E)** Image preview of the selected row. Only a few frames of the selected row are loaded for faster preview. **(F)** Save / load / reset buttons that trigger the saving, loading or clearing of data for the selected rows, with check-boxes to control options for the saving / loading. **(G)** List of data types available for the displayed rows. Saving, loading and clearing data is only done on the selected data types. **(H)** List of processing steps for the calcium imaging pipeline triggered by the Process button. **(J)** Loading bar (in red) for the table updating or the processing pipeline, giving feedback to the user about the progress of the requested action. **(K)** Main table to display the selected sub-set of data files. The table's columns are customizable. **(M)** The Data column has a special coloring system for the loading state of each data type for each row: green text for fully loaded rows, orange for a partially loaded row (e.g. only a couple of imaging frames are loaded for preview), gray for data not loaded.*

just contains another sub-level, or it is a *leaf* level, which contains some actual data files. In the `DataWatcher`'s GUI, users can define which levels they want to display (see `WatchType` filter in Figure 3.31 and in Figure 3.32) and also which specific folder they want to explore (see `Row` filter in Figure 3.31 and in Figure 3.32). The combination of these two filters (levels and specific sub-tree) allows to fully specify the sub-tree that the user wants to explore or display. In addition, the *Keep table* option (Figure 3.31, C bottom) controls whether the previously displayed sub-tree should be cleared from the view or kept when the user requests a search. This allows combining searches of two sub-trees.

To implement this, the `DataWatcher` module goes through such hierarchy using a *recursive*

approach and *regular expressions* (`RegExp`). `RegExp` is a powerful codified language that allows the matching of specific patterns of text. A *recursive* approach implies that the *same* function, `DWProcessFolder`, is called on every level for each encountered item, and this *same* function takes care to recognize which kind of folder each item is, irrespective of the hierarchy level examined. This recursive exploration allows complete flexibility in the way the hierarchy is organized and therefore is suited for any user without the need of hard-coding the specific hierarchy structure for each user. Let us take an example to make the functioning of this recursive function calling explicit.

Usually, the first encountered folder is the *animal* folder. The function examines which kind of folder or file type (called *watchType*) the folder is, based on the folder's name. This association between a folder and a *watchType* is made by testing all *watchType*s sequentially for a possible match against the folder's name, as each *watchType* has an associated regular expression. For example, the *animal* folder *mou_bl_160105_02* would be matched using the *animal watchType*'s regular expression: `^mou_bl_d{6}_d{2}$`. If the folder is a match for one *watchType* and this *watchType* is selected to be displayed via the *watchType* filter, the folder must then pass the *row* filter's test: the folder should also be in the requested sub-tree specified by the *row* filter, in this case the *animal* field of the *row* filter should be set specifically to *mou_bl_160105_02* (our folder's name) or be empty so that any *animal* folder is valid. If the *row* filter is also validating, the folder is further searched. Otherwise if either filter's test is not passed, the folder is not selected for search nor for display and the search moves on.

Once a folder has been validated, the further processing of this folder involves repeating this same examination procedure with all items found in the folder, hence the recursive aspect of this function. Each folder in the sub-tree is therefore searched through, as long as the conditions of the filters are respected. For example, in the *animal* folder mentioned above, let us imagine that there is 2 *day* folders: *2016_03_21* and *2016_04_05*. In addition, let us assume that the *row* filter's *day* field was set to *2016_04_05*. Therefore, when the search process encounters the day *2016_03_21*, it recognizes it as a <*day* folder using the *day watchType*'s regular expression `^d{4}_d{2}_d{2}$`. However, it will not search it further as it is not matching with the *row* filter, set to only accept *2016_04_05*. The other day folder, *2016_04_05*, will on the other hand be recognized as *day* folder and also accepted as being compatible with the sub-tree to search defined by the *row* filter.

Finally, the folders and files found during the search can be *leaf* folders, meaning that they actually contain relevant data files. For example, after the *day* folder mentioned above, there could be a *behavior* folder containing the animal's behavior output files. The search process uses the configuration files to know that this behavior files are to be found in the *behavior* folder. It will

thus search through this *behavior* folder and display in the final table one row for each of these behavior file. The same applies to any *leaf* folder, should it be for imaging files, intrinsic files, etc. These *leaf* files can be read or processed to gain information about them (date, size, type, content, etc.). This information, or *meta-data*, will then be displayed for each item in the overview table, described in the next sub-section. The *Skip meta-data* check-box (Figure 3.31, C bottom) controls whether the meta-data for the found *leaf* data files should be extracted or not. This can be useful as extraction of certain meta-data information (for example file size) can take a great amount of time. The search process can therefore go through the file tree faster by omitting certain steps, depending on the user's need.

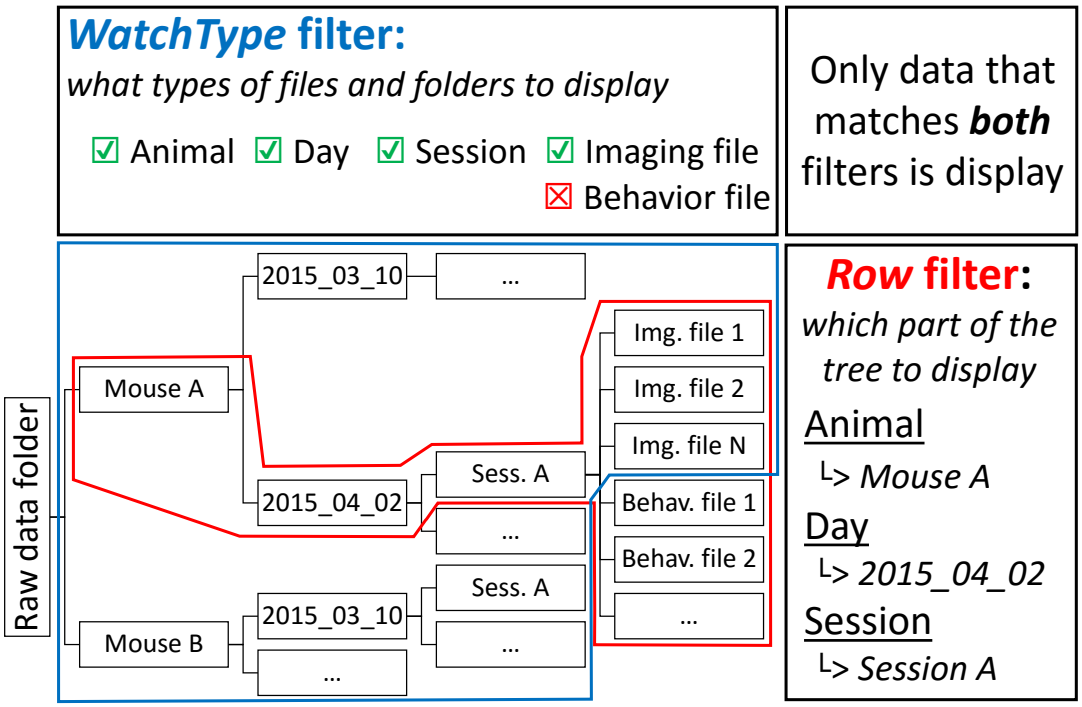

Figure 3.32: The* WatchType *filter *(in blue) is used to select which levels of the file hierarchy and which file types should be displayed. In this example, all levels and files types are requested to be shown, except the behavior files. The* WatchType *filter is combined with the* row *filter (in red), which enables selection of a sub-part of the file hierarchy's tree. In this example, the animal* Mouse A *and the day* 2015_04_02 *and session* Session A *are selected, meaning that only data files from this animal-day-session combination is displayed. For each level (*animal, day, session*), the* row *filter can also be set to empty, meaning that any folder from that level is valid (no filtering on that level). When combining these two filters, only the selected file and folder types for the selected animal/day/session is display (intersection of red and blue area).*

Display of the data set files in a dynamic table

After the search process went through all the files and folders fitting the filters, the gathered information about the file hierarchy's content is then displayed in the main table of the `DataWatcher`. In this table, each row corresponds to a file or folder encountered during the search. For example

in the view presented in Figure 3.31, the first 9 rows correspond to imaging files found in a specific folder (*spot02*) of a specific day (*2015_03_10*) for a specific animal (*mou_bl_150217_05*). Each row is annotated with meta-data during the search and in a post-search annotation step. Information about the origin of the row (animal, day and spot) is added during the search, while other information, like time stamp, file size, row type, etc. are added after the search by a customizable annotation function (`OCIA_annotateTable_*`).

The columns of the table are fully customizable by users, both in terms of their display (ordering, name, etc.) and of their content (what information is stored in each column). This is done through a configuration file that users can easily define before launching the software. The search and annotation steps mentioned before use the user-defined columns to fill the table with information for each row. Since the annotation function is also customizable, the format of the content for each column can also be changed according to the user's own preference. Through this modularity, the table can thus be used for many different purposes, like data management, data processing monitoring or the summarizing of the existing data for an entire project, all without compromising on the precise layout for each user.

The actual data for each row, if any, is not loaded into memory at the search time, it is only referenced in the `DataWatcher`'s main table. The table however contains a field for storing data, but the actual data for each row is only loaded when required. This is implemented in order to avoid loading huge amounts of data into memory at times when this is not wanted. For the same reason, if a row is selected for preview, the data is loaded only partially to memory, just enough for creating a preview. For example in the case of imaging data, only the first few frames of the movie are loaded and then averaged to create the preview. This lowers the memory consumption of the software and increases the speed of preview display, as loading data into memory can be a relatively time-consuming task. Yet, it is still possible and necessary at some times to fully load all the data for a row; this can be done through the `DWLoadRow(this, rowNum, loadType)` function.

The field for storing data mentioned above is somewhat special, as it does not contain only text like all the other field, but it can contain the actual data when it is loaded. The data is stored in this *data* field as a structure containing both the data and information about the type of loading (not loaded, partially loaded or fully loaded). Each row can contain different types of data (raw and processed imaging data, ROI sets, behavior data, calcium traces, etc.) and all of them are stored in parallel in the structure, with their own loading type information. The state of loading for each data type is shown in the display of the table as a colored text (Figure 3.31, M). The text shows whether the data is not loaded (gray), partially loaded (orange) or fully loaded (green). Therefore, users can have an overview of what data is currently loaded in the memory (colored) and what data

is available on the disk but not loaded yet (gray). This feature is an example what can be achieved by accessing the Java components underlying MATLAB, as coloring text in a table requires Java and can not be done with pure MATLAB.

As said above, rows can be selected to be further processed or just to show a preview of their content. For the preview, each row type can implement a `OCIA_getPreview_[ROW_TYPE]` function to display a custom preview, for example a low-resolution image or the average of the frames for a movie or even a color-coded image for the behavior files. This feature mostly uses the partial load of the data as described above. Multiple rows can be selected to be further processed. Selection can be done through two ways: direct selection of the rows by clicking/selecting them or using filters. Filters are a more convenient and faster way to have a specific selection of rows, especially when the table contains already a number of rows.

To create a specific selection, the row filter, also involved in the data set search, can be used. By clicking the *Filter* button at the bottom of the row filter panel (Figure 3.31, B), the displayed rows matching the filtering parameters are selected. Several parameters exist for the row filter, and they are all customizable via a configuration file. In the example view displayed in Figure 3.31, 4 *drop-down*-type filter parameters exist: *animal*, *day*, *spot* (imaging region) and *row type* (imaging row, behavior row, etc.). Each of these have a defined set of values based on what was available but not explored during the search. For example, the search encountered 4 different *animal* folders and 10 *day* folders, but since the filtering parameters were not matching for them, the data files in them was not explored and displayed in the table. However, the search process stored them so that the user can quickly change between different search trees: for example the *day* folders can be quickly changed and a new search launched for another day.

In addition to the *drop-down*-type filter parameters, 4 *text*-type filter exist: general *RegExp*, data load status, row number and run number. The row number and run number parameters can have numbers simple numbers but also a range, for example "'12:15"' or "'[1,2,3:6,7]"'. The general *RegExp* and data load status text filter are more advanced or "'expert-user"' filter parameters as they are using regular expression to match custom columns with custom expressions. In the general *RegExp* field, expressions should use the syntax `COLUMN_NAME = CONTENT AND/OR COLUMN_NAME = CONTENT ...`. A first example not using regular expression but simple text match would be `animal = mou_bl_150217_01 AND rowType = Imaging data AND zoom = 2`, which would find all imaging rows from the specified animal that have a zoom level of 2. The use of regular expression can make this query more precise by adding `... AND comments ~= high`, which would search in the comments text for the "'high"' word, even if it is in the middle of the comments. The data load status text filter uses the same principles, but allows to query the data load type for each row. For example, `data.rawImg.loadStatus = full` would get all the

rows where the raw images are fully loaded. This can be very useful when doing a first processing step and then wanting to move on with only the rows where the processing was successful and the rows are loaded with the output data type. For example, after the calcium imaging processing pipeline, some rows will not pass the quality controls and will therefore not have calcium traces present in their data structure. Specifying `data.caTraces.loadStatus = full` will therefore only select the rows that were fully processed and where calcium data exists for further processing.

Once the wanted rows were selected, several customizable action buttons are available that will perform a custom action only on the selected rows. For example, the calcium imaging processing pipeline can be launched with the *Process* button shown in Figure 3.31 (D). Therefore, the `DataWatcher` can be seen as the starting point of the analysis through these action buttons. The typical workflow of a user would be to open the software, specify some filtering parameters for the file search, do the search, have a look at the existing data files, select some of the data file (manually or using the filters) and then proceed to analyse this selected data.

Finally, a special action button is the *Online analysis* button. Instead of typically moving the selected data files to the next step of processing, this action launches a loop sequence: the table is first updated automatically, then defined rows are selected and processed and some analysis or plotting is performed. The table is then re-updated and another iteration is done, until the online analysis is interrupted. Each steps (search, selection and analysis) can be defined in a configuration file. This mode is very useful when done during experiments, as users can have a fast feedback on what their data actually look like. However this mode requires that all steps can be automatized.

Storage and retrieval of data sets

The `DataWatcher` module takes care of the saving and loading of the data from the disk. This involves the partial and full loading described above, but also the saving and loading of processed data, for example the extracted calcium traces. The file format used by the `OCIA` is the HDF5 format (Hierarchical Data Format version 5). HDF5 has a number of advantages that make it suitable for storing large data sets with complex data in an organized way. HDF5 stores data in a single portable large file that can be compressed and it also enables random reads within the file (all the file does not need to be searched through for finding a specific data set). Furthermore, a number of tools exist to access it from many different programming languages. Furthermore, each data set stored in the file can be annotated with meta-data, so that the origin and experimental context where the data set was created are stored along the data.

The `DataWatcher` stores the data loaded and created in the `OCIA` framework by doing a spare saving and loading. Only the data types requested by the user are saved or loaded. This can be

done using the selection list from the DataWatcher's GUI (Figure 3.31, G). Each data type is saved in its own organized *folder path* within the HDF5 file.

For example, extracted calcium traces for an imaging data file could be stored under the path */animal/day/spot/caTraces/20150310_112400* where as the raw images for the same data file would be under */animal/day/spot/rawImg/20150310_112400*. This allows a nice hierarchical organized storage of files, that can be reused many years later, even more if the appropriate meta-data is saved with the data as mentioned above. The path under which each data set file is saved can be customized by a configuration file. Overall, the DataWatcher creates self-contained data files that are not dependent on the experimenter to be understood and re-used. Furthermore, different HDF5 files can be combined together as the data contained in it is well compartmentalized. It is therefore possible to store the data for all animals in the same single file, that can be compressed for archiving purposes.

3.5.5 Defining Regions Of Interest - ROIDrawer

The ROIDrawer is a module that provides tools for efficiently and quickly label neurons in images from two-photon calcium imaging experiments. It is part of the calcium imaging processing pipeline that the OCIA was developed for in the first place. Originally, this labelling task was done in a much more tedious way using an image processing software called FIJI (Schindelin et al., 2012), part of the ImageJ platform (Schindelin et al., 2015). It quickly appeared that this step was not optimally done by using FIJI and could be made faster, easier and more reliable by integrating it with the rest of the calcium imaging processing pipeline. This however required to create a tool in MATLAB for it, which became the ROIDrawer. The whole calcium imaging processing pipeline will be described in a later section, but the labelling step which is part of it will be described here.

In order to be able to extract relevant calcium signals from the calcium imaging data, a manual or semi-automatic step of neuron labelling is necessary. Indeed, calcium imaging data is recorded from the microscope as images, and these images contain several tens to hundreds of neurons, depending on the imaging field-of-view size. An example image to label is shown in Figure 3.33, (A). Two-photon imaging create an optical section of the neurons present in the brain. Neurons are usually the single units of analysis and therefore the fluorescence collected from them should be grouped together. More technically, each pixel of the image belonging to the same neuron should averaged together in order to obtain a single fluorescence value for each neuron for a given time point. The boundaries of each neuron should thus be delimited or annotated in some form so that an averaging can be performed by the computer in the further steps of the analysis.

The neurons are however not easily defined automatically as their shape is not fully stereotypical, due to their biological diversity in terms of shape and size but also to the optical sectioning

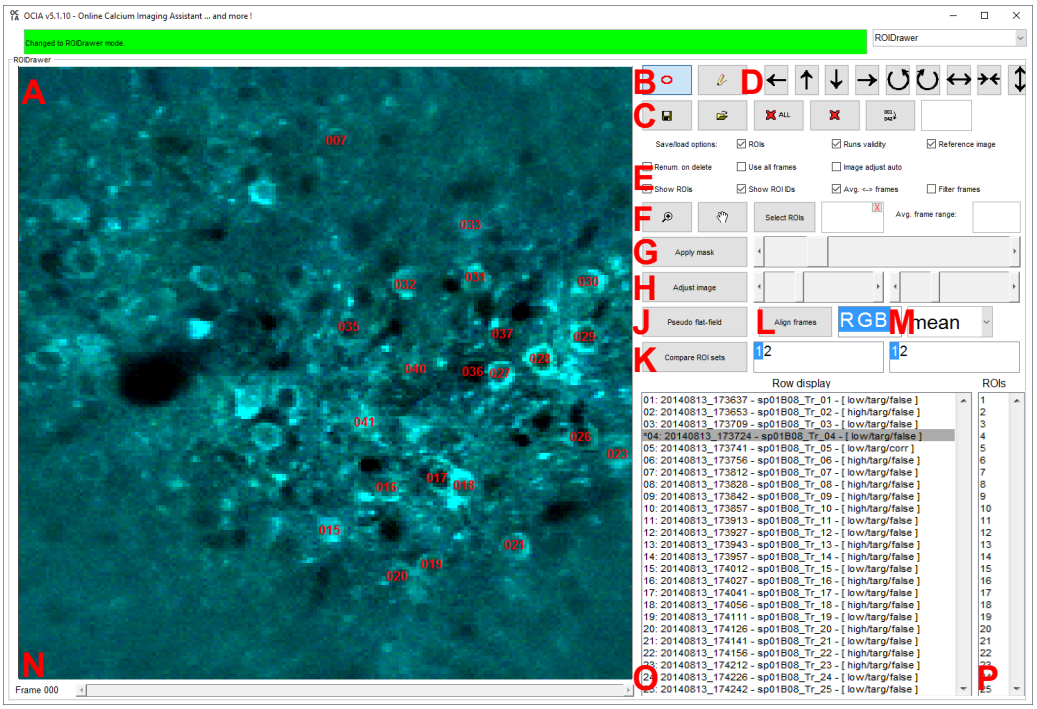

***Figure 3.33:* `ROIDrawer` *module**: a two-photon calcium imaging data Region-Of-Interest defining tool. **(A)** Main display of the image/movie to label. Only half of the ROIs are labelled on this example. **(B)** ROI drawing tools: circular or free-hand. **(C)** Save, load, delete and rename options for the ROIs. **(D)** Transformation tools for the whole ROI set, which helps match ROI sets from the same imaging region on one day and on the next. **(E)** Display option checkboxes. **(F)** Zoom, pan and ROI selection controls. Selection supports range and list input. **(G)** Mask option that shadows all non-labelled pixels. **(H)** Image clipping settings. **(J)** Pseudo-flat-field correction for image smoothing. **(K)** ROI set comparison tool to show the displacement of ROIs from one day to the next. Helps identifying same ROIs for chronic imaging. **(L)** Motion correction on movie frames to sharpen image. **(M)** Color channel control and frame reduction option (mean, max, etc.). **(N)** Current frame number display and frame browser control to run through a movie. **(O)** List of data set rows, each row corresponds to a data file (image or movie). **(P)** ROI selection and display list.*

mentioned above that would give a different picture for a same neuron depending on where it was sectioned. Moreover the labelling provided by the calcium imaging indicator only diffuses to the somata but not to the nucleus of the neurons, giving them a typical *donut*-like shape, a bright ring with a dark center in the middle. This is why a manual labelling (not by a computer) of a Region-Of-Interest (*ROI*) for each neuron is necessary. Some form of automation exist, they will be described below. Furthermore, manual labelling allows greater precision in the inclusion of pixels in the neuron's ROI.

One more problem solved by the `ROIDrawer` is the need to label ROIs for all imaging files. Indeed, calcium imaging experiments typically contain a large number of recordings (movies). In principle, each movie can be slightly different due to movements of the field of view or movements inside the brain tissue. Therefore, labelling done on one movie might not be accurate on a different movie, required the user to label ROIs for each neuron for each imaging file, which can be a tremendous amount of work just for this very fist step of analysis. The `ROIDrawer` and the rest

of the calcium imaging pipeline allows to label ROIs on a single movie and cleverly extrapolate it to relevant imaging data files while still keeping precision in the labelling. This is done by defining a *reference* image on which all neurons are labelled and then *registering* (aligning) all the frames from all the selected imaging movies to the reference image. The registration step is described further below in the calcium imaging processing pipeline section. This way, the labelling process should only be done once per field-of-view, saving a great amount of time for the user.

The `ROIDrawer` provides many tools and features to label neurons in a easy and fast manner, with consistency across different data set files. Here is a list of the features provided by the `ROIDrawer`.

1. Main view: the main view shows the currently labelled image (Figure 3.33, A). The main view supports mouse click events so that users can simply click on the image to label the neurons using the two drawing tools available. The display of the image in the main view can be customized with options like showing or hiding the ROIs or their labels (Figure 3.33, E), changing the shown color channels (Figure 3.33, M), or zooming and panning options (Figure 3.33, F).
2. Drawing tools: elliptic drawing or free hand (Figure 3.33, B). Elliptic drawing provides a quicker labelling as a simple ellipse is shaped around the neuron but it is less precise than the free hand draw which can precisely outline the neuron down to each pixel.
3. Editing: once ROIs have been drawn, it is possible to re-position and re-size them by simply clicking them and then editing them with either the mouse or the keyboard. Furthermore, options to delete and rename ROIs are available to have full control on the ROI set.
4. Saving and loading: labelling of neurons are stored as ROI sets by the `ROIDrawer`. ROI sets contain information about the location and shape of each ROI, their name but also extra information about the *reference* image that was used to defined the ROI set. It also stores information about which imaging file is relevant for this ROI set. Only files marked as relevant for a ROI set are aligned to it. Several ROI sets can be created if the imaging movies for a same field-of-view look very different. This way, all imaging files are always properly labelled. Each of the saving option (ROISet itself, reference image and relevant imaging files) can be activated or not during the saving and loading (Figure 3.33, C), allowing flexible saving and loading operations for the user.
5. Image adjustment: special image adjustment options are available for better seeing the neurons to label. Contrast adjustment options (Figure 3.33, H), *Pseudo-flat-field* correction (Figure 3.33, J) or ROI masking (Figure 3.33, G) are available. The aim of these is to enhance contrast and better show the neurons in regions of the image where a clear outline is difficult to draw visually.

6. Chronic imaging tools: when doing two-photon calcium imaging in a chronic preparation over several days, one needs to identify the same set of neurons across different imaging days. However the shape and size of the field-of-view on one day might look different on the next days. Therefore, a set of ROI set transformation tools is available (Figure 3.33, D) to shift, rotate, expand and shrink the entire ROI set so that it matches the new position of the next day. Furthermore, an ROI set comparison tool is implemented, which shows correspondence between two ROI sets (Figure 3.33, K). This system shows the displacement between ROIs with the same name in ROI sets of the same field of view. This allows easy comparison of ROI sets and guarantees that an ROI corresponds to the same neuron on every imaging day.
7. Shortcuts: each of the function or feature mentioned above can be assigned with a keyboard shortcut to make the tool faster to use.

In summary, the `ROIDrawer` is a quite powerful tool to label ROIs for calcium imaging data, especially in the context of chronic calcium imaging with many imaging files. Having it integrated in the same framework as the calcium processing pipeline allows a very easy transition for users between the different steps of the analysis, as it does not require the usage of an external software, with potential conversion scripts to move from one format to another.

3.5.6 Creation of an automated calcium imaging data processing pipeline

The calcium imaging analysis pipeline was the main and original purpose for which the whole `OCIA` was developed. The purpose of the pipeline is to convert the raw movies recorded by the two-photon microscope into a set of normalized fluorescence time-series for each neuron. This pipeline should ideally be automatized as much as possible, as there are usually a large number of movies and a large number of neurons. The pipeline contains multiple processing steps, which are described further below in this section. Each processing step is not necessarily required for every experiment, and the processing steps can required different parameters depending on the experiment or on the desired output. This is why I originally created the `OCIA` and improved it until it can now offer an automated way of running this calcium imaging processing pipeline, with the possibility to customize which steps should be executed and with which parameters they should be executed.

The processing steps of the calcium imaging data processing pipeline are the following:

1. **Loading of the data**. First, the raw movies should be loaded from the disk. The movies are usually stored in either binary or `TIFF` files. These files should be read and stored in memory. This process is described above in the `DataWatcher` subsection.
2. **Image pre-processing**. Then, the images should be pre-processed to be suitable for the following steps. Indeed, the images can contain multiple types of artefacts due to the record-

ing technique. The removal of these artefacts and the motion correction steps are described separately further below.

3. **Labelling of the neurons**. After the pre-processing of the movies, the neurons should be labelled on a reference image in order to be able to automatically extract the fluorescence time-series. This labelling step is described above in the `ROIDrawer` subsection.
4. **Normalization of the image**. To extract normalized calcium indicator fluorescence time-series, a background normalization step should be done on the movies. Indeed, the fluorescence value recorded in the movies has no unit and is an arbitrary intensity value. Therefore, this intensity should be normalized by subtracting the background intensity from all the images for each movie, in order to have a true "zero" where there is no fluorescence. This is done either by selecting a *background ROI* during the labelling step or by removing a fix value using a percentile of all the intensity values. This latter method is implemented in the `OCIA`, where the first percentile of all pixels from a movie is subtracted from all images.
5. **Extraction of the calcium traces**. Once the movie is normalized, the time-series for each neuron can be extracted using the labelling previously defined. All the pixels within the Region-Of-Interest defined for a neuron are averaged together in each frame. This gives the raw fluorescence F for each time point. This raw fluorescence is then further normalized using the $\Delta F/F$ formula:

   $$\Delta F/F = \frac{F - F_0}{F_0}$$

   The normalization uses F_0 fluorescence level as the baseline fluorescence level. This F_0 can be obtained in various ways from the raw fluorescence F. Possible methods are extracting the mean of the raw fluorescence F, either for the whole trace or for the pre-stimulus time if there are stimulus presentation. A polynomial fit can also be done on the raw trace and used as baseline F_0. The last method, which is the one used in this thesis, is to take a percentile of all the fluorescence values. Typically the 12^{th} percentile for each neuron in each recording is taken as the F_0. This value needs to be however adjusted to the experimental conditions and to the activity of the neurons, as a silent neuron would have its true baseline F_0 at the 50^{th} percentile.

   Note that in the case where ratiometric calcium indicators are used, the ratio R of the two fluorescence channels is calculated and used in place of the raw fluorescence channel F. In this case, the final time-series is usually referred to as $\Delta R/R$.
6. **Generation of stimulus vector**. In the case where stimuli were presented during the calcium imaging, a stimulus vector can be created to mark the stimulus times in relation to the extracted calcium time-series. This stimulus vector can be created by default by the `OCIA` or using custom functions. Each stimulus is encoded in one or several bits of a vector that has

the same length as the calcium time-series. Therefore, each time-point can be marked with an arbitrary number of stimulus type. These stimulus vectors are then used in the `Analyser` module to do analysis and generate plots, for example the peri-stimulus time averages plots.

Automation of the calcium imaging processing pipeline with quality controls

As said above, the execution of all these steps can be controlled by the user, both in terms of their parameters or they can be fully excluded if they are not necessary. This can be done using the GUI controls in the `DataWatcher`'s panel (Figure 3.31, H). Moreover, the inclusion of each processing step in the pipeline and the parameters for each steps can be modified and customized using configuration files. In this way, users can simply select the imaging movies they want to process via the main table of the `DataWatcher`'s panel (Figure 3.31, K) and select the required processing steps (Figure 3.31, H) and launch the fully automated processing pipeline.

The successful completion of the pipeline only requires that the ROIs are already labelled for the selected movies. Otherwise, a warning message will let the user know that this is not done yet. Moreover, the execution of the pipeline can be monitored thanks to a detailed log displayed by the `OCIA` for each processing step. This log also includes quality controls for the steps that require it. Quality controls are an essential requirement in automated processing pipelines, as they show to the user when the data is not suitable for analysis or if something is not conform to the expected outcome. Without quality controls, the pipeline would complete successfully but potentially include erroneous or low-quality data. Parameters for the quality controls, like thresholds of inclusion or exclusion, can be modified using the configuration files.

In addition to the quality controls, debugging plots can be displayed for each processing step. These visual displays of the processing step inputs and outputs help users to better understand what is being done with their data and how each parameter can influence the outcome of the processing pipeline. A feedback on the success of the processing pipeline for each row is finally shown in the *Data* column of the `DataWatcher`'s main table. Rows that do not have a green label in the *Calcium trace* column are imaging movies that had an error in their processing or that did not pass the quality controls. Furthermore, only rows that have valid data can be further used for the analysis in the `Analyser` mode.

The whole pipeline is implemented with a cache-like system that checks what has already been processed and avoids re-processing data that is already existing, saving time and computation power for the user. Finally, the `OCIA` also comes in a *no-GUI* mode, where no graphical interface exists. In addition to this, command line options exist for launching the software with specific tasks or parameters. This allows to run the calcium imaging processing pipeline as batch jobs for

several experiments in parallel, allowing automatized and fast execution of a processing pipeline on multiple computers or on a cluster.

Dealing with image artefacts and motion correction

When recording calcium imaging data with a two-photon microscope in alive animals, many artefacts can be present in the recorded images. Artefacts can be categorized in two classes: recording artefacts and motion artefacts. Both of these artefacts categories can be corrected for, even though sometimes only partially.

The recording artefacts contain artefacts and glitches in the image due to the recording technique or the digitalization of the fluorescence signal into an image. These include for example the first frame of each movie being partially black (no fluorescence) because of the time the shutter needs to move away from the laser's path. Another artefact is the frame jitter, where each line of the image is slightly shifted compared to the next line. This artefact appears if the speed of the X-axis scanning mirror of the microscope does not have a constant speed. The OCIA's calcium imaging processing pipeline provides function to fully remove these artefacts.

The motion artefacts are problems arising due to the recorded biological sample moving under the microscope. This happens in all recording with alive animals and are much more prominent if the animal is awake and even behaving in a task. Motion artefacts are typically corrected in two different ways. First, the lateral motion on the X and Y axis can be corrected on each frame, as described further below. On a second step, the motion on the Z axis, along the optical axis, can only be assessed but not corrected for. Indeed, the motions along the optical axis shift the focus of the microscope up and down, which leads to the recorded imaging plane moving out of focus and therefore not being imaged. Data is therefore missing in the frames where the focus changed too much due to a movement of the animal. Imaging techniques with multiple focal planes being recorded almost simultaneously (*plane hopping*) can compensate for these artefacts by recombining the different planes recorded, but this is not supported by the OCIA.

Lateral movement on the X and Y axis can be corrected by aligning the frames to a reference image. Typically, the reference image is defined as the average of a time period in the movie where movement is limited or as the average of all frames (still containing some movements). Each frame of the movie is then aligned to this reference image using well-known registering algorithms. The algorithm used by the OCIA, called *TurboReg*, is based on the Java code developed by a group at the EPFL (Thevenaz et al., 1998). It is a fast registration method that can be easily parallelized to run faster on computers with multiple cores. Other algorithms exist, some of them allowing to do motion correction on a per-line basis rather than working with the whole frame (Chen et al., 2012).

3.5.7 Analysis and visualization of data sets - `Analyser`

The `Analyser` module takes care of the analysis and visualization of the data. It is designed as an *interactive* analysis and plotting tool. It works mainly with time-series and stimulus vectors, the former being usually extracted from calcium imaging data using the processing pipeline described above. Typically, the images are processing with the pipeline and the extracted calcium time-series are imported into the `Analyser` for analysis and visualization.

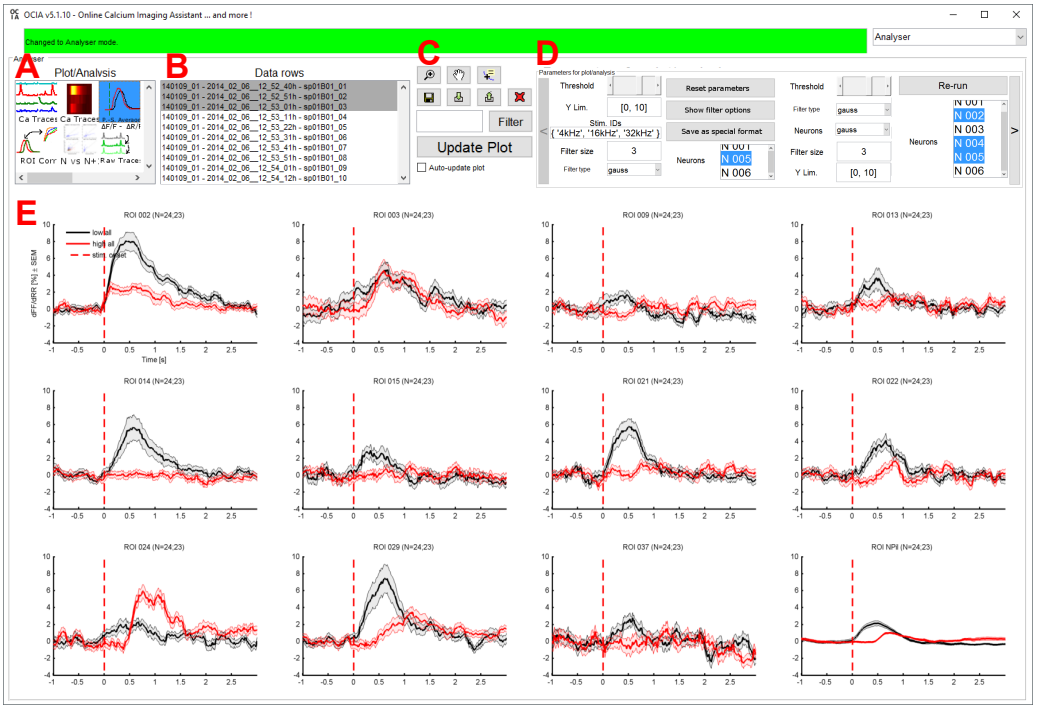

***Figure 3.34: `Analyser` module**: a data visualization and analysis tool. **(A)** Analysis or plot type selection. This list is custom and can be extended simply by adding files to a custom folder, icons being optional. **(B)** List of data set rows, each row corresponds to a data file. **(C)** Top: zoom, pan and data cursor tools to manipulate and examine plots. Middle: save and load options for both the displayed plot but also the analysed output data. Bottom: data set row filter option and update plot button, that re-plots the data or re-runs the analysis. A caching system exists to avoid re-doing analysis with identical parameters. **(D)** Parameter panel for the current plot/analysis. Each plot/analysis has a custom user-defined parameter list that can be easily changed. **(E)** Output display area. The output of each plot/analysis is displayed here into one or multiple plotting regions. The example shown is the peri-stimulus time average response for 11 neurons and the neuropil recorded during a go/no-go discrimination task. Choice of neurons and averaging options can be easily changed using the parameter panel.*

The `Analyser` provides a large set of analysis and plots, which can easily be selected in the GUI (Figure 3.34, A). All these analysis and plots are stored as single function files, creating a base on which to extend. Indeed any custom analysis function can be added to the existing set and will automatically appear in the selection list. In general, each analysis function is also including a plotting function, showing the result of the analysis.

For example, in the view shown in Figure 3.34, a peri-stimulus time average for two different

stimulus types is shown for several neurons. This function builds on the peri-stimulus time averaging function that uses the calcium traces and the stimulus vector. The stimulus type(s) and the neurons to plot can be selected using the parameter panel available in the `Analyser`'s GUI (Figure 3.34, D). Tools are provided to better examine the displayed data: zooming, panning (moving) and data tip (show data value) are available, along with buttons to save the shown plot and/or save the underlying data used to generate the plot. (Figure 3.34, C).

The analysis and exploration of the data is an iterative process, usually done by changing some parameters and running the analysis again. Therefore, an easy way to change the parameters is required. Rather than going in the code and searching for the definition of each parameter, the `Analyser` provides a parameter panel (Figure 3.34, D) to quickly change the parameters without going back to the code.

This parameter panel system is combined with a caching system that automatically saves the results of each analysis when they are executed. This avoids repeating an analysis that has already been done, saving time for the user and increase the interactive aspect of the `Analyser` module. The caching system is aware of the parameter panel and of the dependencies of each analysis to each parameter. Therefore, when an analysis is being run, the caching system checks if a critical parameter has been changed for each analysis step. Only the steps where a critical parameter has been changed will be re-executed, as the change of parameter can lead to a different output of the analysis. In this way, only minimal time is required to examine the effect of an analysis parameter on the output.

3.5.8 Visualization of single trials - `TrialView`

The `TrialView` module is a custom module created for a specific purpose: visualizing single trials for the wide-field calcium imaging with the delayed discrimination experiments. Therefore it is less generic and less customizable as the previously described modules. The precise experimental conditions and resulting data for which this module was created are described in more detail in the *Methods* and *Results* sections. Briefly, animals performed in a auditory *go / no-go* discrimination task with a delayed reporting of the response, combined with wide-field calcium imaging of portion of the cortex.

These experimental conditions, wide-field calcium imaging combined with behavior, produce a great amount of data but more importantly complex data with different types of data sets and different time references that need to be aligned. Indeed, several data types or variables were recorded simultaneously with different means:

1. **Wide-field calcium imaging** recording the cortical activity, which produces a 512-by-512 pixels movie with about 240 frames, usually recorded at 20 Hz, one movie per trial

2. **The behavior monitoring** camera recording the animal, which produces a 720-by-480 pixels movie with about 20'000 frames, usually recorded at 30 Hz, one movie for the entire training session (about 20 minutes).
3. **Licking spout** recording the licking reporting the decision of the animal, which produces a analog time series of about 36'000 data points recorded at a sampling rate of 3 kHz, one time series per trial.
4. **Microphone** recording the played sound stimulation, which produces the same data type as the licking spout (same analog input box).
5. **Wide-field camera trigger signal** recording the triggering time of the wide-field camera, which produces the same data type as the licking spout (same analog input box).
6. **Whisker tracking** camera recording the whiskers' position, which produces high speed images that are converted into a time series down-sampled to the wide-field camera's frame rate, one time series per trial.

A main requirement to analyse this type of experiment was to be able to look at single trials individually with all the above mentioned information and data combined. The aim of the `TrialView` module was to fulfil this requirement by providing a tool that can combine and extract the relevant

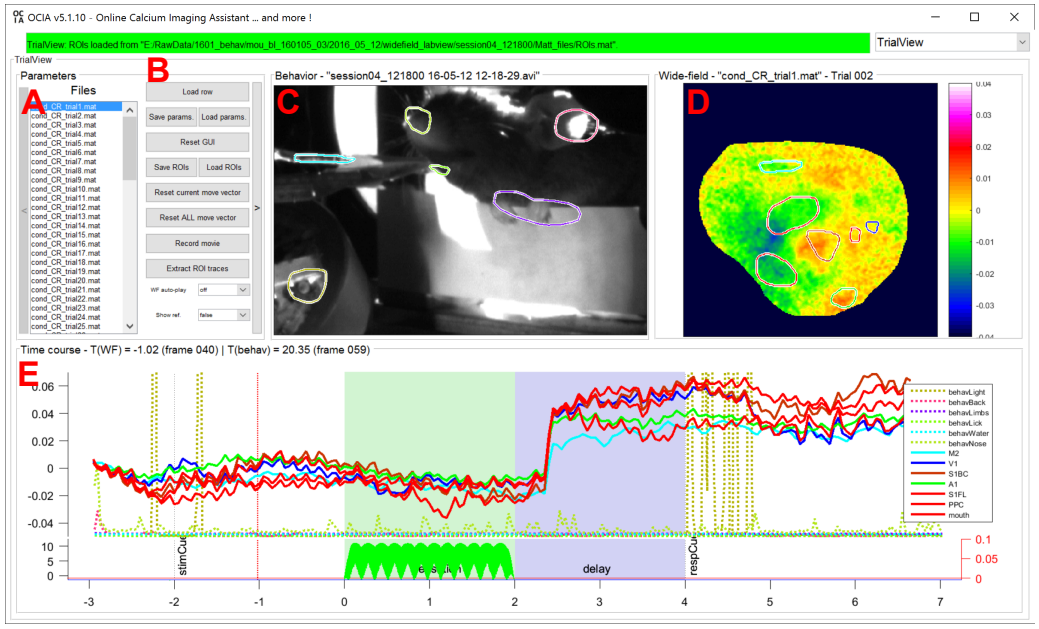

***Figure 3.35: `TrialView` module**: a single trial exploration tool. **(A)** List of the trial files. **(B)** Action buttons: row loading, parameter save and load, GUI reset, ROI set save and load, move vector control options, movie recording, ROI trace extraction. Bottom: display options. **(C)** Behavior movie view with behavior ROIs drawing function. **(D)** Calcium imaging data view with cortical ROI drawing function. **(E)** Time course view of the behavioral variables and the cortical ROI extracted calcium traces. On the bottom, lick trace, sound stimulation, trigger signal and whisker traces can be displayed. On the top part, behavior ROIs and calcium ROIs are overlayed. This allows visual inspection and correlation between the different variables.*

part of each of these data types and display them all in an interactive Graphical User Interface. Given the different time references and frame rates of the different variables, the first challenge accomplished by the `TrialView` module was to bring all these different variables into a common time frame.

When exploring wide-field calcium imaging data, it is necessary to get an idea of both the spatial organisation of activation regions as well as the temporal dynamics of this activation. The `TrialView` module provides this spatio-temporal visualization by showing the spatial organisation in a panel (Figure 3.35, D) and in another panel, the extracted time-series for user-defined Regions-Of-Interest (Figure 3.35, E). This way, users can go back-and-forth between the spatial and the temporal aspect of the recorded cortical activity.

When working with awake behaving animals, each trial is unique as the animals present a large range of variability in their behavior. This variability is often boiled down to a very small amount of variables, in the case of a go / no-go task this can even be just a lick / no lick binary variable describing the whole behavior of the animal. Thanks to the behavior monitoring camera, it was made visible that the animal shows more complexity in the behavior when the body movement is also taken into account and carefully monitored (Dr. Ariel Gilad, personal communication). Moreover, the body movement can greatly influence the activity measured in the cortex with the wide-field imaging. Therefore, looking at single trials is crucial in order to understand the observed cortical activity.

To quantify these body movements, an ROI defining feature was implemented for the behavior movie in a very similar way as for the wide-field imaging movie. Users can define ROIs both for the behavior movie and for the wide-field movie by simply clicking on them and drawing a Region-Of-Interest. In the case of the wide-field movie, the $\Delta F/F$ is computed for the selected region, whereas for the behavior a so-called *frame-to-frame* correlation method is applied. The frame-to-frame correlation $Fr2Fr_{corr}$ for each time point is calculated using the formula:

$$Fr2Fr_{corr}(t_1) = corr(Frame(t_1), Frame(t_2))$$

Frame-to-frame correlation is a very reliable method to detect changes in the behavior movie, therefore being very useful to quantify movements. The two types of time-series are then displayed in a common time frame in the `TrialView`'s GUI (Figure 3.35, E).

Additionally, the `TrialView` module provides a parameter panel, allowing to quickly change parameters for the different display elements (axis limits, colormap, color clipping, synchronization options, etc.) and provides tools to save and load parameters, extracted time-series or an window-capture movie of a whole trial with all the variables displayed in a common window. The time series display panel (Figure 3.35, E) is also made interactive so that users can navigate through the trial

by dragging the mouse or clicking the different time points. Some custom defined action buttons also exist to perform repetitive tasks in an automatized way, like exporting all the behavior vectors for all trials.

Using all these tools, users are able to quickly and efficiently explore trials in an interactive way, enabling the analysis and visualization of the different data types in an integrated framework. This allows comparison and association of the different behavior or experiment variables with the spatio-temporal dynamics of the recorded cortical activity. This module was also used in the analysis of my own data.

3.5.9 Automatization of mouse joint tracking - `JointTracker`

The `JointTracker` module is another custom module created for a specific purpose, similarly to the `TrialView` module. In this case, the aim was to track mouse joints (shoulder, elbow, wrist, etc.) in behavior movies recorded laterally from mice running on a ladder treadmill. The angle between each joint had to be quantified to relate them to the simultaneously recorded motor cortex activity, measured by two-photon imaging. Joints are marked by a black dot to help the tracking.

Previously, a semi-automatic program was used to solve this problem, but the algorithm used by that program was not efficient enough, leading to the manual annotation of the movies, a process that is extremely time consuming. Therefore, a new way of automatically tracking the joints was explored using the *JointTracker* module. The `JointTracker` provides a fully automatic, a semi-automatic and a manual tracking of the mouse joints. It also provides options to pre-processed the videos in order to enhance visibility of the tracked joints.

The automatic and semi-automatic mode use the algorithm described below to track joints. Manual tracking can however sometimes be necessary, in periods of the videos where the joints become less apparent or where the algorithm is not performing optimally. Therefore, a special attention was also made to create a very user-friendly manual tracking experience. Shortcuts and clever mouse interactions were implemented to facilitate the manual tracking and shorten the tracking time. A slider is also present to easily navigate in the movie (Figure 3.36, G), but most of the action are done via the mouse or the keyboard as they are more intuitive and faster input methods.

The algorithm uses a combination of methods to achieve an accurate tracking of the joints. A first reference point needs to be defined for each joint. The algorithm then takes these as reference and tracks the joints on the next frame using always the results of the previous frames, in a sequential manner. The main component of the tracking is the usage of cross-correlations. A reference template image is defined for each joint using the previous frame and a Gaussian

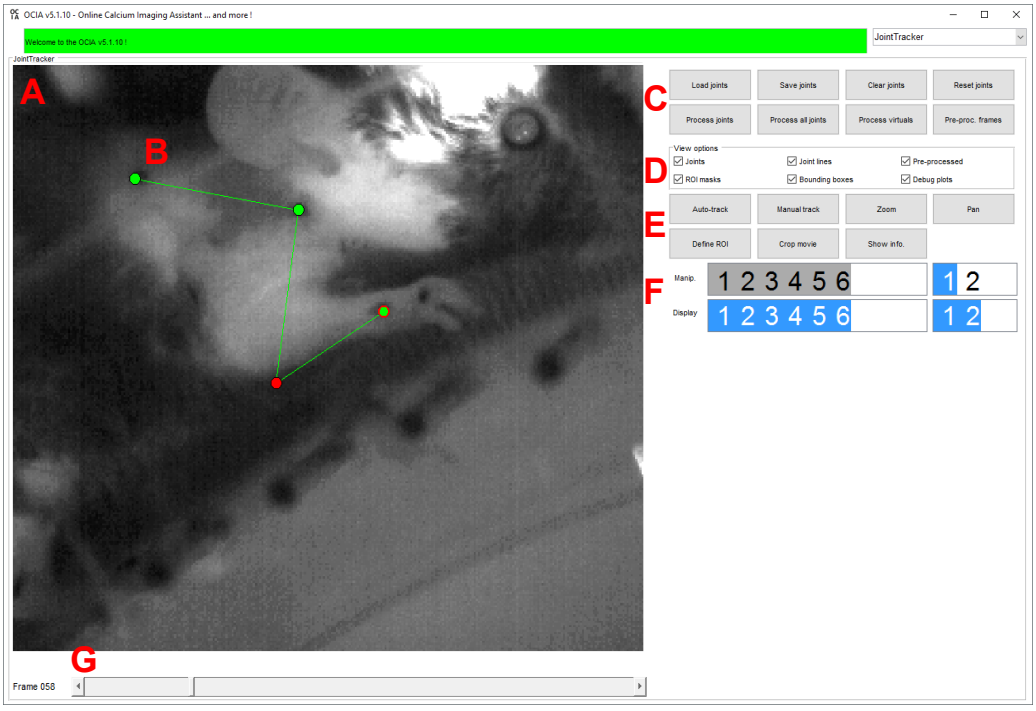

***Figure 3.36: `JointTracker` module**: a mouse joint tracking tool. **(A)** View of the recorded movie. Each joint can be manually clicked and repositioned, or joints can be automatically tracked by the software. **(B)** Joint tracking labels, one point per joint. Different colors label different joint types: manually added joints (black outside, green inside), automatically added joints (red outside, green inside), virtual joints (red inside), etc. **(C)** Save, load and discard options for the joints and processing options for automatically label joints on next frames based on the current joints and user-defined parameters. **(D)** Display options (show/hide joints, joint lines, bounding boxes, debugging plots, etc.). **(E)** Additional view and action buttons: zoom and pan tools, auto tracking, movie pre-processing actions. **(F)** Joint selection options for display and manipulations.*

template matching the joint size. This reference image is then cross-correlated to the current frame, within a delimited region (bounding box) as the joints are not expected to move randomly across the image. The bounding box is dynamically created for each joint, depending on the amount of change in the video since the previous frame. Indeed, a number of change in the video (quantified using the frame-to-frame correlation algorithm described earlier) indicates that the joint might have move more than if the frame is static

The cross-correlation values are weighted using some additional constraints, like the defined distance between the joints which is not supposed to change too much, as the joints are separated by bones that cannot change in length. By combining the cross-correlation values and the expected location of the joints, the most likely current location of the joint is defined and marked as the automatically calculated position of the joint. This position is displayed on the main view (Figure 3.36, A) with dots and lines of different colors, marking the type of joint: automatically annotated, validated, manually tracked, saved joints, etc. (Figure 3.36, B).

This module was not used in the analysis of my own data and was solely created to help other

members of the lab. The main purpose was as said above the mouse joint tracking. However, the flexibility and modularity in the implementation of the algorithm allowed the `JointTracker` to have been used for 2 additional purposes, briefly described below. The flexibility of the algorithm comes among others from the flexibility of its implementation and from the flexible definition of the parameters through a configuration file.

In addition to its original purpose, the `JointTracker` module was used for mouse pup head tracking in a cage and for fiber tip tracking. In the first case, mice were randomly moving in a cage and the amount of movement and the position of the mice across time was tracked using the `JointTracker`, mainly using the manual tracking as the head of the mice was not well defined (black spot on dark background). In the second case, fiber tips of a mouse whisker stimulator were tracked for a jitter quantification experiment. The tips of a glass fiber, marked in black, were semi-automatically tracked using the `JointTracker`, which was possible by slightly adjusting the parameters of the tracking algorithm.

3.5.10 Recording intrinsic signal - `Intrinsic`

The `Intrinsic` module is an experiment controller module created for intrinsic imaging. It uses `MATLAB`'s *Image Acquisition Toolbox* (*imaq*) to grab images from the intrinsic camera. The software is designed to provide feedback to the user during the recording to better control for artefacts and potential problems. It includes a live view panel (Figure 3.37, A), a reference image panel showing the blood vessel pattern (Figure 3.37, B), a set of controls buttons (Figure 3.37, E) to connect/disconnect the hardware and to start/stop the experiment, controls buttons to manipulate and examine the data recorded (Figure 3.37, G, zoom, pan and data tip buttons). Finally, similarly to the other modules described before, an interactive parameter panel also exist in this module to quickly change the experimental parameters. In addition, pre-sets of parameters can also be defined and easily changed to have pre-defined experimental conditions.

Two types of experimental paradigms are implemented: *standard* intrinsic imaging and *Fourier* intrinsic imaging. These paradigms are described in the *Methods* section. Briefly, the standard imaging is trial-based (or repetition-based) stimulus presentation paradigm, where the signal after the stimulus is averaged and normalized to the signal before the stimulus, and the Fourier imaging presents a continuous cycle of a gradual change in a stimulus feature and the signal is then decomposed with a Fourier transform and analysed at the stimulation frequency.

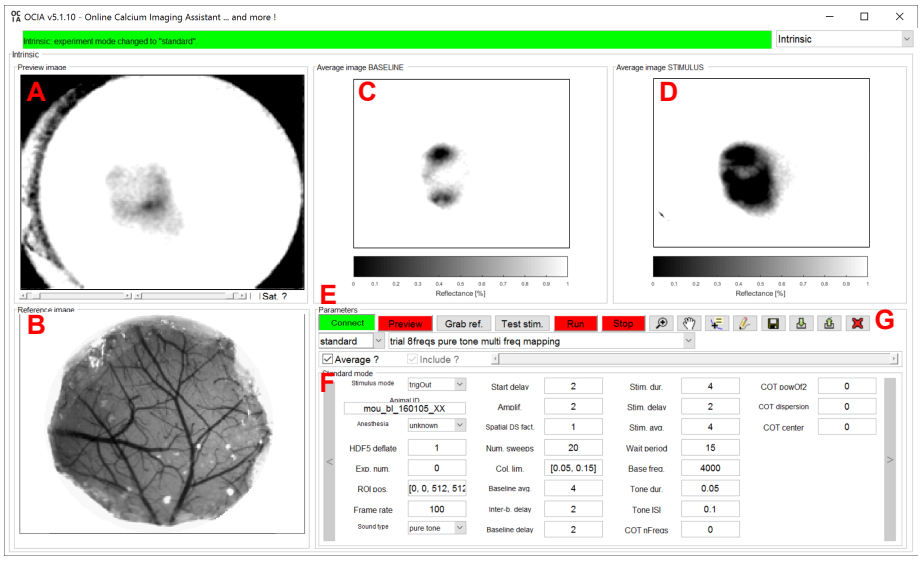

***Figure 3.37: `Intrinsic` module**: a stand-alone intrinsic imaging software. **(A)** Live view. **(B)** Reference image view. **(C)** Average image view of the baseline condition (no stimulus). **(D)** Average image view of the stimulus condition. **(E)** Action buttons: hardware connect, preview mode, reference grabbing, stimulation signal test, experiment run and stop. **(G)** View and action buttons: zoom, pan, data cursor and ROI draw tools, save and load buttons for data as images and MAT files. **(F)** Parameter panel controlling acquisition parameters, stimulation protocol and saving options.*

3.5.11 Control of complex behavior training in real time - `Behavior`

The `Behavior` module is another experiment controller module created for the behavior experiments. Many behavior control software are running on the `LabVIEW` environment, which is very suitable for small applications but can become very complex and difficult to maintain for larger software. The `Behavior` module uses `MATLAB`'s *Data Acquisition Toolbox* (*daq*) to read from and write to digital and analog channels. This module was used for all the behavior experiments described in this thesis.

The tasks that are handled by the `Behavior` module are the following:

1. **Communication with hardware**: as said, the `Behavior` modules uses `MATLAB`'s *daq* toolbox to read and write analog and digital data, allowing the software to communicate with the outside world. This is necessary in an experiment controlling software in order to send triggers, send gating controls and collect analog input data
2. **Trial structure and event handling**: the module has an internal representation of the experimental trial and knows what tasks to perform at what time. It has an internal loop that tracks time and processes events as they come. Among others, delay times are waited, stimuli are presented and triggers are sent when appropriate.
3. **Response detection**: the module can detect in real-time whether a response was made by the animal by monitoring an analog input channel, usually the licking port. It can then deliver

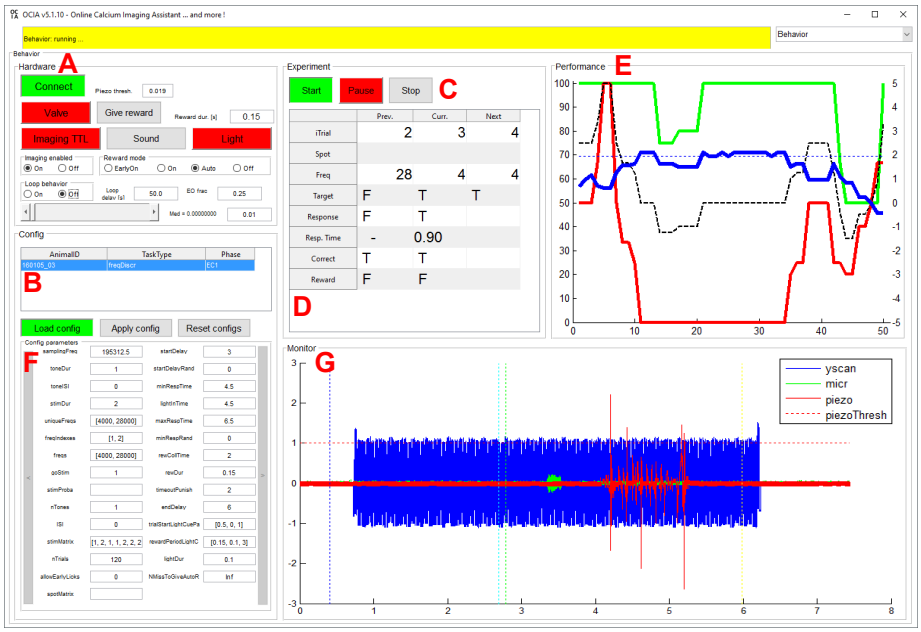

***Figure 3.38:* `Behavior` *module**: a stand-alone behavior control software. **(A)** Hardware panel: action buttons for connecting and setting analog and digital inputs and outputs. **(B)** Configuration panel: a configuration can be selected amongst predefined configurations, usually with one per animal trained. Configurations are stored in a MAT file, which can be generated by a custom script. **(C)** Experiment panel action buttons: start, stop and pause buttons. **(D)** Experiment panel trial table: an overview table of the trial sequence. **(E)** Performance monitoring panel: a plot with running averages of the animal's behavior variables, like hit and false alarm rate, and* d' *sensitivity index for performance. **(F)** Parameter panel: all parameters controlling the trial sequence and features, like sounds to play, timing, etc., generated automatically from a user-defined configuration file. **(G)** Monitoring panel: real-time display of the recorded analog and digital inputs and outputs, like the licking sensory, the sound, the two-photon's scanner's Y mirror, imaging triggers, etc.*

the appropriate outcome, either a water-reward or eventually a punishment air-puff.

4. **Live display**: in order to monitor the behavior of the animal, a live display of the time-line of the trial and of the experiment is shown (Figure 3.37, C and G). The performance of the animal is also updated after every trial and shown using running average performance curves (Figure 3.37, E).
5. **Live parameter adjustment**: like in any experimental software working with live samples, there is a need of adjusting parameters easily and rapidly during the experiment to adapt to changes in the animal's behavior. This can be done using the parameter panel of the `Behavior` module (Figure 3.37, F).

A key element of such a behavior control experiment is the temporal precision. Indeed, if the rewards or stimuli are not delivered with a sufficient precision, the animal's perception of the task will be perturbed. Therefore, several versions of this module where required to improve and achieve a near-millisecond precision. The main technical challenge was to transition from a procedural sequential approach in the first versions, which had some unexpected delays, to a looping system with *MATLAB*'s `timer` object, which allowed constant time between each event.

4 Discussion

4.1 The oddball effect in the auditory cortex

The oddball effect is a well-studied change detection or "surprise" detection phenomenon observed in the brain. In this thesis, it was explored whether it was possible to measure this oddball effect or the stimulus-specific-adaptation (SSA) using supra-threshold recording techniques. Two different recording techniques were used in combination with the same oddball paradigm: juxtacellular electrophysiology recordings and two-photon calcium imaging. In both cases, the oddball effect was observable, as the response to the oddball stimulus was greater than the standard stimulus immediately before. However the differences were not as clear as in recent sub-threshold measurements (Chen et al., 2015). More experiments and controls would however be necessary to complement the results shown in this thesis, in order to study the SSA and the mechanisms it involves in more details.

The oddball effect has also been studied in other modalities, for example in the somatosensory cortex (Musall et al., 2015), where single-whisker stimulus features evoked robust SSA in individual cortical neurons of the somatosensory cortex. As many cortical regions might be involved in the circuits governing the SSA, it would be interesting to study SSA using larger scale approaches, like the wide-field calcium imaging used in this thesis. With such an approach, the temporal flow of the SSA could be addressed on a large scale. It would also be possible to compare the *magnitude* or the oddball effect size in different cortical regions. Furthermore, the modality specificity of the oddball effect could also be studied, by presenting sequences of stimuli in one modality and using an oddball stimulus of a different modality. As the sensory cortex of both modalities could be imaged at the same time, this paradigm could bring insights on the cortical circuits involved in the change detection mechanisms of the brain.

4.2 Mapping frequency tuning in the auditory cortex

4.2.1 Measuring frequency tuning in single neurons

Two different approaches for assessing the frequency tuning of single neurons have been used in this thesis: cell-attached electrophysiology and two-photon calcium imaging. Electrophysiology in cell-attached mode (*juxta-cellular* recording) allows to record supra-threshold spiking activity from a single neuron on the millisecond time-scale, whereas two-photon imaging can record the changes of calcium concentration in multiple neurons, down to a ~10 - 15 millisecond time-scale (77 Hz in this thesis). Electrophysiology was used in combination with two-photon guidance, allowing the specific recording from targeted interneuron types labelled via a genetically modified mouse line (Taniguchi et al., 2011). In the two-photon imaging experiments, cell type was also identified via the use of the same genetically modified mouse line. Two-photon calcium imaging with YC-Nano140 was used to measure the frequency tuning property for multiple neurons at the same time.

In both techniques, the response size from most of the neurons was not very large, as the neurons responded with only few spikes or small calcium transients. This low response property for pure tones in many neurons is sometimes referred to as *sparse coding* (Olshausen and Field, 2004). In this context, sparse coding in the auditory cortex refers to the low amount of neurons encoding auditory information with a high response, with most of the other neurons only weakly responding to the sound. This property is different in each sensory cortex, as for example the visual cortex can show intense sustained firing in response to visual stimuli (Hofer et al., 2011).

The small response amplitude also affected the process of determining the best frequency in the frequency tuning of neurons. Multiple ways of quantifying the tuning for each frequency have been explored (mean evoked response, GLM, response probability, etc.). As the responses are not very large, the tuning curves were found to either be rather flat or multi-peaked. This can however be due to the limitations of the recording technique and calcium indicator used in this thesis (YC-Nano140), as *V-shaped* tuning curves with clear best frequencies have been shown in the literature using electrophysiology (Liang et al., 2014; Guo et al., 2012) or two-photon calcium imaging (Bandyopadhyay et al., 2010; Rothschild et al., 2010; Winkowski and Kanold, 2013; Issa et al., 2014). To have the best chances of capturing the *real* tuning curve of neurons, more sensitive calcium indicators, like the GCaMP family (Chen et al., 2013a), and lower noise in recordings are necessary. In two-photon calcium imaging experiments, noise can originate from multiple sources, among others: optical path alignment defects (misalignment) affecting the focusing capability of the microscope (larger point spread function), damaged or misaligned detection system (photo-

multiplier tubes), electrical noise in the amplification of the detection signal, lack of laser power, scattering of the tissue (especially in deeper recordings).

It should however be noted that many different aspects of the sound stimulus are encoded by the auditory neuron, not just the *pure* frequency. Therefore, it can be that pure tones are not the *ideal* stimulus for getting a maximum response from auditory neurons, especially in the auditory cortex, as it is an already higher stage of processing the auditory information. This non-optimal hypothesis is also the reason why more complex sounds have been used in this thesis, like the *cloud-of-tones*. Finally, differences in activation magnitude can also come from the engagement of the mouse or the attention to the sound. Passively listening to sounds compared to an attentive listening in the context of a behavior task produces different activation level in auditory neurons (Otazu et al., 2009).

4.2.2 Homogeneity and stability of the frequency tuning

Recent advances of genetics allowed the creation of transgenic mouse lines that express genetically encoded calcium indicators proteins in specific layers of the cortex. These transgenic mouse lines allow fantastic opportunities for longitudinal studies of activity patterns in the rodent cortex. In this thesis, the frequency tuning of neurons were measured in chronic experiments, and the stability of the response amplitude and of the frequency tuning was assessed. In addition, two-photon calcium imaging allowed to examine the frequency tuning of a large set of neurons in a local field, giving therefore information about the spatial organization of different properties of neurons that are close to each other.

The homogeneity within a single imaging region was assessed using color maps encoding responsiveness and frequency tuning. Little homogeneity or specific patterns were visible in both frequency and responsiveness maps. The heterogeneity of the frequency tuning on smaller scales has already been reported before (Rothschild et al., 2010). Despite showing a clear tonotopic gradient on larger scales (Guo et al., 2012), the auditory cortex shows a much less homogeneous organization on smaller scales. This heterogeneity has however been shown to be layer specific, as layer 4 neurons show a more homogeneous spatial organization compared to layer 2/3 (Winkowski and Kanold, 2013). Other tuning properties of the neurons regarding the sound stimuli (loudness, response amplitude, response latency) could also be investigated for such layer dependent spatial organization. The limits of the experiments presented in this thesis are the low response levels. Indeed, it is difficult to define frequency tuning of neurons, or any other properties, when only small amplitude responses are measured.

Stability of tuning and of responsiveness was assessed by comparing the best frequency and the response to the best frequency from one day to the next, on several consecutive days. The

frequency tuning of neurons changed severely from one day to the next, whereas the responsiveness showed some relative stability. These results were however measured only on a few days, and the frequency tuning was itself not a very robust measure due to the low responsiveness of neurons (see previous subsection). Others have reported a high degree of stability for frequency tuning and other response properties in the auditory cortex (Galván et al., 2001). Differences from the current results are probably due to the difficulty of defining frequency tuning for neurons with low responsiveness, especially in high recording noise conditions. Therefore a better assessment of the frequency tuning for each neuron, with lower recording noise or more repetitions, should be done in order to confirm the stability or non-stability of the frequency tuning. Furthermore, it would be interesting to assess the stability on different time scales, from the minutes to the days and weeks scales.

4.2.3 The subdivisions of the auditory cortex

Many mapping and tracing experiments have already been done to identify the sub-regions within the auditory cortex (see Introduction, for a review, see Stiebler et al. (1997); Schreiner and Winer (2007)). To have the most precise mapping, the combination of the inputs to the cortex and the tonotopic gradients are used to define the subdivisions of the auditory cortex. In the literature, most studies agree on the location and positioning of the main tonotopic gradients. Indeed, the location of the high frequency "*islands*" and low frequency islands are often coherent (Guo et al., 2012; Issa et al., 2014; Polley, 2006; Kubota et al., 2008). However, variability still exist when assigning these gradients to the 4 main fields of the auditory cortex (A1, AII, AAF and DP). Indeed, the axes of low-to-high frequency preferences can be interpreted in different ways, as several *high-preference* island and *low-preference* islands exist.

The ground truth could be established by combining a functional and anatomical approach. The tonotopy mapping would provide a functional topography, while tracing experiments from and to the different auditory areas would help define their anatomical identity, based on their inputs and outputs. Additionally, unbiased techniques should be used to establish the tonotopy, since for example the electrophysiology recordings tend to be biased to highly responsive neurons, usually from deeper layers. The layer-dependency of the tonotopic maps should also be taken into account, as different layers show differently homogeneous and differently crisp tonotopic maps (Winkowski and Kanold, 2013).

Additionally, the anaesthesia state of the animal has also an effect on the tonotopic maps, which should also not be neglected (Hackett et al., 2011). Most of the studies using deep layer multi unit recordings to assess the tuning using barbiturate anaesthesia find a high precision in the tonotopy. On the other hand, experiments with different conditions, like calcium imaging in the

superficial layers of awake animals, using high-intensity sound level, often find a less clear, lower degree of precision in the tonotopic maps (Hackett et al., 2011).

In this thesis, map-level frequency tuning (tonotopy) was assessed by *standard* and *Fourier* wide-field calcium imaging of the layer 2/3 neurons in isoflurane anaesthetized animals. Standard calcium imaging is an easy but not very accurate and rather slow way of mapping the cortex. Furthermore, it relies on getting a stable, high response amplitude for each frequency mapped. Fourier imaging is a more elegant and faster alternative based on the Fourier transform of the response signal, with presentation of a continuous cyclic stimulus. The phase of the response is used after compensation for response delay. The phase map is then created, giving a higher spatial resolution map with no bias for the response amplitude. Both mapping techniques gave comparable maps but only in very few experiments. This relative unreliability of the output of both techniques prevented to establish clear tonotopic maps, further forbidding the definition of clear subdivisions of the auditory cortex. Ultimately, the electrophysiology recording conditions described above, using deep layer multi unit recordings, remain the major and best method available to get a clear tonotopic mapping (Guo et al., 2012), even though they remain relatively coarse on the spatial scale. Improved sensitivity in calcium indicators or larger fields-of-view would increase the potential of two-photon calcium imaging studies to provide high-quality, reliable tonotopic maps.

4.3 Learning-related changes in the auditory cortex

4.3.1 Training mice in discrimination tasks

In this thesis, many animals have been trained on various auditory discrimination task. The use of mouse or rat behavior has expanded recently, especially when combined with functional recording techniques, such as calcium imaging (Huber et al., 2012; Chen et al., 2013b, 2015; Peron et al., 2015).

Some limitation in mice experiments can however be problematic when not taken care of properly. First, variability in behavior performance exist in every experiment, as the learning experiments are quite complicated both on the experimenter side as on the animal's side. Every source of variability in the experimental protocol should be reduced to a minimum to help the animals build up a stable knowledge base for their learning. However, the learning process involves trial-and-error type of behavior, therefore some level of variability will always remain as the animal's decision is just inherently variable.

Second, factors like attention, motivation and fatigue can nevertheless be controlled to some extent for example by using cues, monitoring water consumption and keeping the learning sessions

reasonably short. In the later learning experiments presented in this thesis, the 5/2 scheme of water scheduling was used. This diminished the water need of the animals on the beginning of the 5-day training period. This led to weekly period variation in the motivation that were accounted for by not using the first day of the week for functional recordings.

Third, in the case of attention, the *go* / *no-go* task also has some limitations. Indeed, distinguishing between a low-motivation state and a misinterpretation of the sound (target versus distractor) cannot be told apart in this paradigm. A two-alternate force choice task would better take care of this issue, as both sounds required a response (Mayrhofer et al., 2013).

In summary, it is possible to train mice for sound discrimination tasks within periods of 5 to 50 days, depending on the difficulty of the task and on the performance level that needs to be achieved. Difficulty of the task is determined by the types of sounds used and by the presence and length of a delay period.

4.3.2 Responsiveness changes in single neurons during learning

Training animals in a discrimination task should produce changes in the brain reflecting the new ability of the animal to perform the task. These changes where studied in this thesis by using a combination of two-photon calcium imaging combined with a sound discrimination task. Establishing such an experiment with recordings in the auditory cortex was one of the aims of this thesis.

In a first set of experiments, the learning period was examined by comparing the *naïve* learning epoch with the *expert* and *late expert* epochs of animals performing a simple discrimination task without delay. These experiments, combined with the chronic two-photon imaging, showed an increase in responsiveness in the expert epoch, with a subsequent decrease of responsiveness. However, information content remained high even in the *late expert* epoch. As said earlier, these experiments may potentially suffer from movement artefacts that occurred during the hearing period of the trial, as the animals were reporting and collecting rewards.

Similar recruitment of silent neurons have been observed in barrel cortex(Margolis et al., 2012). Whisker-evoked responsiveness of layer 2/3 neurons in adult mouse barrel cortex was measured over weeks, first with intact whiskers intact and then during a sensory deprivation context. It was shown that responses to the trimmed whisker stimulation decreased during the sensory deprivation context. However the responses to the spared whisker stimulation increased for the least active neurons, while decreasing for the most active neurons. This recruitment of silent neurons can be compared to the initial increase of responsiveness observed here in the auditory cortex.

In a next set of experiments, using a delay period to avoid the movement artefacts, several learning epochs were compared to examine changes in the activation pattern of single neurons: a *baseline* epoch, a *naïve* epoch, an *expert* epoch and *late expert* epoch. When looking at individual

neurons, it was difficult to see any consistent pattern of change. Neurons that were highly activated on one day for one of the sounds were not necessarily showing the same activation on the next day. Therefore, a population analysis approach was used. This approach highlighted a reduction in responsiveness of the layer 2/3 auditory neurons after the learning. Moreover, the selectivity of these neurons shifted slightly towards the target sound compared to the distractor sound. These two finding will be put in context of the *Darwinian learning* theory in the next section.

However, these recordings have some limitations that should be taken into consideration. An overall reduction in responsiveness could mean that the neuronal networks need less neurons to encode the same amount of information, showing that a specialized network was formed to provide the animal with the required information to perform the task, while the other neurons could go back to a silent state. But it is also possible that a general reduction of the responsiveness is happening due to a degradation of the quality of the recording, due to photo-damage or viral toxicity. This has actually been shown in another set of experiment were neurons suffered from damage that led to their disappearing from the recording region. Therefore, more experiments with better cell health control would be required to confirm that the reduction in responsiveness is not due to damage to the cells. For example, the usage of transgenic mice expressing GECIs would allow to avoid the viral toxicity problem.

The question of the learning related changes in the auditory cortex at the cellular level following a discrimination task has still not been extensively addressed. Xiong et al. (2015) and colleagues showed that corticostriatal connections play an important role in the decision making during an auditory discrimination task using optogenetics and elecrophysiological recordings. They showed that by activating corticostriatal projecting neurons, located mainly in layer 5, they could bias the responses of the animal. While this study shows that neurons in the auditory cortex are involved in the decision making process, the question of how these neurons become involved in such a task remains open. It would be interesting to see how the bias induced by the artificial activation of the neurons evolves over the learning stages. One hypothesis would be that the neurons would not influence the behavior at first, but only in later stages of the learning.

Finally, the learning-related changes observed in this thesis are from cortical layer 2/3. As said before, a heterogeneity of the frequency tuning has however been shown to be layer specific, with layer 4 neurons showing a more homogeneous spatial organization compared to layer 2/3 (Winkowski and Kanold, 2013). Therefore, it would be interesting to investigate how the different layers differ in their responses after a discrimination task. It is also possible to study different layers within a single animal at the same time, thanks to the recent advances in transgenic animals (Madisen et al., 2015). Indeed, different calcium indicators of different spectra can be used by combining different transgenic mouse lines and viral injection approaches. Such experiments

would shed light on the interactions of different layers during the learning process.

4.3.3 *Darwinian learning theory*

The learning process has been shown to influence the tonotopic map (Dahmen and King, 2007). It is known that an expansion of the map in the region corresponding to the trained frequency is occurring. It is however not well known what happens after the learning is done, meaning when the animal has acquired the task and does not improve any more.

According to the *Darwinian learning theory* (Kilgard, 2012), the increase seen in the frequency map should not stay once the learning is done. The theory states that the neurons recruited for performing the task are not all necessary to solve the task and can therefore go back to a more silent state, leaving only a specialized network to encode the task.

One of the aim of this thesis was to test this theory both on the cellular and tonotopic map level. On the cellular level, measurements before, during and after a simple frequency discrimination learning showed the following evolution of the responsiveness and information content of neurons. Responsiveness showed an increase during the learning but subsequent decrease in the after learning epoch. However the information content that also increase during the learning, remained high even after the learning, meaning after the reduction in responsiveness. In further experiments with a delayed learning task, a reduction of responsiveness was also seen in the *late expert* epoch.

Taken together, these results show a tendency to confirm the *Darwinian learning* theory. Indeed, an overall reduction of responsiveness in the last stage of learning can be seen, which is consistent with the re-normalization phase of the *Darwinian learning* theory. However those results have some limitations, either regarding movement artefacts or regarding cell health. Therefore, they would require additional control experiments using for example transgenic mouse lines to confirm the finding of reduction responsiveness on the cellular level.

Regarding the map level, *standard* and *Fourier* calcium imaging techniques were used to measure the tonotopy in the layer 2/3 of the auditory cortex. Unfortunately, neither of these methods showed the consistent recording temporal and spatial stability that is required to show a pre-/post-training change. The standard mapping suffered from a too low spatial resolution to compare precise expansion or reduction of specific tonotopic region. In other words, the area associated for a single frequency was not stable enough in space to be compared in two different days. Furthermore, the Fourier imaging was not stable in time to be compared between two recording sessions. Maps extracted with this method were either very crisp and clear or completely inconsistent. This lack of stability was probably due to differences in anaesthesia or to brain state fluctuations that could not be controlled for.

As the map-level recording techniques did not yield stable results, therefore not allowing the

comparison of tonotopic maps before and after learning to test the *Darwinian learning* theory were not conclusive. Better stability in the recording technique, using for example electrophysiological mapping, would be required to test the expansion and reduction of the trained frequency associated area in a learning task.

The change of size of trained frequency associated tonotopic map regions were already shown at the map level before in rats (Takahashi et al., 2011). In their study Takahashi and colleagues trained rats to detect 20 kHz tones with nose poking. Their results show a clear increase of the total size of different auditory cortical regions (A1, and VAF, ventral auditory field) after 4 days of training, and a subsequent decrease after 20 days. However, they only show a *tendency* to increase for the frequency specific region. It is possible that the increase for the trained frequency is not bigger because the task that they used was only a detection task and not a discrimination task.

All together, it is still not completely clear to what extent the frequency associated tonotopic regions change during and after training and also on what time scale these changes happen. More recently, it was however shown that forelimb training can drive *transient* map reorganization (Pruitt et al., 2016), therefore suggesting that such expansion followed by renormalization process is not only applicable to the auditory modality. Studying this process in the context of a discrimination task, both on the cellular and on the map level is likely to bring more insights on the mechanisms with which frequency and sensory discrimination task learning can happen.

4.3.4 Expert mice performing in a delayed discrimination task

The auditory discrimination learning process does not only involve the auditory cortex, but also different brain regions, like striatum (Xiong et al., 2015) or other neurons from different cortices, which would take part in the *final* network of neurons encoding the task, as stated in the *Darwinian learning* theory (Kilgard, 2012). Therefore, another set of experiments was carried out, using wide-field calcium imaging using layer-specific transgenic animals. This technique allows to record the activity of neurons of a specific layer from almost an entire half hemisphere. It is therefore well suited for studying the flow of activity between the different cortices involved in a learning process. Targeting layer 2/3 is also relevant, as most of the associative connections between cortices are made from and to this layer 2/3.

Animals were trained on a delayed discrimination task that was inspired from the texture discrimination task described before (Chen et al., 2013a). The task was modified to use the auditory modality and a delay period was introduced to avoid movement artefacts in the recording during the sensation period of the trial (original idea from Dr. Ariel Gilad (Gilad et al., *in preparation*). Animals could learn this task, even though the task was more complicated due to the delay period

where they had to refrain from reporting. The refraining from reporting is usually the most difficult part of a task to learn for animals, as they are often impulsive when they are facing the possibility of receiving a reward. This can also be seen in the learning curves, as most of the animals start by having a high *hit* rate, as well as a high *false alarm* rate. The animals learn to refrain to report only after a certain time performing in the task, therefore bringing down their *false alarm* rate.

Since this later experiment was done with a delay, the learning time of the animals was increased. Typically, animals needed over 30 days or more to achieve a high performance level (final *d'* >= 4), which was much above the normal performance level used in these type of tasks (*d'* = 2, Chen et al. (2015)). A special care was taken to only use trials where the animal was quiet and not moving during both the sensation period and the delay period. Therefore, a high performance level was required, in order to have as many quiet trials as possible, which are occurring only in very expert animals. Imaging sessions were only carried out in the later phase of the training, typically when the animal was in a high performance regime (*d'* >= 3).

Movement artefacts are almost always present when dealing with behavior and animals. Therefore, as described above, a special care was taken to analyse, filter and select trials based on the amount of body movement occurring. Trials were the animals was moving its body or its limbs were not included, to avoid contamination of the activity pattern by motor-related activations. This strategy was very effective at removing movement artefacts and helped to obtain a more homogeneous set of trials, containing information relevant to the task and the sounds played, rather than body and limb movement related activations. Such filtering or selection approaches are rarely seen in the current research. This could however be potentially crucial in the understanding of the brain's function during such tasks. Indeed, motor movement is fully part of the behavior of the animal, even if these movements are not immediately relevant for the task. In this experiment, advanced body video analysis and trial data synchronizations were used to automatize the filtering of the trials. This was necessary as the number of trials recorded was very large and manual processing would have required a great amount of time.

The patterns that emerged from the recordings of the cortex using wide-field calcium imaging are based solely on one animal, due to the length of these type of experiments and to time constraint reasons. Nevertheless, some preliminary results and conclusion were drawn from this single mouse, which will be complemented in the future as several other animals are trained currently.

4.3.5 Auditory suppression for *hit* but not *correct rejection* trials

The main differences in activity pattern were observed during the sensation period, when comparing the activation of the auditory cortex between the *hit* and the *correct rejection* trials. While

the *correct rejection* trials showed a slight activation, the activity in the auditory cortex was very much suppressed during *hit* trials. In addition, primary and secondary motor region activation was also observed during the sensation period in *hit* but not *correct rejection* trials. Such auditory suppression was already described before (Otazu et al., 2009; Schneider et al., 2014).

In their study, Otazu and colleagues showed that engaging in an auditory task suppresses responses in auditory cortex. They used multi-unit electrophysiological recordings in rats that were engaged in a two-alternative choice auditory discrimination task with nose poking to report the decision. They compared the response to the stimulus onset of the engaged condition with a passive condition, where rats were not receiving rewards and were therefore just passively exposed to the task. Therefore, the suppression of the auditory cortex in the *hit* trials seen in this thesis is consistent with their finding, if we assume that the mice were more engaged in the *hit* conditions compared to the *correct rejection* condition. Indeed, in the *go* / *no-go* paradigm, the *no-go* sound does not require any action of the mouse, potentially leading to a brief disengagement of the animal until the next trial starts.

A perhaps more likely explanation to the auditory suppression could be suggested by the study from Schneider and colleagues (Schneider et al., 2014). In their study, the authors found that excitatory neurons in the auditory cortex are suppressed before and during movement. They used *in vivo* intracellular recordings combined with optogenetics in behaving mice to show that this suppression is at least partly due to the increased activity of local parvalbumin-positive-containing (PV) interneurons, which receive input from the motor cortex. This is in principle not fully coherent with the suppression seen in this thesis, as the trials were selected for absence of movement. However, two possibilities can conciliate these observations, especially given the motor activation seen at the start of the sound presentation.

First, it should be stated that the movement detection was not absolute. Indeed, the criterion for excluding trials was loose enough to allow small movements that were very short (0.4 sec maximum). Moreover, the method used to detect movement was the analysis of the body camera, which could not detect movements of the rear of the animal (back, tail and hind limbs) nor muscle tensions which did not translate into actual movement (tensions on the holding bar with the front limbs, back arching, etc.). Therefore, it is possible that *hit* trials trigger anticipatory movement in the animal, as it already knows that a reward was potentially coming. In contrast, *correct rejection* trials were never rewarded, therefore the animal could remain more quiet due to the lack of excitation or anticipation for a reward.

Second, it is also proposed by Schneider and colleagues that even the planning of the movement that the animal has not yet execute could also trigger activation in the secondary motor cortex (M2) and that this planning could already trigger a suppression in the auditory cortex via

the auditory projecting motor neurons in M2. Therefore, it would potentially be enough that in the mouse recorded in this thesis, the planning of the movement during the *hit* trials would create the observed motor activation, which in turn would trigger the auditory suppression. It would therefore be interesting to test this hypothesis, by manipulating specifically this motor to auditory link. Auditory projecting motor neurons could be silenced using targeted optogenetics. Additionally, since the suppression is suggested to be mediated by PV interneurons, this specific cell-type could also be targeted by silencing experiments and their contribution be assessed.

These two hypothesises, difference in engagement (Otazu et al., 2009) and more importantly difference in movement or movement planning (Schneider et al., 2014), could explain the difference in activity pattern observed in the auditory cortex between the *hit* and the *correct rejection* trial conditions.

4.3.6 Storing task-related information during a delay period

As the discrimination task described above contained a delay period, the animals had to hold the sensory information collected during the sensation period until the end of the delay period. This involves several hypothetical steps described hereafter. First, the sensory information must flow from the sensory cortex, in this case the auditory cortex, to some temporary storage, the working memory. There, it must be held until the signal to report the decision comes, which is again a sensory cue (visual cue). The sensory information must therefore flow again until the working memory storage to be "*released*" into a motor command.

In the experiments carried out in this thesis, the hypothesis was that one or more cortical regions should show a difference of activation pattern between the *hit* and the *correct rejection* trials during the delay period. Such a region was identified in the posterior part of the cortex, however the delineation and the amplitude of activation of that region were not fully clear. More precisely, a small spot of activation was seen to be reliably higher in the *hit* trials compared to the *correct rejection* trials. This spot was located between the auditory, somatosensory and visual cortices, therefore presumably belonging to the posterior parietal cortex (PPC). However other surrounding regions also showed a tendency to have higher activation in the *correct rejection* trials, but with a much less clear delimitation. Therefore, this activation spot is named PPC hereafter, but does not necessarily correspond to the PPC in all sessions and all animals.

The work from Xiong et al. (2015) shows that corticostriatal neurons are involved in the decision making process. Therefore, already in the auditory cortex, neurons from layer 5 are sending information to pre-motor neurons (striatum). However in their task, no delay was present, meaning that the information perceived and processed at the auditory cortex could *directly* go to the decision making step and issue a motor command (lick left or lick right in their case). Therefore, regions

like the (presumed) PPC or other working memory related cortices are likely not involved in their task.

Interpreting the activation in the small region of a single animal is probably very questionable. Based on the evidences shown in this small preliminary data set, it is not possible to tell what the role of the PPC is in the presented task, or whether or not it holds information related to the delay period, to the perceived sensory information, or both. Additional experiments are required to confirm the existence and location of such a "*retainement*" region. For example, inhibition or activation of that specific region using optogenetics would give useful insights on several aspects. First, the involvement of this region could be tested in the task, by manipulating the activity of the neurons in this region specifically during a specific period of the trial (sensation, delay, etc.). Furthermore, it would be interesting to see in which way activating this presumed PPC would influence the animal's behavior: would an increase in activity help refrain from licking, or on the contrary inhibiting it would abolish the refraining and lead to a more impulsive reporting behavior.

Finally, as in the other parts of this thesis, it would be interesting to explore the layer specificity of the activity patterns presented here, both the auditory suppression and the presumed PPC activation. As the layer 2/3 is the associative connection layer, sending and receiving information to and from the other cortices, it might possible that other layers, that have different targets, show different activation pattern during such a delayed discrimination task.

4.4 Analysis framework and visualization tools for neuroscience

4.4.1 Data types in neuroscience

Experiments in neuroscience often combine different experimental approaches and experimental conditions, but in most of the cases, the recording technique produces time series. Electrophysiology records membrane potentials changes over time, imaging techniques record movies that are then often reduced to time series of cellular signals, and fiber recordings also acquire one or multiple channels over time. Therefore time series are the basic form of functional data that is most common in neuroscience. It is required in many cases that this data goes through some pre-processing step first, to filter or correct recording artefacts, to segment or select features. Therefore, tools that work with time series in a generalized way can potentially be useful to multiple applications.

The time series often come with annotations about the experimental conditions, like the cell type, trial condition, recording region. In addition, the time series are also linked to *event* annotations, representing specific events during the time series. Such event annotations can for example

be stimulus presentation or a behavioral event occurring (whisking, licking, etc.). These events are annotated usually with the time at which they happened during the time series. Therefore, tools that can handle such information in a non-specific manner can also be useful for multiple applications or experiment types.

Once a data set is reduced to one or multiple time series, they are often processed in similar ways. Usually simple operations like averaging, thresholding, separating or fitting based on some criterion are the most common operations to gain some additional knowledge about the data. The next and final step is usually the display of the time series, with some useful information added to the display to better understand what happened during the experiment, that can explain the shape of the time series (activation, burst of activity, silent state, etc.).

The `OCIA` is an analysis framework developed during this thesis and presented here. This framework tries to address the data type concerns explained above and provides neuroscientists with tools to deal with time series and their attached information. The flexibility provided by the different modules and the flexibility for encoding the stimulus vectors allows to work with different time series and stimulus type, independent of the experiment type.

4.4.2 Data management for big and complex data sets

Data management is an increasingly challenging aspect of the data analysis. Indeed, to work with recorded data, there is a need to overview and manage data sets, which are often stored in a hierarchical file system with many levels (animal / day / session / etc.). With the recent methods in neuroscience, the data sets are often too big to be viewed at once and therefore sophisticated filtering and grouping strategies must be used. As a scientist, there is a crucial need to have a good overview of one's data, especially when the quantity of data is getting bigger and bigger. Without a good overview, there can be no good extraction or analysis of meaningful data and therefore no good scientific output. Managing data with advanced tools can allow to gain significant time as repetitive tasks will be automatized rather than executed manually by the scientist.

Storing data on a longer term, either for later usage or for archiving, is also a task that should be done automatically. Experimenters leave the groups they work in and often leave data sets behind. These are then often difficult to re-use or understand, because of a lack of documentation or clear storing strategy. If an automated common way to store and manage data is set up, like for example with the HDF5 files (The HDF Group, 2016) and a good data management software, such lack of re-usability or difficult access to old data would cease to be a problem. HDF5 attaches meta-data to the data sets, which are stored in an organized and durable way. Ideally, the data management software should be linked with good analysis and visualization tools, which would allow a smooth and straightforward transition between storage and data extraction for analysis or

visualization.

The `OCIA`'s `DataWatcher` module was created during this thesis to provide some data management functionalities. It integrates well with the visualization and analysis part of the framework, and allows to flexibly store data in the HDF5 format. It allows accessing any HDF5 file from different experimenters and different experiment types. Unfortunately, the *OCIA* does not provide a solid back-up or archiving system, which task must be done manually by users. Data management software like `openBIS` (Bauch et al., 2011) are more complete solutions to the this challenge, as they cover all aspects of data management, from the archiving, to generic data types, web interface and more, although the `openBIS` software is more suited to the genomic field.

4.4.3 Data-mining and interactive data analysis

The process of analysing data in neuroscience is rarely a straightforward flow of analysis steps. Neuroscience is typically a field where experiments are often at least partially exploratory (or *data-driven*), therefore leading to a process of back-and-forth from single recording examples to pooled analysis or averages.

Despite the large amounts of data collected, there is a great deal of importance in the close examination of the single data points (single neurons, single trials, single evoked responses, etc.). This gives the neuroscientist a "*feeling*" for the data, allowing him to extract the useful knowledge and generalize, in order to build up hypothesis and theories. For this purpose, being able to pick single data points and examples is critical. It is also very important to be able to choose good examples in the context of presentation (meetings, conferences, etc.). This process of *data mining*, where useful information has to be extracted from a large pool of data, is tedious to do without the right tools.

The process of selecting data points, pooling averages but then going back to the single trials/examples to confirm what the average shows, requires interactive tools. Visualization tools with a nice and reactive Graphical User Interface are therefore very handful to interact with the data, instead of running scripts and waiting for them to execute. Typically, being able to see examples of single data points but then also to execute analysis (extracting averages or getting pooled results) should be relatively quick in order to keep this process interactive and maximize efficiency of the scientist.

Having a fast and interactive "*loop*" to go from the single data to the extracted average helps with another aspect of this exploratory analysis, which is the parameter space exploration. One does not always know which parameters are important in an analysis, what values should these parameters take and how they will affect the final result. Hence, an easy interactive exploration of the parameter space by quickly trying out many different parameters is very important and can

speed up the analysis process greatly, but also allow it to be more complete and thorough.

The `Analysis` module of the *OCIA* offers such an interactive analysis tool, with some focus on the interactive part. Indeed, the integrated cache system allows to play with the data and the analysis parameters without having to re-calculate the entire analysis from scratch. It also offers visualization and plotting tools to explore the data sets and extract relevant examples from it. At the same time, higher level analysis, like averages and data pooling, can also be done to get final solid numbers to summarize and quantify the measured variables.

4.4.4 Sharing tools to deal with really large datasets

The software presented in this thesis can obviously not fit all the needs of the neuroscience community and was never intended to fill such a need. Many aspects of it are too simplistic, inflexible and overall this framework is a so-called "*one-man project*", where lack of support is a real problem. The neuroscience community would however greatly benefit from a common set of data formats, analysis tools, visualization tools and data management system. This would allow better sharing and exchange between the large community of scientist trying to understand the brain. In fMRI research, frameworks exist that perform integrated analysis of functional and anatomical data (Eickhoff et al., 2005). Although neuroscience does have many different data types and complex experimental paradigms, other fields of biology already have such community tools and often also common online freely available public databases to share data.

As said, the amount of data and complexity of the data in neuroscience requires advanced analysis tools that can handle large data sets. These data sets often exceeds the single computer memory (RAM) and computing power (CPU). Therefore, a common solution is to use supercomputers or cluster-based computing. This requires the parallelization of the analysis code, which is often not a trivial procedure. Existing tools like the *Spark* and *Thunder* environments (Freeman et al., 2014) are the first solid steps of the neuroscience community to deal with large data sets. Some easy steps of parallelization, like data pre-processing (motion correction, image registration, automatic ROI labelling) could be very useful to share in the community, as they are needed for many groups in relatively similar ways. The Allen Brain Institute participates to this effort through their online databases and their freely available tools, like the Brain Explorer (Lau et al., 2008).

4.5 Summary and outlook

The work described in this thesis covered to main aspects of the current neuroscientists challenges: the experimental and the analytical aspects.

The main topic of this thesis was to establish the study of learning-related neuronal activity pattern changes in the auditory cortex of mice during a sound discrimination task. A set of different methodological approaches were explored to study different aspects of this topic. As prerequisite, an auditory discrimination task was successfully established and combined with two-photon and wide-field calcium imaging. Frequency tuning properties of single neurons and entire tonotopic maps were also measured. The main learning-related changes observed were a presumed decrease in neuronal responsiveness in the later stages of the learning, as well as a trial condition specific decrease in auditory cortex activity during the learning task.

In order to be able to deal with the experimentally produced data sets, an analysis and visualisation framework was created. With the help of the framework, the data collected during the experimental part could be handled. This framework was designed to help with the storage, management, visualisation and analysis of the data collected during the experimental part of this thesis. As the data was obtained using several different recordings methods and therefore composed of many different data types, the framework was developed to be modular and flexible, in order to deal with the complexity of the data and the different data types. The framework is organized into independent but complementary and well integrated modules.

In the coming years, it is very likely that plasticity and learning in sensory cortices will be more and more studied, thanks to the recent transgenic mouse lines and to the increase in behavior experiments. Techniques like the wide-field calcium imaging will probably also be a major focus, as they provide valuable information about the activity flow in entire hemispheres during learning tasks. Furthermore, this technique can easily be combined with various genetic tools and transgenic mice lines, to achieve neuronal cell type or layer specificity.

List of Figures

List of publications

Submitted articles

My main contribution to these articles was through the `OCIA` framework.

van der Bourg, A., Yang, J., Reyes-Puerta, V., Laurenczy, B., Wieckhorst, M., Luhmann, H., Helmchen, F. (2016) *in press*. Layer-Specific Refinement of Sensory Coding in Developing Mouse Barrel Cortex. *Cerebral Cortex*.

Omlor W., Wahl, A.-S., Lütcke, H., Laurenczy, B., Chen, I.-W., Sumanovski, T., van 't Hoff, M., Schwab, M., Helmchen, F. (2016) *submitted*. Contextual Need for Flexibility Enhances Movement Encoding in Motor Cortex.

In preparation

Laurenczy, B., et al. *in preparation*. *OCIA*: An integrated framework for calcium imaging data analysis and visualization.

Laurenczy, B., et al. *in preparation*. Learning-related changes in Neuronal Activity Patterns in the Mouse Auditory Cortex.

Abstracts

Laurenczy, B., Helmchen, F., and Lütcke, H. (2014) Learning-Related Neuronal Circuit Dynamics in Mouse Auditory Cortex Investigated by Chronic Two-Photon Calcium Imaging. Abstract No. 814.05 / CC27 *Society for Neuroscience*.

Laurenczy, B., Helmchen, F., and Lütcke, H. (2014). Learning-Related Neuronal Circuit Dynamics in Mouse Auditory Cortex Investigated by Chronic Two-Photon Calcium Imaging. Abstract No. 40 *Advances and Perspectives in Auditory Neuroscience*.

Acknowledgements

First of all, I am very thankful to my supervisor Prof. Fritjof Helmchen for supervising my work during these 4 years. It has been wonderful and exciting to work in his group, under his positive, patient, encouraging and open-minded supervision. I will always be impressed by his inspiring attitude towards science and by the great, family-like environment he creates in his lab by being a genuinely nice person.

Dr. Henry Lütcke co-supervised the first years of my PhD. He initiated the work on the auditory system and I am proud to have been part of the *A1 team*. I would like to thank him for his help, his availability and his always insightful good advice. Henry is really a great person to work with, and his genuine sharp humour is most refreshing.

I would like to thank my thesis committee members Prof. Richard Hahnloser and Prof. Klaas Enno Stephan for their insightful suggestions during our meetings.

This PhD would have been a whole different and less exciting adventure without my lab-brother Alex, my Padawan Dayra, the almighty Fabian and the Commander Ladan. I would like to thank them for caring and sharing this amazing time with me, for bringing motivation and help on a daily basis through laughs, discussions and good advice. I would like to thank Ariel for accepting me into his wide-field world, full of single trials to look at. Many thanks to the rest of the Helmchen lab family for great scientific discussions and for always interesting group meetings.

I would like to thank the HiFo engineering team, Hansjörg, Marco, Stefan and Martin for their great and always prompt technical support.

I would like to thank my family and friends for their support during these busy years. I would like to thank my parents for the curiosity and perseverance they gifted me through their loving education, my sister and my brother for their always helping, joyful presence, and my friends for being there when needed.

Finally, I would like to thank my wonderful half for her loving support during these 4 years of ups and downs, late evenings and busy weekends, for the balance that she brought and for her astounding understanding.

Bibliography

Aronoff, R. and Petersen, C. (2007). Layer- and column-specific knockout of NMDA receptors in pyramidal neurons of the mouse barrel cortex. *Frontiers in Integrative Neuroscience*, 1(November):1.

Bandyopadhyay, S., Shamma, S. A., and Kanold, P. O. (2010). Dichotomy of functional organization in the mouse auditory cortex. *Nature Neuroscience*, 13(3):361–8.

Barkat, T. R., Polley, D. B., and Hensch, T. K. (2011). A critical period for auditory thalamocortical connectivity. *Nature Neuroscience*, 14(9):1189–94.

Bathellier, B., Ushakova, L., and Rumpel, S. (2012). Discrete neocortical dynamics predict behavioral categorization of sounds. *Neuron*, 76(2):435–449.

Bauch, A., Adamczyk, I., Buczek, P., Elmer, F.-J., Enimanev, K., Glyzewski, P., Kohler, M., Pylak, T., Quandt, A., Ramakrishnan, C., Beisel, C., Malmström, L., Aebersold, R., and Rinn, B. (2011). openBIS: a flexible framework for managing and analyzing complex data in biology research. *BMC Bioinformatics*, 12(1):468.

Berger, T., Borgdorff, A., Crochet, S., Neubauer, F. B., Lefort, S., Fauvet, B., Ferezou, I., Carleton, A., Lüscher, H.-R., and Petersen, C. C. H. (2007). Combined voltage and calcium epifluorescence imaging in vitro and in vivo reveals subthreshold and suprathreshold dynamics of mouse barrel cortex. *Journal of Neurophysiology*, 97(5):3751–62.

Bieszczad, K. M. and Weinberger, N. M. (2010). Representational gain in cortical area underlies increase of memory strength. *Proceedings of the National Academy of Sciences*, 107(8):3793–3798.

Bozza, T. C. and Mombaerts, P. (2001). Olfactory coding: Revealing intrinsic representations of odors.

Brown, M., Irvine, D. R. F., and Park, V. N. (2004). Perceptual learning on an auditory frequency discrimination task by cats: association with changes in primary auditory cortex. *Cerebral Cortex*, 14(9):952–65.

Cang, J., Kalatsky, V. A., Löwel, S., and Stryker, M. P. (2005). Optical imaging of the intrinsic signal as a measure of cortical plasticity in the mouse. *Visual Neuroscience*, 22(5):685–691.

Castillo, P. E. (2012). Presynaptic LTP and LTD of excitatory and inhibitory synapses. *Cold Spring Harbor Perspectives in Biology*, 4(2).

Chen, I.-W., Helmchen, F., and Lutcke, H. (2015). Specific Early and Late Oddball-Evoked Responses in Excitatory and Inhibitory Neurons of Mouse Auditory Cortex. *Journal of Neuroscience*, 35(36):12560–12573.

Chen, J. L., Carta, S., Soldado-Magraner, J., Schneider, B. L., and Helmchen, F. (2013a). Behaviour-dependent recruitment of long-range projection neurons in somatosensory cortex. *Nature*, 499(7458):336–340.

Chen, T., Xue, Z., Wang, C., Qu, Z., Wong, K. K., and Wong, S. T. (2012). Motion correction for cellular-resolution multi-photon fluorescence microscopy imaging of awake head-restrained mice using speed embedded HMM. *Computerized Medical Imaging and Graphics*, 36(3):171–182.

Chen, T.-W., Wardill, T. J., Sun, Y., Pulver, S. R., Renninger, S. L., Baohan, A., Schreiter, E. R., Kerr, R. A., Orger, M. B., Jayaraman, V., Looger, L. L., Svoboda, K., and Kim, D. S. (2013b). Ultrasensitive fluorescent proteins for imaging neuronal activity. *Nature*, 499(7458):295–300.

Chen, X., Leischner, U., Rochefort, N. L., Nelken, I., and Konnerth, A. (2011). Functional mapping of single spines in cortical neurons in vivo. *Nature*, 475(7357):501–5.

Conner, J. M., Chiba, A. A., and Tuszynski, M. H. (2005). The basal forebrain cholinergic system is essential for cortical plasticity and functional recovery following brain injury. *Neuron*, 46(2):173–9.

Conner, J. M., Culberson, A., Packowski, C., Chiba, A. A., and Tuszynski, M. H. (2003). Lesions of the Basal forebrain cholinergic system impair task acquisition and abolish cortical plasticity associated with motor skill learning. *Neuron*, 38(5):819–29.

Dahmen, J. C. and King, A. J. (2007). Learning to hear: plasticity of auditory cortical processing. *Current Opinion in Neurobiology*, 17(4):456–464.

Denk, W., Strickler, J., and Webb, W. (1990). Two-photon laser scanning fluorescence microscopy. *Science*, 248(4951):73–76.

Denker, A. and Rizzoli, S. O. (2010). Synaptic vesicle pools: An update.

Douglas, R. J. and Martin, K. A. (2004). NEURONAL CIRCUITS OF THE NEOCORTEX. *Annual Review of Neuroscience*, 27(1):419–451.

Eggermont, J. J. (2015). The auditory cortex and tinnitus - a review of animal and human studies. *European Journal of Neuroscience*, 41(5):665–676.

Eickhoff, S. B., Stephan, K. E., Mohlberg, H., Grefkes, C., Fink, G. R., Amunts, K., and Zilles, K. (2005). A new SPM toolbox for combining probabilistic cytoarchitectonic maps and functional imaging data. *NeuroImage*, 25(4):1325–1335.

Elhilali, M., Fritz, J. B., Chi, T.-S., and Shamma, S. A. (2007). Auditory cortical receptive fields: stable entities with plastic abilities. *The Journal of neuroscience : the official journal of the Society for Neuroscience*, 27(39):10372–82.

Freeman, J., Vladimirov, N., Kawashima, T., Mu, Y., Sofroniew, N. J., Bennett, D. V., Rosen, J., Yang, C.-T., Looger, L. L., and Ahrens, M. B. (2014). Mapping brain activity at scale with cluster computing. *Nature Methods*, 11(9):941–950.

Friauf, E., Fischer, A. U., and Fuhr, M. F. (2015). Synaptic plasticity in the auditory system: a review.

Froemke, R. C. and Martins, A. R. O. (2011). Spectrotemporal dynamics of auditory cortical synaptic receptive field plasticity. *Hearing Research*, 279(1-2):149–161.

Galván, V. V., Chen, J., and Weinberger, N. M. (2001). Long-term frequency tuning of local field potentials in the auditory cortex of the waking guinea pig. *Journal of the Association for Research in Otolaryngology : JARO*, 2(3):199–215.

Gobel, W. and Helmchen, F. (2007). In Vivo Calcium Imaging of Neural Network Function. *Physiology*, 22(6):358–365.

Graber, M. H., Helmchen, F., and Hahnloser, R. H. R. (2013). Activity in a Premotor Cortical Nucleus of Zebra Finches Is Locally Organized and Exhibits Auditory Selectivity in Neurons but Not in Glia. *PLoS ONE*, 8(12):e81177.

Grewe, B. F. and Helmchen, F. (2009). Optical probing of neuronal ensemble activity. *Current Opinion in Neurobiology*, 19(5):520–529.

Grewe, B. F., Voigt, F. F., van 't Hoff, M., and Helmchen, F. (2011). Fast two-layer two-photon imaging of neuronal cell populations using an electrically tunable lens. *Biomedical optics express*, 2(7):2035–2046.

Grienberger, C., Adelsberger, H., Stroh, A., Milos, R.-I., Garaschuk, O., Schierloh, A., Nelken, I., and Konnerth, A. (2012). Sound-evoked network calcium transients in mouse auditory cortex in vivo. *The Journal of Physiology*, 590(4):899–918.

Grienberger, C. and Konnerth, A. (2012). Imaging Calcium in Neurons.

Grinvald, A. and Hildesheim, R. (2004). VSDI: a new era in functional imaging of cortical dynamics. *Nature Reviews Neuroscience*, 5(11):874–885.

Guo, W., Chambers, A. R., Darrow, K. N., Hancock, K. E., Shinn-Cunningham, B. G., and Polley, D. B. (2012). Robustness of Cortical Topography across Fields, Laminae, Anesthetic States, and Neurophysiological Signal Types. *Journal of Neuroscience*, 32(27):9159–9172.

Guo, Z. V., Li, N., Huber, D., Ophir, E., Gutnisky, D., Ting, J. T., Feng, G., and Svoboda, K. (2014). Flow of cortical activity underlying a tactile decision in mice. *Neuron*, 81(1):179–94.

Hackett, T. A. (2015). Anatomic organization of the auditory cortex. *Handbook of Clinical Neurology*, 129:27–53.

Hackett, T. A., Rinaldi Barkat, T., O'Brien, B. M. J., Hensch, T. K., and Polley, D. B. (2011). Linking Topography to Tonotopy in the Mouse Auditory Thalamocortical Circuit. *Journal of Neuroscience*, 31(8):2983–2995.

Harris, K. D., Bartho, P., Chadderton, P., Curto, C., de la Rocha, J., Hollender, L., Itskov, V., Luczak, A., Marguet, S. L., Renart, A., and Sakata, S. (2011). How do neurons work together? Lessons from auditory cortex. *Hearing Research*, 271(1-2):37–53.

Heffner, R. S. and Heffner, H. E. (1985). Hearing range of the domestic cat. *Hearing Research*, 19(1):85–88.

Helmchen, F. (2009). *Two-Photon Functional Imaging of Neuronal Activity*. CRC Press/Taylor & Francis.

Helmchen, F. (2011). Calibration of Fluorescent Calcium Indicators. *Cold Spring Harbor Protocols*, 2011(8):pdb.top120–pdb.top120.

Helmchen, F. and Denk, W. (2005). Deep tissue two-photon microscopy. *Nature Methods*, 2(12):932–940.

Helmchen, F. and Waters, J. (2002). Ca2+ imaging in the mammalian brain in vivo. *European Journal of Pharmacology*, 447(2-3):119–129.

Herry, C. and Johansen, J. P. (2014). Encoding of fear learning and memory in distributed neuronal circuits. *Nature Neuroscience*, 17(12):1644–1654.

Hodgkin, A. L. and Huxley, A. F. (1952). A quantitative description of membrane current and its application to conduction and excitation in nerve. *The Journal of Physiology*, 117(4):500–544.

Hofer, S. B., Ko, H., Pichler, B., Vogelstein, J., Ros, H., Zeng, H., Lein, E., Lesica, N., and Mrsic-flogel, T. D. (2011). Differential connectivity and response dynamics of excitatory and inhibitory neurons in visual cortex. *Nature Neuroscience*, 14(8):1045–1052.

Holtmaat, A., Bonhoeffer, T., Chow, D. K., Chuckowree, J., Paola, D., Hofer, S. B., Hübener, M., Keck, T., Knott, G., Lee, A., Mostany, R., Mrsic-flogel, T. D., Nedivi, E., Portera-cailliau, C., Svoboda, K., Trachtenberg, J. T., Wilbrecht, L., Paola, V., and Lee, W.-C. (2009). Long-term, high-resolution imaging in the mouse neocortex through a chronic cranial window. *Nature Protocols*, 4(8):1128–1144.

Horikawa, K., Yamada, Y., Matsuda, T., Kobayashi, K., Hashimoto, M., Matsu-ura, T., Miyawaki, A., Michikawa, T., Mikoshiba, K., and Nagai, T. (2010). Spontaneous network activity visualized by ultrasensitive Ca2+ indicators, yellow Cameleon-Nano. *Nature Methods*, 7(9):729–732.

Hromádka, T. and Zador, A. M. (2009). Representations in auditory cortex. *Current Opinion in Neurobiology*, 19(4):430–433.

Huber, D., Gutnisky, D. A., Peron, S. P., O'Connor, D. H., Wiegert, J. S., Tian, L., Oertner, T. G., Looger, L. L., and Svoboda, K. (2012). Multiple dynamic representations in the motor cortex during sensorimotor learning. *Nature*, 484(7395):473–478.

Issa, J. B., Haeffele, B. D., Agarwal, A., Bergles, D. E., Young, E. D., and Yue, D. T. (2014). Multiscale Optical Ca2+ Imaging of Tonal Organization in Mouse Auditory Cortex. *Neuron*.

Kalatsky, V. A., Polley, D. B., Merzenich, M. M., Schreiner, C. E., and Stryker, M. P. (2005). Fine functional organization of auditory cortex revealed by Fourier optical imaging. *Proceedings of the National Academy of Sciences of the United States of America*, 102(37):13325–30.

Kalatsky, V. A. and Stryker, M. P. (2003). New paradigm for optical imaging: temporally encoded maps of intrinsic signal. *Neuron*, 38(4):529–45.

Kepecs, A. and Fishell, G. (2014). Interneuron cell types are fit to function. *Nature*, 505(7483):318–326.

Kerr, J., Kock, C., Greenberg, D. S., Bruno, R., Sakmann, B., and Helmchen, F. (2007). Spatial organization of neuronal population responses in layer 2/3 of rat barrel cortex. *The Journal of Neuroscience*, 27(48):13316–13328.

Kerr, J. N. D., Greenberg, D., and Helmchen, F. (2005). Imaging input and output of neocortical networks in vivo. *Proceedings of the National Academy of Sciences of the United States of America*, 102(39):14063–8.

Kilgard, M. (2003). Cholinergic Modulation of Skill Learning and Plasticity. *Neuron*, 38(5):678–680.

Kilgard, M. P. (2012). Harnessing plasticity to understand learning and treat disease. *Trends in Neurosciences*, 35(12):715–722.

Kilgard, M. P. and Merzenich, M. M. (1998). Cortical Map Reorganization Enabled by Nucleus Basalis Activity. *Science*, 279(5357):1714–1718.

King, A. J., Bajo, V. M., Bizley, J. K., Campbell, R. A. A., Nodal, F. R., Schulz, A. L., and Schnupp, J. W. H. (2007). Physiological and behavioral studies of spatial coding in the auditory cortex. *Hearing Research*, 229(1-2):106–115.

Koay, G., Heffner, R. S., and Heffner, H. E. (2002). Behavioral audiograms of homozygous medJ mutant mice with sodium channel deficiency and unaffected controls. *Hearing Research*, 171(1-2):111–118.

Kössl, M., Hechavarria, J., Voss, C., Schaefer, M., and Vater, M. (2015). Bat auditory cortex - model for general mammalian auditory computation or special design solution for active time perception? *European Journal of Neuroscience*, 41(5):518–532.

Kubota, Y., Kamatani, D., Tsukano, H., Ohshima, S., Takahashi, K., Hishida, R., Kudoh, M., Takahashi, S., and Shibuki, K. (2008). Transcranial photo-inactivation of neural activities in the mouse auditory cortex. *Neuroscience Research*, 60(4):422–430.

Langer, D., van 't Hoff, M., Keller, A. J., Nagaraja, C., Pfäffli, O. A., Göldi, M., Kasper, H., and Helmchen, F. (2013). HelioScan: A software framework for controlling in vivo microscopy setups with high hardware flexibility, functional diversity and extendibility. *Journal of Neuroscience Methods*, 215(1):38–52.

Lantz, C. (2014). Visual defects in a mouse model of fetal alcohol spectrum disorder. *Frontiers in Pediatrics*, 2(October):107.

Lau, C., Ng, L., Thompson, C., Pathak, S., Kuan, L., Jones, A., Hawrylycz, M., Carninci, P., Kasukawa, T., Katayama, S., and Toga, A. (2008). Exploration and visualization of gene expression with neuroanatomy in the adult mouse brain. *BMC Bioinformatics*, 9(1):153.

Letzkus, J. J., Wolff, S. B. E., Meyer, E. M. M., Tovote, P., Courtin, J., Herry, C., and Lüthi, A. (2011). A disinhibitory microcircuit for associative fear learning in the auditory cortex. *Nature*, 480(7377):331–5.

Liang, F., Bai, L., Tao, H. W., Zhang, L. I., and Xiao, Z. (2014). Thresholding of auditory cortical representation by background noise. *Frontiers in Neural Circuits*, 8:133.

Llano, D. A. and Sherman, S. M. (2008). Evidence for nonreciprocal organization of the mouse auditory thalamocortical-corticothalamic projection systems. *The Journal of Comparative Neurology*, 507(2):1209–1227.

Lynch, M. A. (2004). Long-Term Potentiation and Memory. *Physiological Reviews*, 84(1):87–136.

Madisen, L., Garner, A. R., Shimaoka, D., Chuong, A. S., Klapoetke, N. C., Li, L., van der Bourg, A., Niino, Y., Egolf, L., Monetti, C., Gu, H., Mills, M., Cheng, A., Tasic, B., Nguyen, T. N., Sunkin, S. M., Benucci, A., Nagy, A., Miyawaki, A., Helmchen, F., Empson, R. M., Knöpfel, T., Boyden, E. S., Reid, R. C., Carandini, M., and Zeng, H. (2015). Transgenic mice for intersectional targeting of neural sensors and effectors with high specificity and performance. *Neuron*, 85(5):942–58.

Madisen, L., Zwingman, T. A., Sunkin, S. M., Oh, S. W., Zariwala, H. A., Gu, H., Ng, L. L., Palmiter, R. D., Hawrylycz, M. J., Jones, A. R., Lein, E. S., and Zeng, H. (2010). A robust and high-throughput Cre reporting and characterization system for the whole mouse brain. *Nature Neuroscience*, 13(1):133–140.

Malmierca, M. S. and Ryugo, D. K. (2012). Auditory System. In *The Mouse Nervous System*. Elsevier.

Margolis, D. J., Lütcke, H., Schulz, K., Haiss, F., Weber, B., Kügler, S., Hasan, M. T., and Helmchen, F. (2012). Reorganization of cortical population activity imaged throughout long-term sensory deprivation. *Nature Neuroscience*, 15(11):1539–1546.

Mayrhofer, J. M., Skreb, V., von der Behrens, W., Musall, S., Weber, B., and Haiss, F. (2013). Novel two-alternative forced choice paradigm for bilateral vibrotactile whisker frequency discrimination in head-fixed mice and rats. *Journal of Neurophysiology*, 109(1):273–284.

Mueller, T. (2012). What is the Thalamus in Zebrafish? *Frontiers in Neuroscience*, 6(MAY):64.

Musall, S., Haiss, F., Weber, B., and von der Behrens, W. (2015). Deviant Processing in the Primary Somatosensory Cortex. *Cerebral Cortex*, page bhv283.

Näätänen, R., Gaillard, A. W., and Mäntysalo, S. (1978). Early selective-attention effect on evoked potential reinterpreted. *Acta psychologica*, 42(4):313–29.

Nagai, T., Yamada, S., Tominaga, T., Ichikawa, M., and Miyawaki, A. (2004). Expanded dynamic range of fluorescent indicators for Ca(2+) by circularly permuted yellow fluorescent proteins. *Proceedings of the National Academy of Sciences of the United States of America*, 101(29):10554–10559.

Neher, E. and Sakmann, B. (1992). The patch clamp technique. *Scientific American*, 266(3):44–51.

Nelken, I. (2004). Large-Scale Organization of Ferret Auditory Cortex Revealed Using Continuous Acquisition of Intrinsic Optical Signals. *Journal of Neurophysiology*, 92(4):2574–2588.

Nimmerjahn, A. and Helmchen, F. (2012). In Vivo Labeling of Cortical Astrocytes with Sulforhodamine 101 (SR101). *Cold Spring Harbor protocols*, 2012(3).

Nimmerjahn, A., Kirchhoff, F., Kerr, J. N. D., and Helmchen, F. (2004). Sulforhodamine 101 as a specific marker of astroglia in the neocortex in vivo. *Nature Methods*, 1(1):31–37.

Ohkura, M., Sasaki, T., Kobayashi, C., Ikegaya, Y., and Nakai, J. (2012). An Improved Genetically Encoded Red Fluorescent Ca2+ Indicator for Detecting Optically Evoked Action Potentials. *PLoS ONE*, 7(7):e39933.

Olshausen, B. and Field, D. (2004). Sparse coding of sensory inputs. *Current Opinion in Neurobiology*, 14(4):481–487.

Otazu, G. H., Tai, L.-H., Yang, Y., and Zador, A. M. (2009). Engaging in an auditory task suppresses responses in auditory cortex. *Nature Neuroscience*, 12(5):646–654.

Pena, J. L. and DeBello, W. M. (2010). Auditory Processing, Plasticity, and Learning in the Barn Owl. *ILAR Journal*, 51(4):338–352.

Peron, S., Chen, T.-W., and Svoboda, K. (2015). Comprehensive imaging of cortical networks. *Current Opinion in Neurobiology*, 32:115–123.

Pi, H.-J., Hangya, B., Kvitsiani, D., Sanders, J. I., Huang, Z. J., and Kepecs, A. (2013). Cortical interneurons that specialize in disinhibitory control. *Nature*, 503(7477):521–4.

Pilz, G.-A., Carta, S., Stäuble, A., Ayaz, A., Jessberger, S., and Helmchen, F. (2016). Functional Imaging of Dentate Granule Cells in the Adult Mouse Hippocampus. *The Journal of Neuroscience*, 36(28):7407–7414.

Polley, D. B. (2006). Perceptual Learning Directs Auditory Cortical Map Reorganization through Top-Down Influences. *Journal of Neuroscience*, 26(18):4970–4982.

Polley, D. B., Kvašňák, E., and Frostig, R. D. (2004). Naturalistic experience transforms sensory maps in the adult cortex of caged animals. *Nature*, 429(May):67–71.

Pruitt, D. T., Schmid, A. N., Danaphongse, T. T., Flanagan, K. E., Morrison, R. A., Kilgard, M. P., Rennaker, R. L., and Hays, S. A. (2016). Forelimb training drives transient map reorganization in ipsilateral motor cortex. *Behavioural Brain Research*, 313:10–16.

Reed, A., Riley, J., Carraway, R. S., Carrasco, A., Perez, C. A., Jakkamsetti, V., and Kilgard, M. P. (2011). Cortical map plasticity improves learning but is not necessary for improved performance. *Neuron*, 70(1):121–31.

Rothschild, G., Nelken, I., and Mizrahi, A. (2010). Functional organization and population dynamics in the mouse primary auditory cortex. *Nature Neuroscience*, 13(3):353–360.

Sando, R., Baumgaertel, K., Pieraut, S., Torabi-Rander, N., Wandless, T. J., Mayford, M., and Maximov, A. (2013). Inducible control of gene expression with destabilized Cre. *Nature Methods*, 10(11):1085–8.

Schindelin, J., Arganda-Carreras, I., Frise, E., Kaynig, V., Longair, M., Pietzsch, T., Preibisch, S., Rueden, C., Saalfeld, S., Schmid, B., Tinevez, J.-Y., White, D. J., Hartenstein, V., Eliceiri, K., Tomancak, P., and Cardona, A. (2012). Fiji: an open-source platform for biological-image analysis. *Nature Methods*, 9(7):676–82.

Schindelin, J., Rueden, C. T., Hiner, M. C., and Eliceiri, K. W. (2015). The ImageJ ecosystem: An open platform for biomedical image analysis. *Molecular Reproduction and Development*, 82(7-8):518–529.

Schneider, D. M., Nelson, A., and Mooney, R. (2014). A synaptic and circuit basis for corollary discharge in the auditory cortex. *Nature*, 513(7517):189–94.

Schreiner, C. E. and Winer, J. A. (2007). Auditory cortex mapmaking: principles, projections, and plasticity. *Neuron*, 56(2):356–65.

Sheng, M. and Kim, M. J. (2002). Postsynaptic signaling and plasticity mechanisms. *Science (New York, N.Y.)*, 298(5594):776–780.

Squires, N. K., Squires, K. C., and Hillyard, S. A. (1975). Two varieties of long-latency positive waves evoked by unpredictable auditory stimuli in man. *Electroencephalography and Clinical Neurophysiology*, 38(4):387–401.

Stiebler, I., Neulist, R., Fichtel, I., and Ehret, G. (1997). The auditory cortex of the house mouse: left-right differences, tonotopic organization and quantitative analysis of frequency representation. *Journal of Comparative Physiology A: Sensory, Neural, and Behavioral Physiology*, 181(6):559–571.

Stosiek, C., Garaschuk, O., Holthoff, K., and Konnerth, A. (2003). In vivo two-photon calcium imaging of neuronal networks. *Proceedings of the National Academy of Sciences of the United States of America*, 100(12):7319–7324.

Svoboda, K. and Yasuda, R. (2006). Principles of Two-Photon Excitation Microscopy and Its Applications to Neuroscience.

Takahashi, H., Yokota, R., Funamizu, A., Kose, H., and Kanzaki, R. (2011). Learning-stage-dependent, field-specific, map plasticity in the rat auditory cortex during appetitive operant conditioning. *Neuroscience*, 199:243–58.

Taniguchi, H., He, M., Wu, P., Kim, S., Paik, R., Sugino, K., Kvitsani, D., Fu, Y., Lu, J., Lin, Y., Miyoshi, G., Shima, Y., Fishell, G., Nelson, S. B., and Huang, Z. J. (2011). A Resource of Cre Driver Lines for Genetic Targeting of GABAergic Neurons in Cerebral Cortex. *Neuron*, 71(6):995–1013.

The HDF Group (2016). Hierarchical Data Format, version 5. *The HDF Group*.

Thevenaz, P., Ruttimann, U., and Unser, M. (1998). A pyramid approach to subpixel registration based on intensity. *IEEE Transactions on Image Processing*, 7(1):27–41.

Trujillo, M. and Razak, K. A. (2013). Altered cortical spectrotemporal processing with age-related hearing loss. *Journal of Neurophysiology*, 110(12):2873–2886.

Tsien, R. Y. (1989). Fluorescent Probes of Cell Signaling. *Annual Review of Neuroscience*, 12(1):227–253.

Ulanovsky, N., Las, L., and Nelken, I. (2003). Processing of low-probability sounds by cortical neurons. *Nature Neuroscience*, 6(4):391–398.

Watson, C., Paxinos, G., and Puelles, L. (2012). *The Mouse Nervous System*, volume 36. Elsevier.

Weinberger, N. M. (1995). Dynamic Regulation of Receptive Fields and Maps in the Adult Sensory Cortex. *Annual Review of Neuroscience*, 18(1):129–158.

Weinberger, N. M. (2003). The nucleus basalis and memory codes: auditory cortical plasticity and the induction of specific, associative behavioral memory. *Neurobiology of Learning and Memory*, 80(3):268–84.

Weinberger, N. M. (2004). Specific long-term memory traces in primary auditory cortex. *Nature reviews. Neuroscience*, 5(4):279–90.

Winer, J. A. and Lee, C. C. (2007). The distributed auditory cortex. *Hearing Research*, 229(1-2):3–13.

Winkowski, D. E. and Kanold, P. O. (2013). Laminar Transformation of Frequency Organization in Auditory Cortex. *Journal of Neuroscience*, 33(4):1498–1508.

Wolff, S. B. E., Gründemann, J., Tovote, P., Krabbe, S., Jacobson, G. a., Müller, C., Herry, C., Ehrlich, I., Friedrich, R. W., Letzkus, J. J., and Lüthi, A. (2014). Amygdala interneuron subtypes control fear learning through disinhibition. *Nature*, 509(7501):453–8.

Xiong, Q., Znamenskiy, P., and Zador, A. M. (2015). Selective corticostriatal plasticity during acquisition of an auditory discrimination task. *Nature*, 521(7552):348–51.

Zepeda, A., Arias, C., and Sengpiel, F. (2004). Optical imaging of intrinsic signals: Recent developments in the methodology and its applications.

Zhao, Y., Araki, S., Wu, J., Teramoto, T., Chang, Y.-F., Nakano, M., Abdelfattah, A. S., Fujiwara, M., Ishihara, T., Nagai, T., and Campbell, R. E. (2011). An Expanded Palette of Genetically Encoded Ca2+ Indicators. *Science*, 333(6051):1888–1891.

Znamenskiy, P. and Zador, A. M. (2013). Corticostriatal neurons in auditory cortex drive decisions during auditory discrimination. *Nature*, 497(7450):482–5.